EUROPEAN ORGANISATION FOR NUCLEAR RESEARCH (CERN)

Submitted to: JHEP

CERN-PH-EP-2015-229
23rd December 2015

arXiv:1509.06047v2 [hep-ex] 22 Dec 2015

Search for flavour-changing neutral current top quark decays $t \to Hq$ in pp collisions at $\sqrt{s} = 8$ TeV with the ATLAS detector

The ATLAS Collaboration

Abstract

A search for flavour-changing neutral current decays of a top quark to an up-type quark ($q = u, c$) and the Standard Model Higgs boson, where the Higgs boson decays to $b\bar{b}$, is presented. The analysis searches for top quark pair events in which one top quark decays to Wb, with the W boson decaying leptonically, and the other top quark decays to Hq. The search is based on pp collisions at $\sqrt{s} = 8$ TeV recorded in 2012 with the ATLAS detector at the CERN Large Hadron Collider and uses an integrated luminosity of 20.3 fb^{-1}. Data are analysed in the lepton-plus-jets final state, characterised by an isolated electron or muon and at least four jets. The search exploits the high multiplicity of b-quark jets characteristic of signal events, and employs a likelihood discriminant that uses the kinematic differences between the signal and the background, which is dominated by $t\bar{t} \to WbWb$ decays. No significant excess of events above the background expectation is found, and observed (expected) 95% CL upper limits of 0.56% (0.42%) and 0.61% (0.64%) are derived for the $t \to Hc$ and $t \to Hu$ branching ratios respectively. The combination of this search with other ATLAS searches in the $H \to \gamma\gamma$ and $H \to WW^*, \tau\tau$ decay modes significantly improves the sensitivity, yielding observed (expected) 95% CL upper limits on the $t \to Hc$ and $t \to Hu$ branching ratios of 0.46% (0.25%) and 0.45% (0.29%) respectively. The corresponding combined observed (expected) upper limits on the $|\lambda_{tcH}|$ and $|\lambda_{tuH}|$ couplings are 0.13 (0.10) and 0.13 (0.10) respectively. These are the most restrictive direct bounds on tqH interactions measured so far.

© 2015 CERN for the benefit of the ATLAS Collaboration.
Reproduction of this article or parts of it is allowed as specified in the CC-BY-3.0 license.

Contents

1 Introduction **2**

2 ATLAS detector **4**

3 Object reconstruction **5**

4 Data sample and event preselection **6**

5 Background and signal modelling **7**

6 Analysis strategy **9**
- 6.1 Event categorisation 10
- 6.2 Discrimination of signal from background 10
  - 6.2.1 Signal probability 11
  - 6.2.2 Background probability 13
  - 6.2.3 Final discriminant 14

7 Systematic uncertainties **14**
- 7.1 Luminosity 17
- 7.2 Reconstructed objects 18
- 7.3 Background modelling 18
- 7.4 Signal modelling 20

8 Statistical analysis **20**

9 Results **21**
- 9.1 $H \to b\bar{b}$ 21
- 9.2 $H \to \gamma\gamma$ 23
- 9.3 $H \to W^+W^-, \tau^+\tau^-$ 23
- 9.4 Combination of searches 29

10 Conclusion **33**

Appendix **35**

A Pre-fit and post-fit event yields in the $t\bar{t} \to WbHq, H \to b\bar{b}$ search **35**

B Pre-fit event yields in the $t\bar{t} \to WbHq, H \to WW^*, \tau\tau$ search **35**

1. Introduction

Following the observation of a Higgs boson by the ATLAS and CMS collaborations [1, 2], a comprehensive programme of measurements of its properties is underway looking for deviations from the Standard Model (SM) predictions. An interesting possibility is the presence of flavour-changing neutral current (FCNC) interactions between the Higgs boson, the top quark, and a u- or c-quark, tqH ($q = u, c$). Since the Higgs boson is lighter than the top quark, with a measured mass $m_H = 125.09 \pm 0.24$ GeV [3], such interactions would manifest themselves as FCNC top quark decays, $t \to Hq$. In the SM, such decays are extremely suppressed relative to the dominant $t \to Wb$ decay mode, since tqH interactions are forbidden at the tree level and even suppressed at higher-orders in the perturbative expansion due to the Glashow–Iliopoulos–Maiani (GIM) mechanism [4]. As a result, the SM predictions for the $t \to Hq$ branching ratios are exceedingly small: BR$(t \to Hu) \sim 10^{-17}$ and BR$(t \to Hc) \sim 10^{-15}$ [5–8]. On the other hand, large enhancements in these branching ratios are possible in some beyond-SM scenarios, where the GIM suppression can be relaxed and/or new particles can contribute to the loops, yielding effective couplings orders of magnitude larger than those of the SM. Examples include quark-singlet models [9], two-Higgs-doublet models (2HDM) of type I, with explicit flavour conservation, and of type II, such as the minimal supersymmetric SM (MSSM) [10–12], or supersymmetric models with R-parity violation [13]. In those scenarios, typical branching ratios can be as high as BR$(t \to Hq) \sim 10^{-5}$. An even larger branching ratio of BR$(t \to Hc) \sim 10^{-3}$ can be reached in 2HDM without explicit flavour conservation (type III), since a tree-level FCNC coupling is not forbidden by any symmetry [14–16]. While other FCNC top couplings, $tq\gamma$, tqZ, tqg, are also enhanced relative to the SM prediction in those scenarios beyond the SM, the largest enhancements are typically for the tqH couplings, and in particular the tcH coupling. See ref. [7] for a review.

Searches for $t \to Hq$ decays have been performed by the ATLAS and CMS collaborations, taking advantage of the large samples of $t\bar{t}$ events collected during Run 1 of the LHC. In these searches, one of the top quarks is required to decay into Wb, while the other top quark decays into Hq, yielding $t\bar{t} \to WbHq$.[1] Assuming SM decays for the Higgs boson and $m_H = 125$ GeV, the most sensitive single-channel searches have been performed in the $H \to \gamma\gamma$ decay mode which, despite the tiny branching ratio of BR$(H \to \gamma\gamma) \simeq 0.2\%$, is characterised by very small background and excellent diphoton mass resolution. The resulting observed (expected) 95% confidence level (CL) upper limits on BR$(t \to Hq)$ are 0.79% (0.51%) and 0.69% (0.81%), respectively from the ATLAS [17] and CMS [18] collaborations. These searches are insensitive to the difference between $t \to Hu$ and $t \to Hc$, and thus the above limits can be interpreted as applying to the sum BR$(t \to Hu)$+BR$(t \to Hc)$. The CMS Collaboration has also reinterpreted searches in multilepton (three or four leptons) final states [18] in the context of $t\bar{t} \to WbHq$ with $H \to WW^*, \tau\tau$, resulting in an observed (expected) upper limit of BR$(t \to Hc) < 1.28\%$ (1.17%) at the 95% CL. Multilepton searches are able to exploit a significantly larger branching ratio for the Higgs boson decay compared to the $H \to \gamma\gamma$ decay mode, and are also characterised by relatively small backgrounds. However, in general they do not have good mass resolution,[2] so any excess would be hard to interpret as originating from $t \to Hq$ decays. The combination of CMS searches in diphoton and multilepton (three or four leptons) final states yields an observed (expected) upper limit of BR$(t \to Hc) < 0.56\%$ (0.65%) at the 95% CL [18].

Upper limits on the branching ratios BR$(t \to Hq)$ $(q = u, c)$ can be translated to upper limits on the non-flavour-diagonal Yukawa couplings λ_{tqH} appearing in the following Lagrangian:

$$\mathcal{L}_{\mathrm{FCNC}} = \lambda_{tcH}\bar{t}Hc + \lambda_{tuH}\bar{t}Hu + h.c. \qquad (1)$$

The branching ratio BR$(t \to Hq)$ is estimated as the ratio of its partial width [8] to the SM $t \to Wb$ partial width [19], which is assumed to be dominant. Both predicted partial widths include next-to-leading-order

---

[1] In the following $WbHq$ is used to denote both $W^+bH\bar{q}$ and its charge conjugate, $HqW^-\bar{b}$. Similarly, $WbWb$ is used to denote $W^+bW^-\bar{b}$.

[2] An exception is the $H \to ZZ^* \to \ell^+\ell^-\ell'^+\ell'^-$ $(\ell, \ell' = e, \mu)$ decay mode, which has a very small branching ratio and thus is not promising for this search.

(NLO) QCD corrections. Using the expression derived in ref. [17], the coupling $|\lambda_{tqH}|$ can be extracted as $|\lambda_{tqH}| = (1.92 \pm 0.02)\sqrt{\mathrm{BR}(t \to Hq)}$.

The results presented in this paper fill a gap in the current programme of searches for $t \to Hq$ decays at the LHC by considering the dominant decay mode $H \to b\bar{b}$, which has $\mathrm{BR}(H \to b\bar{b}) \simeq 58\%$. This search is focused on the $t\bar{t} \to WbHq$ $(q = u, c)$ process, with $W \to \ell\nu$ $(\ell = e, \mu, \tau)$ and $H \to b\bar{b}$, resulting in a lepton-plus-jets final state with high b-jet multiplicity, which can be effectively exploited to suppress the overwhelming $t\bar{t}$ background. Early studies of the prospects for this search at the LHC were performed in ref. [20]. Only events with an electron or muon, including those produced via leptonically decaying taus, are considered. The lepton-plus-jets final state also allows the kinematic reconstruction of the final state and in particular the dijet invariant mass spectrum from the $H \to b\bar{b}$ decay, providing additional handles that would help in detecting $t\bar{t} \to WbHq$ events. Most of this paper is devoted to the discussion of this particular search, for which background estimation techniques, systematic uncertainties and statistical treatment closely follow those used in recent ATLAS searches using the same final-state signature [21, 22]. This paper also includes a reinterpretation of the ATLAS search for $t\bar{t}H$ associated production, with $H \to WW^*, ZZ^*, \tau\tau$, resulting in multilepton final states [23]. This reinterpretation only considers the final states with a significant expected contribution from $t\bar{t} \to WbHq$, $H \to WW^*, \tau\tau$ signal, namely two same-charge leptons with and without an identified hadronic tau lepton and three leptons. A combination of the three ATLAS searches for $t\bar{t} \to WbHq$, probing the $H \to b\bar{b}$, $H \to WW^*, \tau\tau$, and $H \to \gamma\gamma$ decay modes, is performed and bounds are set on $\mathrm{BR}(t \to Hc)$ and $\mathrm{BR}(t \to Hu)$, as well as on the corresponding non-flavour-diagonal Yukawa couplings.

This paper is organised as follows. A brief description of the ATLAS detector is provided in section 2. Subsequent sections are devoted to a detailed discussion of the $t\bar{t} \to WbHq, H \to b\bar{b}$ search, covering the object reconstruction (section 3), the data sample and event preselection (section 4), the modelling of the backgrounds and the signal (section 5), the analysis strategy (section 6), and the systematic uncertainties (section 7). Section 8 provides a discussion of the statistical methods used. Section 9 presents the results obtained by the three individual ATLAS searches as well as their combination. Finally, the conclusions are given in section 10.

2. ATLAS detector

The ATLAS detector [24] consists of the following main subsystems: an inner tracking system, electromagnetic and hadronic calorimeters, and a muon spectrometer. The inner detector provides tracking information from silicon pixel and microstrip detectors in the pseudorapidity[3] range $|\eta| < 2.5$ and from a straw-tube transition radiation tracker covering $|\eta| < 2.0$, all immersed in a 2 T axial magnetic field provided by a superconducting solenoid. The electromagnetic (EM) sampling calorimeter uses lead as the absorber material and liquid-argon (LAr) as the active medium, and is divided into barrel ($|\eta| < 1.475$) and end-cap ($1.375 < |\eta| < 3.2$) regions. Hadron calorimetry is also based on the sampling technique, with either scintillator tiles or LAr as the active medium, and with steel, copper, or tungsten as the absorber material. The calorimeters cover $|\eta| < 4.9$. The muon spectrometer measures the deflection of muons with $|\eta| < 2.7$ using multiple layers of high-precision tracking chambers located in a toroidal field of approximately 0.5 T and 1 T in the central and end-cap regions of ATLAS, respectively. The muon spectrometer is also instrumented with separate trigger chambers covering $|\eta| < 2.4$. A three-level trigger system [25] is used to select interesting events. The first-level trigger is implemented in custom electronics and uses a subset of detector information to reduce the event rate to at most 75 kHz. This is followed by two software-based trigger levels exploiting the full detector information and yielding a typical recorded event rate of 400 Hz during 2012.

---

[3] ATLAS uses a right-handed coordinate system with its origin at the nominal interaction point (IP) in the centre of the detector and the z-axis coinciding with the axis of the beam pipe. The x-axis points from the IP to the centre of the LHC ring, and the y-axis points upward. Cylindrical coordinates (r,ϕ) are used in the transverse plane, ϕ being the azimuthal angle around the beam pipe. The pseudorapidity is defined in terms of the polar angle θ as $\eta = -\ln\tan(\theta/2)$.

3. Object reconstruction

Electron candidates [26] are reconstructed from energy clusters in the EM calorimeter that are matched to reconstructed tracks in the inner detector. Electron clusters are required to have a transverse energy E_{T} greater than 25 GeV and $|\eta_{\mathrm{cluster}}| < 2.47$, excluding the transition region $1.37 < |\eta_{\mathrm{cluster}}| < 1.52$ between sections of the EM calorimeter. The longitudinal impact parameter of the electron track with respect to the event's primary vertex (see section 4), z_0, is required to be less than 2 mm. Electrons are required to satisfy "tight" quality requirements [26] based on calorimeter, tracking and combined variables that provide good separation between prompt electrons and jets. To reduce the background from non-prompt electrons resulting from semileptonic decays of b- or c-hadrons, and from jets with a high fraction of their energy deposited in the EM calorimeter, electron candidates must also satisfy calorimeter- and track-based isolation requirements. The calorimeter isolation variable is based on the energy sum of cells within a cone of size $\Delta R = \sqrt{(\Delta\phi)^2 + (\Delta\eta)^2} = 0.2$ around the direction of each electron candidate, and an η-dependent requirement is made, giving an average efficiency of 90% across η for prompt electrons from Z boson decays. This energy sum excludes cells associated with the electron cluster and is corrected for leakage from the electron cluster itself as well as for energy deposits from additional pp interactions within the same bunch crossing ("pileup"). A further 90%-efficient isolation requirement is made on the track transverse momentum (p_{T}) sum around the electron (excluding the electron track itself) in a cone of size $\Delta R = 0.3$.

Muon candidates [27, 28] are reconstructed from track segments in the various layers of the muon spectrometer that are matched with tracks found in the inner detector. The final candidates are refitted using the complete track information from both detector systems and are required to have $p_{\mathrm{T}} > 25$ GeV and $|\eta| < 2.5$. The longitudinal impact parameter of the muon track with respect to the primary vertex, z_0, is required to be less than 2 mm. Muons are required to satisfy a p_{T}-dependent track-based isolation requirement: the scalar sum of the p_{T} of the tracks within a cone of variable size $\Delta R = 10\ \mathrm{GeV}/p_{\mathrm{T}}^{\mu}$ around the muon (excluding the muon track itself) must be less than 5% of the muon p_{T} (p_{T}^{μ}). This requirement has good signal efficiency and background rejection even under high-pileup conditions, as well as in boosted configurations where the muon is close to a jet. For muons from W boson decays in simulated $t\bar{t}$ events, the average efficiency of the isolation requirement is about 95%.

Jets are reconstructed with the anti-k_t algorithm [29–31] with a radius parameter $R = 0.4$, using calibrated topological clusters [32, 33] built from energy deposits in the calorimeters. Prior to jet finding, a local cluster calibration scheme [34] is applied to correct the topological cluster energies for the non-compensating response of the calorimeter, as well as for the energy lost in dead material and via out-of-cluster leakage. The corrections are obtained from simulations of charged and neutral particles. After energy calibration [35], jets are required to have $p_{\mathrm{T}} > 25$ GeV and $|\eta| < 2.5$. To reduce the contamination due to jets originating from pileup interactions, a requirement on the absolute value of the jet vertex fraction (JVF) variable above 0.5 is applied to jets with $p_{\mathrm{T}} < 50$ GeV and $|\eta| < 2.4$. This requirement ensures that at least 50% of the scalar sum of the p_{T} of the tracks with $p_{\mathrm{T}} > 1$ GeV associated with a jet comes from tracks originating from the primary vertex. During jet reconstruction, no distinction is made between identified electrons and jet energy deposits. Therefore, if any of the jets lie within $\Delta R = 0.2$ of a selected electron, the closest jet is discarded in order to avoid double-counting of electrons as jets. Finally, any electron or muon within $\Delta R = 0.4$ of a selected jet is discarded.

Jets containing b-hadrons are identified (b-tagged) via an algorithm [36] that uses multivariate techniques to combine information from the impact parameters of displaced tracks as well as topological properties of secondary and tertiary decay vertices reconstructed within the jet. For each jet, a value for the multivariate b-tagging discriminant is calculated. The jet is considered b-tagged if this value is above a given threshold. The threshold used in this search corresponds to 70% efficiency to tag a b-quark jet, with a light-jet[4] rejection factor of ~130 and a charm-jet rejection factor of 5, as determined for jets with $p_{\mathrm{T}} > 20$ GeV and $|\eta| < 2.5$ in simulated $t\bar{t}$ events.

The missing transverse momentum ($E_{\mathrm{T}}^{\mathrm{miss}}$) is constructed [37] from the vector sum of all calorimeter energy deposits contained in topological clusters. All topological cluster energies are corrected using the local cluster calibration scheme discussed previously in the context of the jet energy calibration. Those topological clusters associated with a high-p_{T} object (e.g. jet or electron) are further calibrated using their respective energy corrections. In addition, contributions from the p_{T} of selected muons are included in the calculation of $E_{\mathrm{T}}^{\mathrm{miss}}$.

4. Data sample and event preselection

This search is based on pp collision data at $\sqrt{s} = 8$ TeV collected by the ATLAS experiment between April and December 2012. Only events recorded with a single-electron or single-muon trigger under stable beam conditions and for which all detector subsystems were operational are considered. The corresponding integrated luminosity is 20.3 ± 0.6 fb^{-1} [38]. Single-lepton triggers with different p_{T} thresholds are combined in a logical OR in order to increase the overall efficiency. The p_{T} thresholds are 24 or 60 GeV for the electron triggers and 24 or 36 GeV for the muon triggers. The triggers with the lower p_{T} threshold include isolation requirements on the candidate lepton, resulting in inefficiencies at high p_{T} that are recovered by the triggers with higher p_{T} threshold.

Events satisfying the trigger selection are required to have at least one reconstructed vertex with at least five associated tracks with $p_{\mathrm{T}} > 400$ MeV, consistent with originating from the beam collision region in the x–y plane. The average number of pp interactions per bunch crossing is approximately 20, resulting in several vertices reconstructed per event. If more than one vertex is found, the hard-scatter primary vertex is taken to be the one which has the largest sum of the squared transverse momenta of its associated tracks. For the event topologies considered in this paper, this requirement leads to a probability to reconstruct and select the correct hard-scatter primary vertex larger than 99%.

Preselected events are required to have exactly one electron or muon, as defined in section 3, that matches, within $\Delta R = 0.15$, the lepton candidate reconstructed by the trigger. In addition, at least four jets are required, of which at least two must be b-tagged.

---

[4] Light-jet denotes a jet originating from the hadronisation of a light quark (u, d, s) or gluon.

5. Background and signal modelling

After the event preselection, the main background is $t\bar{t} \to WbWb$ production, possibly in association with jets, denoted by $t\bar{t}$+jets in the following. Single top quark production and production of a W boson in association with jets (W+jets) contribute to a lesser extent. Small contributions arise from multijet, Z+jets and diboson (WW, WZ, ZZ) production, as well as from the associated production of a vector boson V ($V = W, Z$) or a Higgs boson and a $t\bar{t}$ pair ($t\bar{t}V$ and $t\bar{t}H$). Signal and all backgrounds are estimated from simulation and normalised to their theoretical cross sections, with the exception of the multijet background, which is estimated with data-driven methods [39].

Simulated samples of $t\bar{t}$ events are generated with the NLO generator Powheg-Box 2.0 [40–43] using the CT10 [44] set of parton distribution functions (PDF). The nominal sample is interfaced to Pythia 6.425 [45] for parton showering and hadronisation with the CTEQ6L1 PDF set and the Perugia2011C [46] set of optimised parameters for the underlying event (UE) description, referred to as the "UE tune". An alternative sample, used to study the uncertainty related to the hadronisation model, is interfaced to Herwig v6.520 [47] with the CTEQ6L1 PDF set and Jimmy v4.31 [48] to simulate the UE. All samples are generated assuming a top quark mass of 172.5 GeV and top quark decays exclusively through $t \to Wb$. The $t\bar{t}$ process is normalised to a cross section of 253^{+15}_{-16} pb, computed using Top++ v2.0 [49] at next-to-next-to-leading order (NNLO) in QCD, including resummation of next-to-next-to-leading logarithmic (NNLL) soft gluon terms [50–54], and using the MSTW 2008 NNLO [55, 56] PDF set. Theoretical uncertainties result from variations of the factorisation and renormalisation scales, as well as from uncertainties on the PDF and α_S. The latter two represent the largest contribution to the overall theoretical uncertainty on the cross section and were calculated using the PDF4LHC prescription [57] with the MSTW 2008 68% CL NNLO, CT10 NNLO [44, 58] and NNPDF2.3 5f FFN [59] PDF sets. In the case where a non-zero $\mathrm{BR}(t \to Hq)$ is assumed, an additional factor of $[1-\mathrm{BR}(t \to Hq)]^2$ is applied to the sample normalisation. It is not possible to generate the $t\bar{t} \to WbHq$ signal with Powheg-Box, and a different event generator is used instead, as discussed below.

The $t\bar{t}$ samples are generated inclusively, but events are categorised depending on the flavour content of additional particle jets not originating from the decay of the $t\bar{t}$ system.[5] Details about this categorisation scheme can be found in ref. [21]. In this way, a distinction is made between $t\bar{t}+b\bar{b}$, $t\bar{t}+c\bar{c}$ and $t\bar{t}$+light-jets events. The first two categories are generically referred to as $t\bar{t}$+HF events (with HF standing for "heavy flavour"), while the latter category also includes events with no additional jets. The modelling of $t\bar{t}$+HF in Powheg-Box+Pythia is via the parton-shower evolution. To study uncertainties related to this simplified description, an alternative $t\bar{t}$+jets sample is generated with Madgraph5 1.5.11 [60] using the CT10 PDF set. It includes tree-level diagrams with up to three additional partons (including b- and c-quarks) and is interfaced to Pythia 6.425.

Since the best possible modelling of the $t\bar{t}$+jets background is a key aspect of this search, a correction is applied to simulated $t\bar{t}$ events in Powheg-Box+Pythia based on the ratio of the differential cross sections measured in data and simulation at $\sqrt{s} = 7$ TeV as a function of top quark p_T and $t\bar{t}$ system p_T [61]. This correction significantly improves agreement between simulation and data at $\sqrt{s} = 8$ TeV in distributions such as the jet multiplicity and the p_T of decay products of the $t\bar{t}$ system [21], and is applied only to $t\bar{t}$+light-jets and $t\bar{t} + c\bar{c}$ events. The modelling of the $t\bar{t} + b\bar{b}$ background is improved by reweighting the Powheg-Box+Pythia prediction to an NLO prediction of $t\bar{t} + b\bar{b}$ with massive b quarks and including parton showering [62], based on Sherpa+OpenLoops [63, 64] using the CT10 PDF set. Such treatment is not possible for the $t\bar{t} + c\bar{c}$ background since a corresponding NLO prediction is not currently available. More details about the modelling of the $t\bar{t}$+jets background can be found in ref. [21].

---

[5] Particle jets are reconstructed by clustering stable particles excluding muons and neutrinos using the anti-k_t algorithm with a radius parameter $R = 0.4$.

Samples of single-top-quark backgrounds corresponding to the t-channel, s-channel, and Wt production mechanisms are generated with Powheg-Box 2.0 [65, 66] using the CT10 PDF set and interfaced to Pythia 6.425 with the CTEQ6L1 PDF set in combination with the Perugia2011C UE tune. Overlaps between the $t\bar{t}$ and Wt final states are avoided using the "diagram removal" scheme [67]. The single-top-quark samples are normalised to the approximate NNLO theoretical cross sections [68–70], calculated using the MSTW 2008 NNLO PDF set.

Samples of W/Z+jets events are generated with up to five additional partons using the Alpgen v2.14 [71] LO generator with the CTEQ6L1 PDF set and interfaced to Pythia v6.426. To avoid double-counting of partonic configurations generated by both the matrix-element calculation and the parton shower, a parton–jet matching scheme ("MLM matching") [72] is employed. The W+jets samples are generated separately for W+light-jets, $Wb\bar{b}$+jets, $Wc\bar{c}$+jets, and Wc+jets. The Z+jets samples are generated separately for Z+light-jets, $Zb\bar{b}$+jets, and $Zc\bar{c}$+jets. Overlap between $VQ\bar{Q}$+jets ($V = W, Z$ and $Q = b, c$) events generated from the matrix-element calculation and those generated from parton-shower evolution in the W/Z+light-jets samples is avoided via an algorithm based on the angular separation between the extra heavy quarks: if $\Delta R(Q, \bar{Q}) > 0.4$, the matrix-element prediction is used, otherwise the parton-shower prediction is used. Both the W+jets and Z+jets background contributions are normalised to their inclusive NNLO theoretical cross sections [73]. Further corrections are applied to W/Z+jets events in order to better describe data in the preselected sample. Normalisation factors for each of the W+jets categories ($Wb\bar{b}$+jets, $Wc\bar{c}$+jets, Wc+jets and W+light-jets) are derived for events with one lepton and at least four jets by simultaneously analysing six different event categories, defined by the b-tag multiplicity (0, 1 and ≥2) and the sign of the lepton charge [74]. The b-tag multiplicity provides information about the heavy-flavour composition of the W+jets background, while the lepton charge is used to determine the normalisation of each component, exploiting the expected charge asymmetry for W+jets production in pp collisions as predicted by Alpgen. In the case of Z+jets events, a correction to the heavy-flavour fraction is derived to reproduce the relative rates of Z+2-jets events with zero and one b-tagged jet observed in data. In addition, the Z boson p_{T} spectrum is compared between data and the simulation in Z+2-jets events, and a reweighting function is derived in order to improve the modelling. This reweighting function is also applied to the W+jets simulated sample and it was verified that this correction further improves the agreement between data and simulation for W+jets events. In any case, W/Z+jets events constitute a very small background in this analysis after final event selection.

The $WW/WZ/ZZ$+jets samples are generated with up to three additional partons using Alpgen v2.13 and the CTEQ6L1 PDF set, interfaced to Herwig v6.520 and Jimmy v4.31 for parton showering, hadronisation and UE modelling. The MLM parton–jet matching scheme is used. The WW+jets samples require at least one of the W bosons to decay leptonically, while the WZ/ZZ+jets samples require one Z boson to decay leptonically and other boson decays inclusively. Additionally, WZ+jets samples requiring the W boson to decay leptonically and the Z boson to decay hadronically, are generated with up to three additional partons (including massive b- and c-quarks) using Sherpa v1.4.1 and the CT10 PDF set. All diboson samples are normalised to their NLO theoretical cross sections [75].

Samples of $t\bar{t}V$ events, including $t\bar{t}WW$, are generated with up to two additional partons using Madgraph5 1.3.28 with the CTEQ6L1 PDF set, and interfaced to Pythia 6.425 with the AUET2B UE tune [76]. A sample of $t\bar{t}H$ events is generated with the PowHel framework [77], which combines the Powheg-Box generator and NLO matrix elements obtained from the HELAC-Oneloop package [78]. The sample is generated using the CT10nlo PDF set [44]. Showering is performed with Pythia 8.1 [79] using the CTEQ6L1 PDF set and the AU2 UE tune [76, 80]. Inclusive decays of the Higgs boson are assumed in the generation of the $t\bar{t}H$ sample. The $t\bar{t}V$ samples are normalised to the NLO cross-section predictions [81]. The $t\bar{t}H$ sample is normalised using the NLO cross section [82–84] and the Higgs decay branching ratios [85–88] collected in ref. [89].

The multijet background contributes to the selected data sample via several production and misreconstruction mechanisms. In the electron channel, it consists of non-prompt electrons (from semileptonic b- or c-hadron decays) as well as misidentified photons (e.g. from a conversion of a photon into an e^+e^- pair) or jets with a high fraction of their energy deposited in the EM calorimeter. In the muon channel, the multijet background is predominantly from non-prompt muons. Its normalisation and shape are estimated directly from data by using the “matrix method” technique [39], which exploits differences in lepton-identification-related properties between prompt and isolated leptons and leptons that are either non-isolated or result from the misidentification of photons or jets. Further details can be found in ref. [22].

The $t\bar{t} \to WbHq$ signal process is modelled using the Protos v2.2 [90, 91] LO generator with the CTEQ6L1 PDF set, and interfaced to Pythia 6.426 and the Perugia2011C UE tune. Two separate samples are generated corresponding to $t\bar{t} \to WbHc$ and $t\bar{t} \to WbHu$, with the W boson forced to decay leptonically, $W \to \ell\nu$ ($\ell = e, \mu, \tau$), The top quark and Higgs boson masses are set to 172.5 GeV and 125 GeV, respectively. The Higgs boson is allowed to decay to all SM particles with branching ratios as given in ref. [89]. The signal sample is normalised to the same NNLO cross section as used for the $t\bar{t} \to WbWb$ sample, and the corresponding branching ratios: $\sigma(t\bar{t} \to W(\to \ell\nu)bHq) = 2\mathrm{BR}(t \to Hq)[1 - \mathrm{BR}(t \to Hq)]\mathrm{BR}(W \to \ell\nu)\sigma_{t\bar{t}}$, with $\mathrm{BR}(W \to \ell\nu) = 0.324$ and $\mathrm{BR}(t \to Hq)$ depending on the branching ratio being tested. Typically a reference branching ratio of $\mathrm{BR}(t \to Hq) = 1\%$ is used. The case of both top quarks decaying into Hq is neglected in the analysis given existing upper limits on $\mathrm{BR}(t \to Hq)$ (see section 1). In order to improve the modelling of the signal kinematics, a two-step reweighting procedure is applied: the first step is designed to correct the spectrum of top quark p_{T} and $t\bar{t}$ system p_{T} to match that of the uncorrected $t\bar{t} \to WbWb$ Powheg-Box+Pythia sample; the second step involves the same correction to the top quark p_{T} and $t\bar{t}$ system p_{T} applied to the $t\bar{t}$+jets background (see discussion above).

Finally, all generated samples are processed through a simulation [92] of the detector geometry and response using Geant4 [93]. Additional minimum-bias pp interactions are simulated with the Pythia 8.1 generator with the MSTW 2008 LO PDF set and the A2 UE tune [94]. They are overlaid on the simulated signal and background events according to the luminosity profile of the recorded data. The contributions from these pileup interactions are modelled both within the same bunch crossing as the hard-scattering process and in neighbouring bunch crossings. All simulated samples are processed through the same reconstruction software as the data. Simulated events are corrected so that the object identification efficiencies, energy scales, and energy resolutions match those determined from data control samples.

6. Analysis strategy

This section presents an overview of the analysis strategy followed by the $t\bar{t} \to WbHq, H \to b\bar{b}$ search.

6.1. Event categorisation

Given the focus on the $W \to \ell\nu$ and $H \to b\bar{b}$ decay modes, the $t\bar{t} \to WbHq$ signal is expected to have typically four jets, of which three or four are b-tagged. The latter case corresponds to the $t\bar{t} \to WbHc$ signal where the charm quark, as well as the three b-quark jets, are b-tagged. Additional jets can also be present because of initial- or final-state radiation. In order to optimise the sensitivity of the search, the selected events are categorised into different channels depending on the number of jets (4, 5 and ≥6) and on the number of b-tagged jets (2, 3 and ≥4). Therefore, the total number of analysis channels considered in this search is nine: (4 j, 2 b), (4 j, 3 b), (4 j, 4 b), (5 j, 2 b), (5 j, 3 b), (5 j, ≥4 b), (≥6 j, 2 b), (≥6 j, 3 b), and (≥6 j, ≥4 b), where (n j, m b) indicates n selected jets and m b-tagged jets.

The overall rate and composition of the $t\bar{t}$+jets background strongly depends on the jet and b-tag multiplicities, as illustrated in figure 1. The $t\bar{t}$+light-jets background is dominant in events with exactly two or three b-tagged jets, with the two b-quarks from the top quark decays being tagged in both cases, and a charm quark from the hadronic W boson decay also being tagged in the latter case. Contributions from $t\bar{t}+c\bar{c}$ and $t\bar{t}+b\bar{b}$ become significant as the jet and b-tag multiplicities increase, with the $t\bar{t}+b\bar{b}$ background being dominant for events with ≥6 jets and ≥4 b-tags.

In the channels with four or five jets and three or at least four b-tags, which dominate the sensitivity of this search, selected signal events have a $H \to b\bar{b}$ decay in more than 95% of the events. The channels most sensitive to the $t\bar{t} \to WbHu$ and $t\bar{t} \to WbHc$ signals are (4 j, 3 b) and (4 j, 4 b) respectively. Because of the better signal-to-background ratio in the (4 j, 4 b) channel, this analysis is expected to have better sensitivity for $t\bar{t} \to WbHc$ than for $t\bar{t} \to WbHu$ signal. The rest of the channels have significantly lower signal-to-background ratios, but they are useful for calibrating the $t\bar{t}$+jets background prediction and constraining the related systematic uncertainties (see section 7) through a likelihood fit to data (see section 8). This strategy was first used in the ATLAS search for $t\bar{t}H$ associated production, with $H \to b\bar{b}$ [21], and is adopted in this analysis. A table summarising the observed and expected yields before the fit to data in each of the analysis channels can be found in appendix A.

6.2. Discrimination of signal from background

After event categorisation, the signal-to-background ratio is very low even in the most sensitive analysis channels, and a suitable discriminating variable between signal and background needs to be constructed in order to improve the sensitivity of the search. A powerful discriminant between signal and background can be defined as:

$$D(\mathbf{x}) = \frac{P^{\mathrm{sig}}(\mathbf{x})}{P^{\mathrm{sig}}(\mathbf{x}) + P^{\mathrm{bkg}}(\mathbf{x})}, \tag{2}$$

where $P^{\mathrm{sig}}(\mathbf{x})$ and $P^{\mathrm{bkg}}(\mathbf{x})$ represent the probability density functions (pdf) of a given event under the signal hypothesis ($t\bar{t} \to WbHq$) and under the background hypothesis ($t\bar{t} \to WbWb$) respectively. Both pdfs are functions of $\mathbf{x}$, representing the four-momentum vectors of all final-state particles at the reconstruction level: the lepton (ℓ), the neutrino (ν; reconstructed as discussed below), and the N_{jets} selected jets in a given analysis channel.

Since both signal and background result from the $t\bar{t}$ decay, there are few experimental handles available to discriminate between them. The most prominent features are the different resonances present in the decay (i.e. the Higgs boson in the case of $t\bar{t} \to WbHq$ and a hadronically decaying W boson in the case of $t\bar{t} \to WbWb$), and the different flavour content of the jets forming those resonances. This is the main

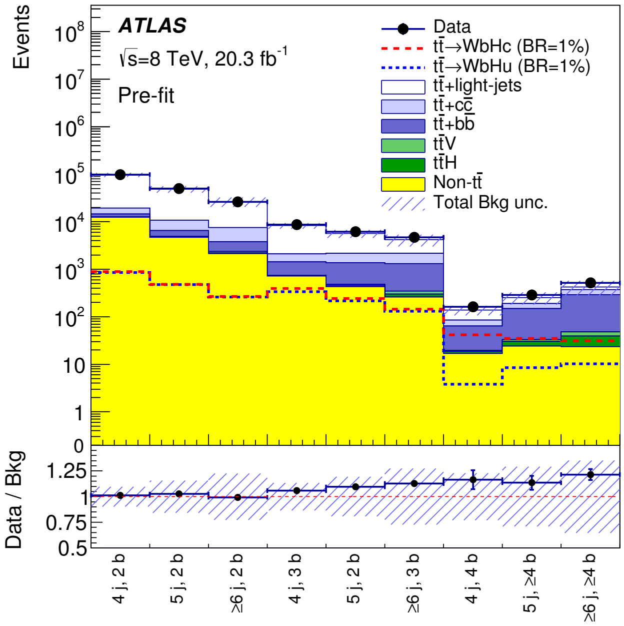

Figure 1: Comparison between the data and background prediction for the yields in each of the analysis channels considered before the fit to data (pre-fit). Backgrounds are normalised to their nominal cross sections discussed in section 5. The expected $t\bar{t} \to WbHc$ and $t\bar{t} \to WbHu$ signals (dashed histograms) are shown separately normalised to $\mathrm{BR}(t \to Hq) = 1\%$. The $t\bar{t} \to WbWb$ background is normalised to the SM prediction. The small contributions from W/Z+jets, single top, diboson and multijet backgrounds are combined into a single background source referred to as "Non-$t\bar{t}$". The bottom panel displays the ratio of data to the SM background ("Bkg") prediction. The hashed area represents the total uncertainty on the background.

information exploited in the construction of $P^{\mathrm{sig}}(\mathbf{x})$ and $P^{\mathrm{bkg}}(\mathbf{x})$ in this analysis, so that $\mathbf{x}$ is extended to include not only the four-momenta of jets $\mathbf{p}_{\mathrm{jet}}$, but also the value of their multivariate b-tagging discriminant $\mathbf{w}_{\mathrm{jet}}$, i.e., $\mathbf{x} \equiv \{p_\ell, p_\nu, (p_{\mathrm{jet}_i}, w_{\mathrm{jet}_i})\}$ $(i = 1, \ldots, N_{\mathrm{jets}})$. There is also some angular information from the different spins of the daughter resonances (Higgs and W boson) that could be exploited, but it is expected to be subleading in importance and is neglected in this analysis.

The calculation of $P^{\mathrm{sig}}(\mathbf{x})$ and $P^{\mathrm{bkg}}(\mathbf{x})$ is discussed in detail in sections 6.2.1 and 6.2.2 respectively. In the following, b_ℓ denotes the b-quark jet from the semileptonic top quark decay, q_h and b_h denote the light-quark jet ($q_h = u$ or c) and b-quark jet from the hadronic top quark decay in background and signal events respectively, q_1 and q_2 denote the up-type-quark jet (u or c) and down-type-quark jet (d or s) from the W boson decay respectively, and b_1 and b_2 denote the two b-quark jets from the Higgs boson decay. The level of separation achieved between signal and background with the resulting discriminant D is illustrated in section 6.2.3.

6.2.1. Signal probability

The construction of $P^{\mathrm{sig}}(\mathbf{x})$ will now be described step by step to illustrate the method. If the partonic origin of each jet were known [see figure 2(a)], $P^{\mathrm{sig}}(\mathbf{x})$ would be defined in this analysis as the product of the normalised pdfs for each of the reconstructed invariant masses in the event: the semileptonic top quark mass ($M_{\ell\nu b_\ell}$), the hadronic top quark mass ($M_{b_1 b_2 q_h}$) and the Higgs boson mass ($M_{b_1 b_2}$). Since $M_{b_1 b_2 q_h}$ and $M_{b_1 b_2}$ are correlated, their difference in quadrature, $X_{b_1 b_2 q_h} \equiv M_{b_1 b_2 q_h} \ominus M_{b_1 b_2}$, is used instead of $M_{b_1 b_2 q_h}$. Therefore the expression for P^{sig} just making use of the above kinematic information, denoted by $P^{\mathrm{sig}}_{\mathrm{kin}}$, is:

$$P^{\mathrm{sig}}_{\mathrm{kin}}(\mathbf{x}) = P^{\mathrm{sig}}(M_{\ell\nu b_\ell}) P^{\mathrm{sig}}(X_{b_1 b_2 q_h}) P^{\mathrm{sig}}(M_{b_1 b_2}). \tag{3}$$

The distributions of these invariant masses are obtained from simulated signal events using the reconstructed lepton and/or jets corresponding to the correct parton–jet assignment, determined by matching a given quark (before final-state radiation) to the closest jet with $\Delta R < 0.3$. The corresponding pdfs are constructed as unit-normalised one-dimensional histograms. To compute $M_{\ell\nu b_\ell}$, the neutrino four-momentum is needed, which is reconstructed as follows. Initially, the x and y components of the neutrino momentum, $p_{x,\nu}$ and $p_{y,\nu}$, are identified with those of the reconstructed $E_{\mathrm{T}}^{\mathrm{miss}}$ vector. The z component of the neutrino momentum, $p_{z,\nu}$, is inferred by solving $M_W^2 = (p_\ell + p_\nu)^2$, with $M_W = 80.4$ GeV being the W boson mass. If two real solutions ("2sol") exist, they are sorted according to their absolute value of $|p_{z,\nu}|$ i.e., $|p_{z,\nu 1}| < |p_{z,\nu 2}|$. It is found that in 62% of the cases $p_{z,\nu 1}$ is closer than $p_{z,\nu 2}$ to the generator-level neutrino $p_{z,\nu}$. In this case, two different pdfs are constructed, one for each solution, and $P^{\mathrm{sig}}_{\mathrm{2sol}}(M_{\ell\nu b_\ell})$ is defined as the average of the two pdfs weighted by their fractions (0.62 for $p_{z,\nu 1}$ and 0.38 for $p_{z,\nu 2}$). If no real solution ("nosol") exists, which happens in about 30% of the cases, the $p_{x,\nu}$ and $p_{y,\nu}$ components are scaled by a common factor until the discriminant of the quadratic equation is exactly zero, yielding only one solution for $p_{z,\nu}$. This solution for $p_{z,\nu}$ is used to compute $M_{\ell\nu b_\ell}$, from which the corresponding $P^{\mathrm{sig}}_{\mathrm{nosol}}(M_{\ell\nu b_\ell})$ is constructed. In the calculation of $P^{\mathrm{sig}}_{\mathrm{kin}}(\mathbf{x})$ from equation (3), $P^{\mathrm{sig}}(M_{\ell\nu b_\ell})$ is identified with $P^{\mathrm{sig}}_{\mathrm{2sol}}(M_{\ell\nu b_\ell})$ or with $P^{\mathrm{sig}}_{\mathrm{nosol}}(M_{\ell\nu b_\ell})$, depending on how many neutrino solutions can be found for the event.

In practice, the partonic origin of the jets is not known, so it is necessary to evaluate $P^{\mathrm{sig}}(\mathbf{x})$ by averaging over the N_p possible parton–jet assignments, which dilutes the kinematic information. At this point b-tagging information can be used to suppress the impact from parton–jet assignments that are inconsistent with the correct parton flavours as follows:

$$P^{\mathrm{sig}}(\mathbf{x}) = \frac{\sum_{k=1}^{N_p} P^{\mathrm{sig}}_{\mathrm{btag}}(\mathbf{x}^k) P^{\mathrm{sig}}_{\mathrm{kin}}(\mathbf{x}^k)}{\sum_{k=1}^{N_p} P^{\mathrm{sig}}_{\mathrm{btag}}(\mathbf{x}^k)}, \tag{4}$$

where $P^{\mathrm{sig}}_{\mathrm{kin}}(\mathbf{x})$ is given by equation (3) and $P^{\mathrm{sig}}_{\mathrm{btag}}(\mathbf{x})$ is defined as:

$$P^{\mathrm{sig}}_{\mathrm{btag}}(\mathbf{x}) = P_b(\mathrm{jet}_1) P_b(\mathrm{jet}_2) P_b(\mathrm{jet}_3) P_{q_h}(\mathrm{jet}_4), \tag{5}$$

with jet_i ($i = 1, \ldots, 4$) representing the parton–jet assignment being evaluated, and $P_f(\mathrm{jet}_i)$ denoting the probability that jet i, characterised by its four-momentum p_{jet_i} and b-tagging weight value w_{jet_i}, originates from a parton with flavour f (b, c, or l; l for light parton). The calibration of the b-tagging algorithm is performed for fixed thresholds on the multivariate b-tagging discriminant variable, corresponding to different average b-tagging efficiencies in $t\bar{t}$ events of 60%, 70%, and 80%, also referred to as "operating points" (OP). The corresponding thresholds are denoted by $w^{\mathrm{OP}}_{\mathrm{cut}}$, with OP = 60%, 70%, or 80%. Parameterisations of the b-tagging efficiencies for different jet flavours as functions of jet p_{T} and η are available for each of these operating points, $\epsilon^{\mathrm{OP}}_f(p_{\mathrm{T}}, \eta)$, which can be used to compute P_f as follows: if the jet b-tagging weight falls between the thresholds for operating points OP_1 and OP_2, $w^{\mathrm{OP}_1}_{\mathrm{cut}} < w_{\mathrm{jet}} \leq w^{\mathrm{OP}_2}_{\mathrm{cut}}$, then

$P_f = \epsilon_f^{\mathrm{OP}_1} - \epsilon_f^{\mathrm{OP}_2}$; alternatively, if the jet b-tagging weight is below (above) the threshold corresponding to the 80% (60%) operating point, then $P_f = 1 - \epsilon_f^{80\%}$ ($P_f = \epsilon_f^{60\%}$).

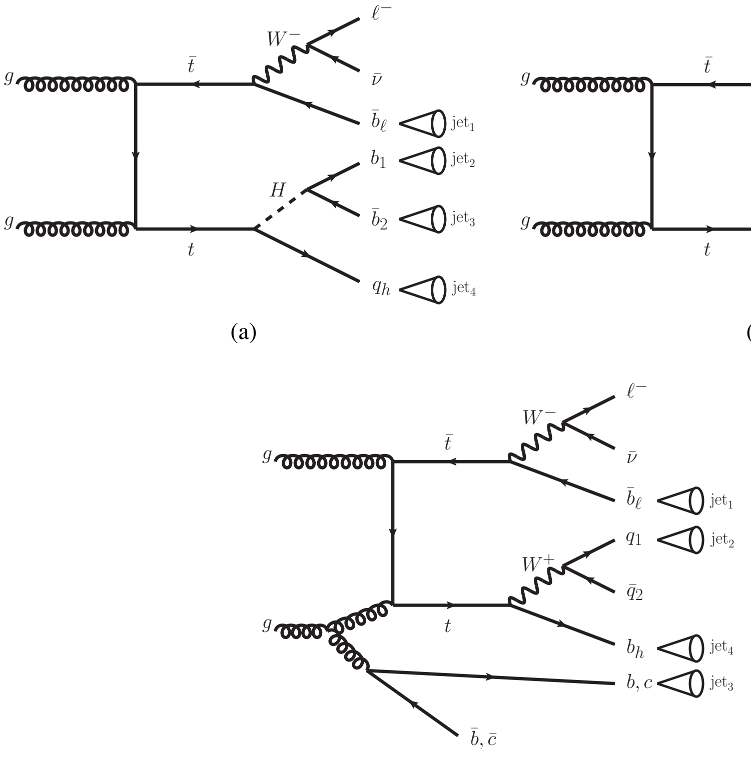

(a) (b) (c)

Figure 2: Representative Feynman diagrams illustrating the partonic configurations and parton–jet assignments considered in the construction of (a) the signal probability and (b) and (c) the background probability used in the definition of the final discriminant (see text for details).

6.2.2. Background probability

The calculation of P^{bkg} follows a similar approach to that discussed in section 6.2.1, although it is slightly more complicated to account for the varying fraction and different kinematic features of the $t\bar{t}$+light-jets, $t\bar{t} + c\bar{c}$ and $t\bar{t} + b\bar{b}$ backgrounds as a function of the analysis channel. This is particularly relevant in the (4 j, 3 b) and (4 j, 4 b) channels, which dominate the sensitivity of the search. While $t\bar{t}$+light-jets events often have both jets from the hadronic W boson decay among the four selected jets [see figure 2(b)], this is seldom the case for $t\bar{t} + b\bar{b}$ and $t\bar{t} + c\bar{c}$ events, especially in the (4 j, 4 b) channel. In this case the four b-tagged jets typically originate from the two b-quarks from the top quark decays, the charm quark from the W boson decay, and an extra heavy-flavour quark (b or c) produced in association with the $t\bar{t}$ system, while the jet associated with the down-type quark from the W boson decay is not reconstructed [see figure 2(c)].

To account for this, the following kinematic variables are considered: $M_{\ell\nu b_\ell}$, $X_{q_1 j b_h}$ and $M_{q_1 j}$, with $X_{q_1 j b_h} \equiv M_{q_1 j b_h} \ominus M_{q_1 j}$, were j denotes an extra quark-jet which can either originate from the W boson decay (q_2) or from an extra heavy-quark (b or c) produced in association with the $t\bar{t}$ system. For each of these possibilities, occurring in a fraction f_j of the cases, corresponding pdfs are constructed. As a generalisation of equation (4), the expression for $P^{\mathrm{bkg}}(\mathbf{x})$ becomes:

$$P^{\mathrm{bkg}}(\mathbf{x}) = \frac{\sum_{k=1}^{N_p} \sum_{j\in\{b,c,q_2\}} f_j P_{\mathrm{btag}}^{\mathrm{bkg},j}(\mathbf{x}^k) P_{\mathrm{kin}}^{\mathrm{bkg},j}(\mathbf{x}^k)}{\sum_{k=1}^{N_p} \sum_{j\in\{b,c,q_2\}} f_j P_{\mathrm{btag}}^{\mathrm{bkg},j}(\mathbf{x}^k)}, \tag{6}$$

with

$$P_{\mathrm{kin}}^{\mathrm{bkg},j}(\mathbf{x}) = P^{\mathrm{bkg}}(M_{\ell\nu b_\ell}) P^{\mathrm{bkg}}(X_{q_1 j b_h}) P^{\mathrm{bkg}}(M_{q_1 j}), \tag{7}$$

and

$$P_{\mathrm{btag}}^{\mathrm{bkg},j}(\mathbf{x}) = P_b(\mathrm{jet}_1) P_{q_1}(\mathrm{jet}_2) P_j(\mathrm{jet}_3) P_b(\mathrm{jet}_4). \tag{8}$$

where $P_f(\mathrm{jet}_i)$ are computed as discussed in section 6.2.1. In the above expression, $P_j = P_l$ for $j = q_2$, the down-type quark in the W boson decay, and $P_{q_1} = f_c P_c + (1 - f_c) P_l$, where f_c is the fraction of events where the up-type quark from the W boson decay assigned to the jet is a charm quark. This fraction is different in each analysis channel, primarily depending on the b-tag multiplicity requirements. It varies from ~ 50% for events in the (4 j, 2 b) channel to ~ 90% for events in the (4 j, 4 b) channel.

6.2.3. Final discriminant

The final discriminant D is computed for each event as given in equation (2), using the definitions for P^{sig} and P^{bkg} given in equations (4) and (6), respectively. Since this analysis has higher expected sensitivity to a $t\bar{t} \to WbHc$ signal than to a $t\bar{t} \to WbHu$ signal and, in order to allow probing of the BR($t \to Hu$) versus BR($t \to Hc$) plane, the discriminant optimised for $t\bar{t} \to WbHc$ is used for both the Hc and Hu decay modes. It was verified that using the $t\bar{t} \to WbHc$ discriminant for the $t\bar{t} \to WbHu$ search does not result in a significant sensitivity loss. Figure 3 compares the shape of the D distribution between the $t\bar{t} \to WbHc$ and $t\bar{t} \to WbHu$ signals and the $t\bar{t} \to WbWb$ background in each of the channels considered in this analysis.

7. Systematic uncertainties

Several sources of systematic uncertainty are considered that can affect the normalisation of signal and background and/or the shape of their corresponding final discriminant distributions. Each source of systematic uncertainty is considered to be uncorrelated with the other sources. Correlations of a given systematic uncertainty are maintained across processes and channels. Table 1 presents a list of all systematic uncertainties considered in the analysis and indicates whether they are taken to be normalisation-only, or to affect both shape and normalisation.

The leading sources of systematic uncertainty vary depending on the analysis channel considered, but they typically originate from $t\bar{t}$+jets modelling (including $t\bar{t}$+HF) and b-tagging. For example, the total systematic uncertainty in the background normalisation in the (4 j, 4 b) channel, which dominates the sensitivity in the case of the $t\bar{t} \to WbHc$ search, is approximately 20%, with the largest contributions originating from $t\bar{t}$+HF normalisation, b-tagging efficiency, c-tagging efficiency, light-jet tagging efficiency

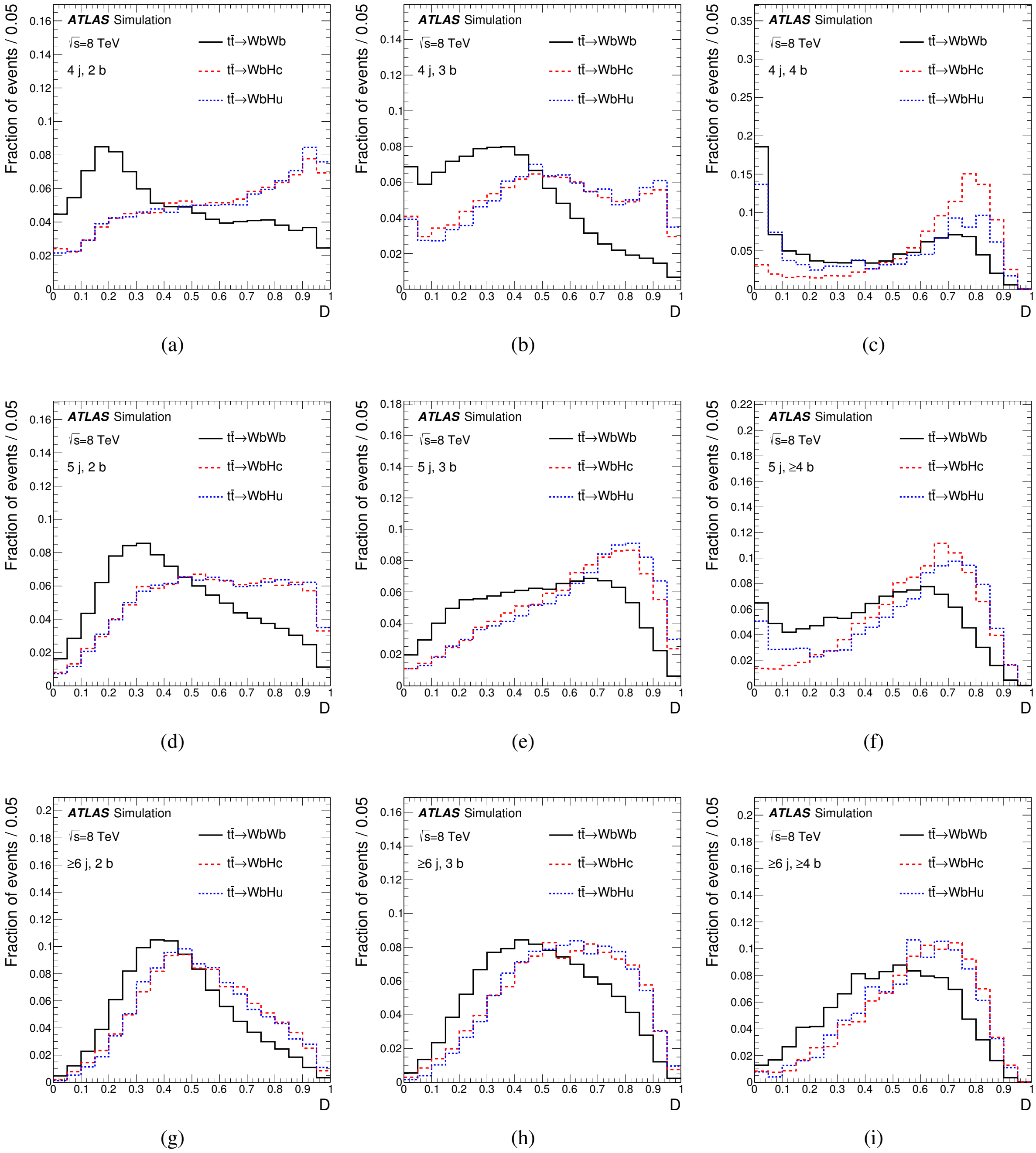

(a) (b) (c)

(d) (e) (f)

(g) (h) (i)

Figure 3: Comparison of the shape of the D discriminant distribution between the $t\bar{t} \rightarrow WbHc$ (red dashed) and $t\bar{t} \rightarrow WbHu$ (blue dotted) signals, and the $t\bar{t} \rightarrow WbWb$ background (black solid) in each of the channels considered in the analysis: (a) (4 j, 2 b), (b) (4 j, 3b), (c) (4 j, 4 b), (d) (5 j, 2 b), (e) (5 j, 3 b), (f) (5 j, ≥4 b), (g) (≥6 j, 2 b), (h) (≥6 j, 3 b), and (i) (≥6 j, ≥4 b).

Systematic uncertainty	Type	Components
Luminosity	N	1
Reconstructed Objects		
Electron	SN	5
Muon	SN	6
Jet reconstruction	SN	1
Jet vertex fraction	SN	1
Jet energy scale	SN	22
Jet energy resolution	SN	1
Missing transverse momentum	SN	2
b-tagging efficiency	SN	6
c-tagging efficiency	SN	4
Light-jet tagging efficiency	SN	12
High-p_{T} tagging	SN	1
Background Model		
$t\bar{t}$ cross section	N	1
$t\bar{t}$ modelling: p_{T} reweighting	SN	9
$t\bar{t}$ modelling: parton shower	SN	3
$t\bar{t}$+HF: normalisation	N	2
$t\bar{t}$+$c\bar{c}$: p_{T} reweighting	SN	2
$t\bar{t}$+$c\bar{c}$: generator	SN	4
$t\bar{t}$+$b\bar{b}$: NLO shape	SN	8
W+jets normalisation	N	3
W p_{T} reweighting	SN	1
Z+jets normalisation	N	3
Z p_{T} reweighting	SN	1
Single top normalisation	N	3
Single top model	SN	1
Diboson normalisation	N	3
$t\bar{t}V$ cross section	N	1
$t\bar{t}V$ model	SN	1
$t\bar{t}H$ cross section	N	1
$t\bar{t}H$ model	SN	2
Multijet normalisation	N	4
Signal Model		
$t\bar{t}$ cross section	N	1
Higgs boson branching ratios	N	3
$t\bar{t}$ modelling: p_{T} reweighting	SN	9
$t\bar{t}$ modelling: p_{T} reweighting non-closure	N	1
$t\bar{t}$ modelling: parton shower	N	1

Table 1: List of systematic uncertainties considered. An “N” means that the uncertainty is taken as affecting only the normalisation for all relevant processes and channels, whereas “SN” means that the uncertainty is taken on both shape and normalisation. Some of the systematic uncertainties are split into several components for a more accurate treatment.

and $t\bar{t}$ cross section. However, as shown in section 9, the fit to data in the nine analysis channels allows the overall background uncertainty to be reduced significantly, to approximately 4.4%. The reduced uncertainty results from the significant constraints provided by the data on some systematic uncertainties, as well as the anti-correlations among sources of systematic uncertainty resulting from the fit to the data. The total systematic uncertainty on the $t\bar{t} \to WbHc$ signal normalisation in the (4 j, 4 b) channel is approximately 17%, with similar contributions from uncertainties related to b-tagging and overall signal modelling. After the fit, this uncertainty is reduced to 7.8%. Table 2 presents a summary of the systematic uncertainties for the $t\bar{t} \to WbHc$ search and their impact on the normalisation of the signal and the main backgrounds in the (4 j, 4 b) channel.

The following sections describe each of the systematic uncertainties considered in the analyses.

	Pre-fit				Post-fit			
	$WbHc$	$t\bar{t}$+LJ	$t\bar{t} + c\bar{c}$	$t\bar{t} + b\bar{b}$	$WbHc$	$t\bar{t}$+LJ	$t\bar{t} + c\bar{c}$	$t\bar{t} + b\bar{b}$
Luminosity	±2.8	±2.8	±2.8	±2.8	±2.6	±2.6	±2.6	±2.6
Lepton efficiencies	±1.5	±1.5	±1.5	±1.5	±1.5	±1.5	±1.5	±1.5
Jet energy scale	±3.3	±2.9	±2.3	±5.8	±1.4	±1.2	±1.8	±4.1
Jet efficiencies	±1.2	–	±1.9	±1.7	±0.9	–	±1.4	±1.2
Jet energy resolution	–	±1.2	±2.8	±2.9	–	–	±1.0	±1.1
b-tagging eff.	±7.9	±5.5	±5.2	±10	±5.7	±3.9	±3.7	±6.6
c-tagging eff.	±7.0	±6.6	±13	±3.5	±6.3	±6.0	±11	±3.2
Light-jet tagging eff.	±0.8	±18	±3.2	±1.5	±0.6	±13	±2.3	±1.1
$t\bar{t}$: reweighting	±5.9	±2.7	±4.2	–	±3.8	±1.9	±2.3	–
$t\bar{t}$: parton shower	±5.4	±4.8	±10	±4.9	±1.7	±1.5	±6.5	±3.1
$t\bar{t}$+HF: normalisation	–	–	±50	±50	–	–	±32	±16
$t\bar{t}$+HF: modelling	–	–	–	±7.7	–	–	–	±7.4
Signal modelling	±6.9	–	–	–	±6.9	–	–	–
Theor. cross sections	±6.2	±6.2	±6.2	±6.2	±3.9	±3.9	±3.9	±3.9
Total	±17	±22	±54	±53	±7.8	±14	±28	±15

Table 2: $t\bar{t} \to WbHc, H \to b\bar{b}$ search: summary of the systematic uncertainties considered in the (4 j, 4 b) channel and their impact (in %) on the normalisation of the signal and the main backgrounds, before and after the fit to data. The $t\bar{t} \to WbHc$ signal and the $t\bar{t}$+light-jets background are denoted by "$WbHc$" and "$t\bar{t}$+LJ" respectively. Only sources of systematic uncertainty resulting in a normalisation change of at least 0.5% are displayed. The total post-fit uncertainty can differ from the sum in quadrature of individual sources due to the anti-correlations between them resulting from the fit to the data.

7.1. Luminosity

The uncertainty on the integrated luminosity is 2.8%, affecting the overall normalisation of all processes estimated from the simulation. It is estimated from a calibration of the luminosity scale derived from beam-separation scans performed in November 2012, following the same methodology as that detailed in ref. [38].

7.2. Reconstructed objects

Uncertainties associated with leptons arise from the reconstruction, identification and trigger. These efficiencies are measured using tag-and-probe techniques on $Z \to \ell^+\ell^-$ ($\ell = e, \mu$) data and simulated samples. The small differences found are corrected for in the simulation. Negligible sources of uncertainty originate from the corrections applied to adjust the lepton momentum scale and resolution in the simulation to match those in data. The combined effect of all these uncertainties results in an overall normalisation uncertainty on the signal and background of approximately 1.5%.

Uncertainties associated with jets arise from the efficiency of jet reconstruction and identification based on the JVF variable, as well as the jet energy scale and resolution. The largest contribution results from the jet energy scale, whose uncertainty dependence on jet p_{T} and η is split into 22 uncorrelated sources that are treated independently in the analysis. It affects the normalisation of signal and backgrounds by approximately 3–4% in the most sensitive search channels, (4 j, 3 b) and (4 j, 4 b), and up to 12% in the channels with ≥6 jets.

Uncertainties associated with energy scales and resolutions of leptons and jets are propagated to $E_{\mathrm{T}}^{\mathrm{miss}}$. Additional uncertainties originating from the modelling of the underlying event, in particular its impact on the p_{T} scale and resolution of unclustered energy, are negligibly small.

The leading uncertainties associated with reconstructed objects in this analysis originate from the modelling of the b-, c-, and light-jet-tagging efficiencies in the simulation, which is corrected to match the efficiencies measured in data control samples [36, 95] through dedicated scale factors. Uncertainties on these factors include a total of six independent sources affecting b-jets and four independent sources affecting c-jets. Each of these uncertainties has a different jet-p_{T} dependence. Twelve sources of uncertainty affecting light jets are considered, which depend on jet p_{T} and η. The above sources of systematic uncertainty are taken as uncorrelated between b-jets, c-jets, and light-jets. They have their largest impact in the (4 j, 4 b) channel, resulting in 10%, 13%, and 18% normalisation uncertainties on the $t\bar{t} + b\bar{b}$, $t\bar{t} + c\bar{c}$, and $t\bar{t}$+light-jets background associated with the uncertainties on the b-, c-, and light-jet-tagging scale factors, respectively. An additional uncertainty is included due to the extrapolation of these scale factors to jets with p_{T} beyond the kinematic reach of the data calibration samples used ($p_{\mathrm{T}} > 300$ GeV for b- and c-jets, and $p_{\mathrm{T}} > 750$ GeV for light-jets), taken to be correlated among the three jet flavours. This uncertainty has a very small impact in this analysis (e.g. $< 0.2\%$ on the signal and background normalisations in the (4 j, 4 b) channel).

7.3. Background modelling

A number of sources of systematic uncertainty affecting the modelling of $t\bar{t}$+jets are considered. A brief summary is provided below, with further details available in ref. [21], as the uncertainty treatment is identical. An uncertainty of +6.1%/−6.4% is assumed for the inclusive $t\bar{t}$ production cross section [49], including contributions from varying the factorisation and renormalisation scales, and uncertainties arising from the PDF, α_{S}, and the top quark mass. Uncertainties associated with the reweighting procedure applied to $t\bar{t}$+light-jets and $t\bar{t}+c\bar{c}$ processes include the nine leading sources of uncertainty in the differential cross-section measurement at $\sqrt{s} = 7$ TeV [61]. Additional uncertainties assigned to the modelling of the $t\bar{t}+c\bar{c}$ background include a 50% normalisation uncertainty, the full differences between applying and not applying the reweightings of the top quark and $t\bar{t}$ p_{T} spectra, as well as smaller uncertainties associated with the choice of LO generator. Uncertainties affecting the modelling of $t\bar{t}+b\bar{b}$ production include a normalisation uncertainty of 50% (taken to be uncorrelated with the same uncertainty assigned to the $t\bar{t}+c\bar{c}$ background) and shape uncertainties (including inter-category migration effects) associated with the NLO prediction from Sherpa+OpenLoops, which is used for reweighting of the default Powheg-Box $t\bar{t}+b\bar{b}$ prediction. These include three different scale variations, a different shower-recoil model scheme, and two alternative PDF sets (MSTW and NNPDF). Additional uncertainties are assessed for the contributions to the $t\bar{t}+b\bar{b}$ background originating from multiple parton interactions or final-state radiation from top decay products, which are not part of the NLO prediction. Finally, an uncertainty due to the choice of parton shower and hadronisation model is derived by comparing events produced by Powheg-Box interfaced to Pythia or Herwig. This uncertainty is taken to be uncorrelated between the $t\bar{t}$+light-jets, $t\bar{t}+c\bar{c}$ and $t\bar{t}+b\bar{b}$ processes.

Uncertainties affecting the modelling of the W+jets background include a 7% normalisation uncertainty for events with ≥4 jets coming from the data-driven normalisation procedure. The corresponding normalisation uncertainty for Z+jets is 5% for events with ≥2 jets. In addition, a 24% normalisation uncertainty is added in quadrature for each additional inclusive jet-multiplicity bin beyond the one where the background is normalised, based on a comparison among different algorithms for merging LO matrix elements and parton shower simulations [96]. For example, W+jets events with exactly 4 jets, exactly 5 jets and ≥ 6 jets are assigned normalisation uncertainties of 7%, $7\% \oplus 24\% = 25\%$ and $7\% \oplus 24\% \oplus 24\% = 35\%$. Finally, the full size of the W and Z boson p_{T} correction, after symmetrisation, is taken as a systematic uncertainty. The above uncertainties are taken as uncorrelated between W+jets and Z+jets.

Uncertainties affecting the modelling of the single-top-quark background include a +5%/−4% uncertainty on the total cross section, which is estimated as a weighted average of the theoretical uncertainties on t-, Wt- and s-channel production [68–70]. Similarly to the case of W/Z+jets, an additional 24% normalisation uncertainty is added in quadrature for each additional inclusive jet-multiplicity bin above ≥3 jets. An additional systematic uncertainty on Wt-channel production concerning the separation between $t\bar{t}$ and Wt at NLO [97] is assessed by comparing the nominal sample, which uses the so-called "diagram subtraction" scheme, with an alternative sample using the "diagram removal" scheme.

Uncertainties on the diboson background normalisation include 5% from the NLO theoretical cross sections [75] and additional 24% normalisation uncertainties added in quadrature for each additional inclusive jet-multiplicity bin above ≥2 jets. Uncertainties on the $t\bar{t}V$ and $t\bar{t}H$ normalisations are 15% and +9%/−12% respectively, from the uncertainties on their respective NLO theoretical cross sections [81, 89, 98]. Additional small uncertainties arising from scale variations, which change the amount of initial-state radiation and thus the event kinematics, are also considered.

Uncertainties on the data-driven multijet background estimate receive contributions from the limited sample size in data, particularly at high jet and b-tag multiplicities, as well as from the uncertainty on the rate of fake leptons, estimated in different control regions (e.g. selected with a requirement on either the maximum $E_{\mathrm{T}}^{\mathrm{miss}}$ or m_{T}^{W}). A combined normalisation uncertainty of 50% due to all these effects is assigned, which is taken as correlated across jet and b-tag multiplicity bins, but uncorrelated between electron and muon channels. No explicit shape uncertainty is assigned since the large statistical uncertainties associated with the multijet background prediction, which are uncorrelated between bins in the final discriminant distribution, effectively cover all possible shape uncertainties.

7.4. Signal modelling

Several normalisation and shape uncertainties are taken into account for the $t\bar{t} \to WbHq$ signal. The uncertainty on the $t\bar{t}$ cross section (see above) also applies to the $t\bar{t} \to WbHq$ signal and is taken to be the same as, and fully correlated with, that assigned to the $t\bar{t} \to WbWb$ background. Uncertainties on the $H \to b\bar{b}$ branching ratio are taken into account following the recommendation in ref. [89]: ±1.1% ($\Delta\alpha_\mathrm{S}$), ±1.4% (Δm_b) and ±0.8% (theory). Additional modelling uncertainties originate from non-closure of the reweighting procedure applied to correct the distributions of top quark p_T and $t\bar{t}$ system p_T from Protos to match those from the uncorrected Powheg-Box+Pythia simulation, and the uncertainties associated with the further reweighting in the same variables to match the differential cross-section measurements at $\sqrt{s} = 7$ TeV, taken to be fully correlated with those assigned to the $t\bar{t}$+light-jets background. Finally, an uncertainty from the choice of parton shower and hadronisation model is estimated by comparing the $t\bar{t} \to WbWb$ yields between Powheg-Box+Pythia and Powheg-Box+Herwig in the channels with two b-tags, which are enriched in $t\bar{t}$+light-jets, and thus taken to be representative of what would be the signal acceptance uncertainty due to differences in extra jet radiation and b-quark fragmentation between the two parton shower/hadronisation models.

8. Statistical analysis

The distributions of the final discriminants in each of the analysis channels considered are combined to test for the presence of a signal. The statistical analysis is based on a binned likelihood function $L(\mu, \theta)$ constructed as a product of Poisson probability terms over all bins considered in the search. In the case of several searches being combined, the product of Poisson probability terms is extended over all bins considered in all searches. The function $L(\mu, \theta)$ depends on the signal-strength parameter μ, defined as a multiplicative factor to the yield for $t\bar{t} \to WbHq$ signal events normalised to a reference branching ratio $\mathrm{BR}_\mathrm{ref}(t \to Hq) = 1\%$, and θ, a set of nuisance parameters that encode the effect of systematic uncertainties on the signal and background expectations and are implemented in the likelihood function as Gaussian or log-normal priors with their width parameters corresponding to the size of the respective uncertainties. The relationship between μ and the corresponding $\mathrm{BR}(t \to Hq)$ is:

$$\mu = \frac{\mathrm{BR}(t \to Hq)[1 - \mathrm{BR}(t \to Hq)]}{\mathrm{BR}_\mathrm{ref}(t \to Hq)[1 - \mathrm{BR}_\mathrm{ref}(t \to Hq)]}. \tag{9}$$

For a given μ value, the SM $t\bar{t} \to WbWb$ background contribution is scaled accordingly in order to preserve the inclusive $t\bar{t}$ cross section. The corresponding multiplicative factor would be $[1 - \mathrm{BR}(t \to Hq)]^2$, with $\mathrm{BR}(t \to Hq)$ being a function of μ as can be derived from equation (9):

$$\mathrm{BR}(t \to Hq) = \frac{1 - \sqrt{1 - 4\mathrm{BR}_\mathrm{ref}(t \to Hq)(1 - \mathrm{BR}_\mathrm{ref}(t \to Hq))\mu}}{2}. \tag{10}$$

Therefore, the total number of signal and background events in a given bin depends on μ and θ. The best-fit $\mathrm{BR}(t \to Hq)$ is obtained by performing a binned likelihood fit to the data under the signal-plus-background hypothesis, i.e. maximising the likelihood function $L(\mu, \theta)$ over μ and θ. The nuisance parameters θ allow variations of the expectations for signal and background according to the corresponding systematic uncertainties, and their fitted values correspond to the deviations from the nominal expectations that globally provide the best fit to the data. This procedure allows a reduction of the impact of systematic uncertainties on the search sensitivity by taking advantage of the highly populated background-dominated channels included in the likelihood fit.

The test statistic q_μ is defined as the profile likelihood ratio: $q_\mu = -2\ln(L(\mu, \hat{\hat{\theta}}_\mu)/L(\hat{\mu}, \hat{\theta}))$, where $\hat{\mu}$ and $\hat{\theta}$ are the values of the parameters that maximise the likelihood function (with the constraint $0 \leq \hat{\mu} \leq \mu$), and $\hat{\hat{\theta}}_\mu$ are the values of the nuisance parameters that maximise the likelihood function for a given value of μ. Statistical uncertainties in each bin of the discriminant distributions are also taken into account via dedicated nuisance parameters in the fit. The test statistic q_μ is implemented in the RooFit package [99, 100] and is used to measure the compatibility of the observed data with the background-only hypothesis by setting $\mu = 0$ in the profile likelihood ratio: $q_0 = -2\ln(L(0, \hat{\hat{\theta}}_0)/L(\hat{\mu}, \hat{\theta}))$. The p-value (referred to as p_0) representing the compatibility of the data with the background-only hypothesis is estimated by integrating the distribution of q_0 from background-only pseudo-experiments, approximated using the asymptotic formulae given in ref. [101], above the observed value of q_0. The observed p_0-value is checked for each explored signal scenario. In the absence of any significant excess above the background expectation, upper limits on μ, and thus on BR$(t \to Hq)$ via equation (10), are derived by using q_μ in the CL$_\mathrm{s}$ method [102, 103]. Values of BR$(t \to Hq)$ yielding CL$_\mathrm{s}$<0.05, where CL$_\mathrm{s}$ is computed using the asymptotic approximation [101], are excluded at ≥95% CL.

9. Results

This section presents the results obtained from the individual searches for $t\bar{t} \to WbHq$, as well as their combination.

9.1. $H \to b\bar{b}$

Following the statistical analysis discussed in section 8, a binned likelihood fit under the signal-plus-background hypothesis is performed on the distributions of the final discriminant in the nine analysis channels considered. Figures 4–6 show a comparison of the data and prediction in the final discriminant in each of the analysis channels, both pre- and post-fit to data, in the case of the $t\bar{t} \to WbHc$ search. The post-fit yields can be found in appendix A. The best-fit branching ratio obtained is BR$(t \to Hc)$ = [0.17 ± 0.12 (stat.) ± 0.17 (syst.)]%, assuming that BR$(t \to Hu) = 0$. A similar fit is performed for the $t\bar{t} \to WbHu$ search, yielding BR$(t \to Hu)$ = [−0.07 ± 0.17 (stat.) ± 0.28 (syst.)]%, assuming that BR$(t \to Hc) = 0$. The different measured values for the two branching ratios is the result of the different sensitivities of the $t\bar{t} \to WbHc$ and $t\bar{t} \to WbHu$ searches, as discussed in section 6.1.

The large number of events in the analysis channels considered, together with their different background compositions, allows the fit to place constraints on the combined effect of several sources of systematic uncertainty. As a result, an improved background prediction is obtained with significantly reduced uncertainty, not only in the signal-depleted channels, but also in the most sensitive analysis channels for this search, (4 j, 3 b) and (4 j, 4 b). The channels with two b-tags are used to constrain the leading uncertainties affecting the $t\bar{t}$+light-jets background prediction, while the channels with ≥5 jets and ≥3 b-tags are sensitive to the uncertainties affecting the $t\bar{t}$+HF background prediction. In particular, one of the main corrections applied by the fit is an increase of the $t\bar{t} + b\bar{b}$ normalisation by approximately 20% relative to the nominal prediction by adjusting the corresponding nuisance parameter. This results in an improved agreement between data and prediction in the (5 j, ≥4 b) and (≥6 j, ≥4 b) channels, where the $t\bar{t} + b\bar{b}$ process provides a significant, or, in the latter case, dominant background contribution.[6] In addition, the corresponding uncertainty is reduced from the initial 50% down to about 16%. This correction is in agreement with that found in ref. [21]. However, in contrast with ref. [21], the $t\bar{t} + b\bar{b}$ normalisation is not one of the leading uncertainties affecting this search, since the $t\bar{t} + b\bar{b}$ background is subdominant in the (4 j, 3 b) channel, and it has a very different final discriminant shape from that of the signal in the (4 j, 4 b) channel.

As an illustration, figure 7 provides a summary of the leading 15 systematic uncertainties affecting the $t\bar{t} \to WbHc$ search, quantifying their impact on the signal strength μ, both before and after the fit, and displaying the constraints provided by the data on the associated nuisance parameters. The pre-fit impact on μ is estimated by fixing the corresponding nuisance parameter at $\theta_0 \pm \Delta\theta$, where θ_0 is the nominal value of the nuisance parameter and $\Delta\theta$ is its pre-fit uncertainty, and performing the fit again. The difference between the default and modified μ, $\Delta\mu$, represents the effect of the systematic uncertainty in question on μ. The same procedure is followed to estimate the post-fit impact on μ, but the corresponding nuisance parameter is instead fixed at $\hat{\theta} \pm \sigma_\theta$, where $\hat{\theta}$ is the fitted value of the nuisance parameter and σ_θ is its post-fit uncertainty. For reference, $\Delta\mu = 0.05$ corresponds to $\Delta\text{BR}(t \to Hc) \simeq 0.05\%$.

Prior to the fit, the systematic uncertainties with the largest impact on μ are the leading uncertainty for light-jet tagging and the uncertainty on the $t\bar{t}$ background associated with the choice of parton shower and hadronisation models. The significant impact from light-jet tagging results from the large fraction of $t\bar{t}$+light-jets background present in the (4 j, 4 b) channel, which peaks at high values of the final discriminant, like the signal, and thus cannot be strongly constrained by the fit. Because of this, this uncertainty remains the leading one after the fit. In contrast, the uncertainty related to $t\bar{t}$ modelling is significantly constrained by the fit since it has a large impact (∼5–16%) on the $t\bar{t}$+light-jets background normalisation in the highly populated channels with two b-tags. As a result, this uncertainty is ranked only fourth in importance after the fit, becoming comparable to uncertainties such as the choice of renormalisation scale for $t\bar{t} + b\bar{b}$, the leading uncertainty for c-jet tagging and the $t\bar{t} + c\bar{c}$ normalisation. Of these, the nuisance parameter associated with the choice of the renormalisation scale for $t\bar{t} + b\bar{b}$ is slightly pulled (by half of the prior uncertainty) to improve agreement with the data in the (4 j, 4 b) and (5 j, 4 b) channels. In these channels, this uncertainty causes variations of up to ∼5% in the bin contents in some regions of the final discriminant, i.e. distorting its shape compared to that of the nominal prediction, but the sensitivity is not sufficient to constrain it significantly. The leading uncertainty from c-tagging causes small (few percent) distortions in the shape of the background, and also cannot be constrained by the fit. In contrast, the fit is sensitive to the $t\bar{t} + c\bar{c}$ normalisation and the second-leading uncertainty for c-tagging,[7] through the comparison of data and predictions across channels with different b-tag multiplicity, yielding results in agreement with the nominal predictions but with half the initial uncertainties.

Other nuisance parameters have a smaller impact on the signal extraction and typically have small pulls or constraints. One exception is the nuisance parameter associated with the $t\bar{t}$ cross section, which affects the signal extraction indirectly through the existing small fraction of non-$t\bar{t}$ background, and after the fit is found to be consistent with the nominal prediction but is constrained owing to the large number of $t\bar{t}$ events. On the other hand, a slight pull is obtained for the nuisance parameter associated with one of the uncertainties for the top quark p_{T} and $t\bar{t}$ system p_{T} reweightings, which is used by the fit to improve agreement between data and prediction in the channels with two b-tags but which has very small effect on the background prediction in the signal region.

---

[6] The overall change in $t\bar{t} + b\bar{b}$ normalisation can be different across channels due to the different impact of other nuisance parameters affecting $t\bar{t} + b\bar{b}$ modelling, such as that related to parton shower and hadronisation, which is changed by the fit by half of the prior uncertainty.

[7] The main effect of this uncertainty is a change in normalisation for the background with almost no effect on its shape in the final discriminant.

In the absence of a significant excess in data above the background expectation, 95% CL limits are set on BR($t \to Hc$) and BR($t \to Hu$). The observed (expected) 95% CL upper limits on the branching ratios are BR($t \to Hc$) $< 0.56\%\,(0.42\%)$ and BR($t \to Hu$) $< 0.61\%\,(0.64\%)$. These upper limits can be translated into corresponding observed (expected) limits on the couplings of $|\lambda_{tcH}| < 0.14\,(0.12)$ and $|\lambda_{tuH}| < 0.15\,(0.15)$.

9.2. $H \to \gamma\gamma$

A search for $t\bar{t} \to WbHq, H \to \gamma\gamma$ published by the ATLAS Collaboration uses a data set corresponding to an integrated luminosity of 4.5 fb^{-1} at $\sqrt{s}$ = 7 TeV and 20.3 fb^{-1} at $\sqrt{s}$ = 8 TeV [17]. The event selection requires at least two reconstructed photon candidates and additional requirements to select $t \to Wb$ decays. Events are categorised into two channels, leptonic and hadronic, depending on the W boson decay modes. The leptonic channel selects events with exactly one lepton (e or μ), at least two jets, and at least one b-tagged jet. The hadronic channel selects events with no reconstructed lepton, at least four jets, and at least one b-tagged jet. In both channels, additional requirements are made to select events compatible with $t\bar{t} \to WbHq$ production by exploiting the invariant masses of the reconstructed top quark candidates. Finally, the diphoton mass ($m_{\gamma\gamma}$) distribution of the selected events is analysed using a sideband technique in order to estimate the background in the signal region, defined to be 122 GeV $\leq m_{\gamma\gamma} \leq$ 129 GeV.

Based on the above strategy, this search has essentially no discrimination power between $t\bar{t} \to WbHc$ and $t\bar{t} \to WbHu$ signals, because their selection acceptances are very close, although not identical. To facilitate combining it with the other searches discussed in this paper, minor modifications to the inputs were made with respect to the published result, all having a negligible impact on the result. They include updates to the $t\bar{t}$ cross-section uncertainty and the uncertainty model for Higgs branching ratios, as well as the separate treatment of $t\bar{t} \to WbHc$ and $t\bar{t} \to WbHu$ signals taking into account their slightly different acceptances. The best-fit branching ratios obtained are BR($t \to Hc$) = $[0.22 \pm 0.26\,(\text{stat.}) \pm 0.10\,(\text{syst.})]\%$ and BR($t \to Hu$) = $[0.23 \pm 0.27\,(\text{stat.}) \pm 0.10\,(\text{syst.})]\%$ under the assumptions that BR($t \to Hu$) = 0 and BR($t \to Hc$) = 0 respectively. The observed (expected) 95% CL upper limits on the branching ratios from ref. [17] remain the best estimates, BR($t \to Hq$) $< 0.79\%\,(0.51\%)$. The corresponding limits on the couplings are $|\lambda_{tqH}| < 0.17\,(0.14)$. These limits can be understood as applying to the sum of the $t \to Hc$ and $t \to Hu$ decay modes, or only to one of them, if the other decay mode is assumed to have a branching ratio equal to zero. In the former case, BR($t \to Hq$) $\equiv$ BR($t \to Hc$) + BR($t \to Hu$) and $|\lambda_{tqH}| \equiv \sqrt{|\lambda_{tcH}|^2 + |\lambda_{tuH}|^2}$.

9.3. $H \to W^+W^-, \tau^+\tau^-$

The $H \to WW^*$ and $H \to \tau\tau$ decay modes are predicted to have significant branching ratios, of 21.5% and 6.3% respectively. The resulting signatures for signal events, $t\bar{t} \to WbHq \to W^{\pm}W^{\pm}W^{\mp}bq$ and $t\bar{t} \to WbHq \to W^{\pm}\tau^{\pm}\tau^{\mp}bq$, can be effectively exploited to suppress backgrounds in the case of multilepton final states.

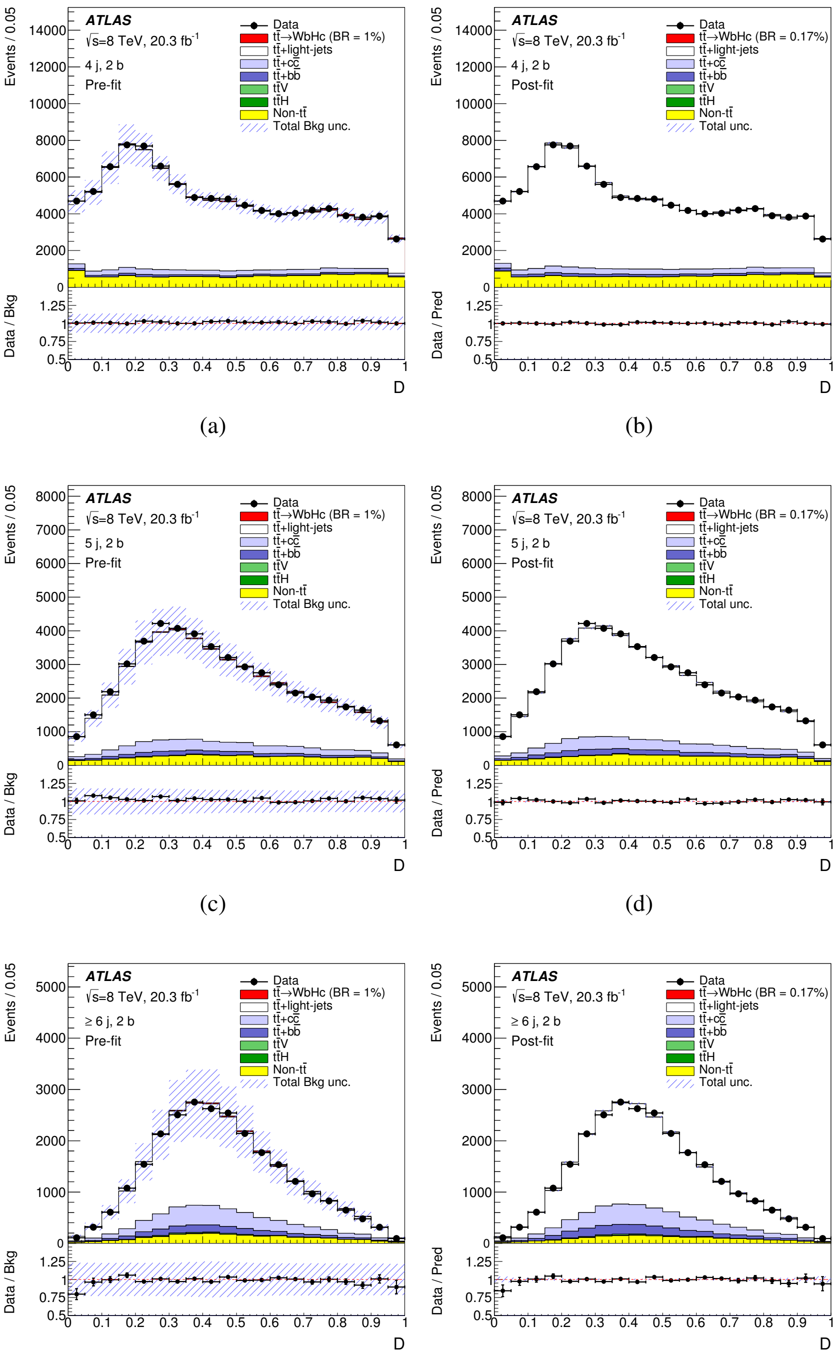

(a) (b)

(c) (d)

(e) (f)

Figure 4: $t\bar{t} \to WbHc, H \to b\bar{b}$ search: comparison between the data and prediction for the distribution of the D discriminant used in the (4 j, 2 b) channel (a) before the fit and (b) after the fit, in the (5 j, 2 b) channel (c) before the fit and (d) after the fit, and in the (≥6 j, 2 b) channel (e) before the fit and (f) after the fit. The fit is performed on data under the signal-plus-background hypothesis. In the pre-fit distributions the $t\bar{t} \to WbHc$ signal (solid red) is normalised to BR($t \to Hc$) = 1% and the $t\bar{t} \to WbWb$ background is normalised to the SM prediction, while in the post-fit distributions both signal and $t\bar{t} \to WbWb$ background are normalised using the best-fit BR($t \to Hc$). The small contributions from W/Z+jets, single top, diboson and multijet backgrounds are combined into a single background source referred to as "Non-$t\bar{t}$". The bottom panels display the ratios of data to either the SM background prediction before the fit ("Bkg") or the total signal-plus-background prediction after the fit ("Pred"). The hashed area represents the total uncertainty on the background.

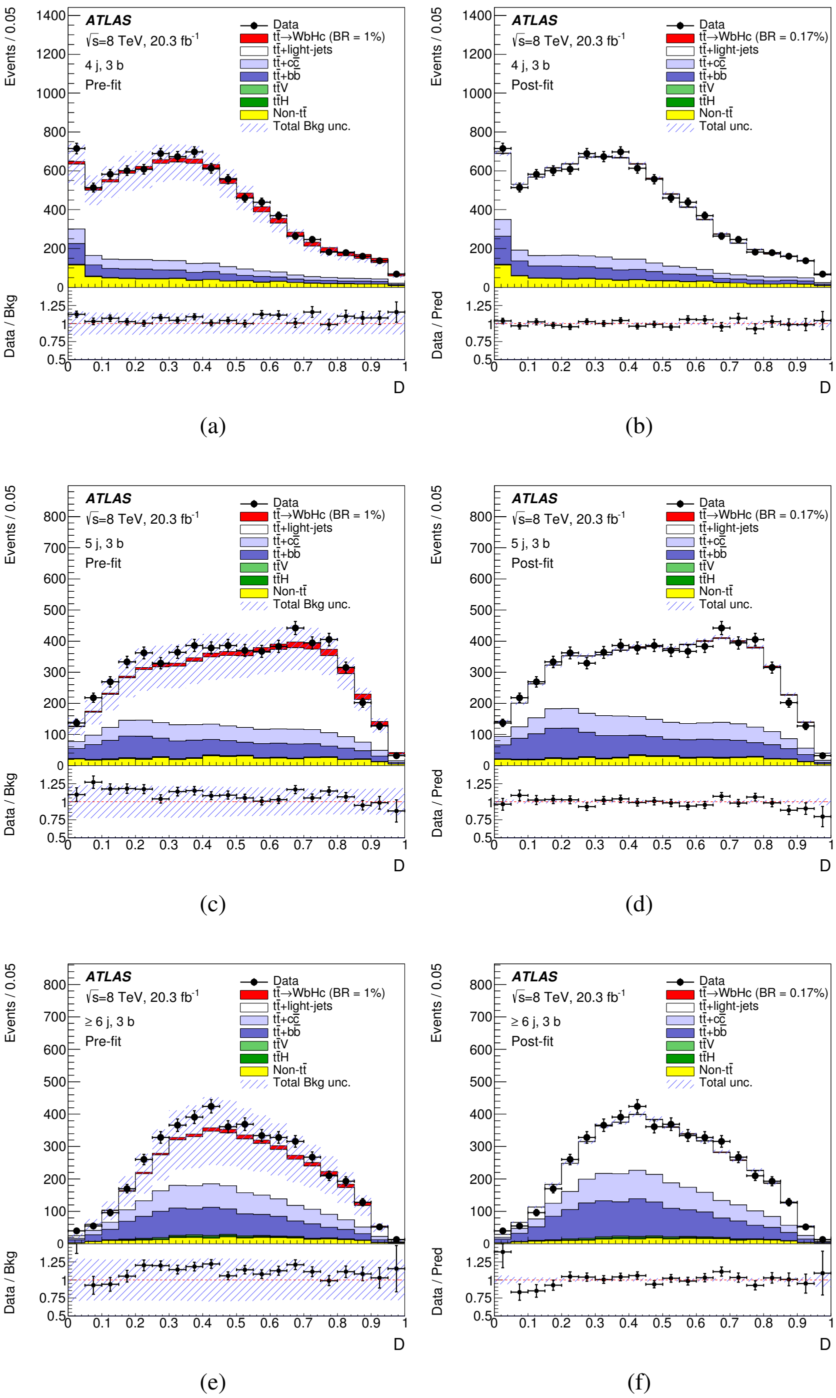

(a) (b) (c) (d) (e) (f)

Figure 5: $t\bar{t} \rightarrow WbHc, H \rightarrow b\bar{b}$ search: comparison between the data and prediction for the distribution of the D discriminant used in the (4 j, 3 b) channel (a) before the fit and (b) after the fit, in the (5 j, 3 b) channel (c) before the fit and (d) after the fit, and in the (≥6 j, 3 b) channel (e) before the fit and (f) after the fit. The fit is performed on data under the signal-plus-background hypothesis. In the pre-fit distributions the $t\bar{t} \rightarrow WbHc$ signal (solid red) is normalised to BR$(t \rightarrow Hc) = 1\%$ and the $t\bar{t} \rightarrow WbWb$ background is normalised to the SM prediction, while in the post-fit distributions both signal and $t\bar{t} \rightarrow WbWb$ background are normalised using the best-fit BR$(t \rightarrow Hc)$. The small contributions from W/Z+jets, single top, diboson and multijet backgrounds are combined into a single background source referred to as "Non-$t\bar{t}$". The bottom panels display the ratios of data to either the SM background prediction before the fit ("Bkg") or the total signal-plus-background prediction after the fit ("Pred"). The hashed area represents the total uncertainty on the background.

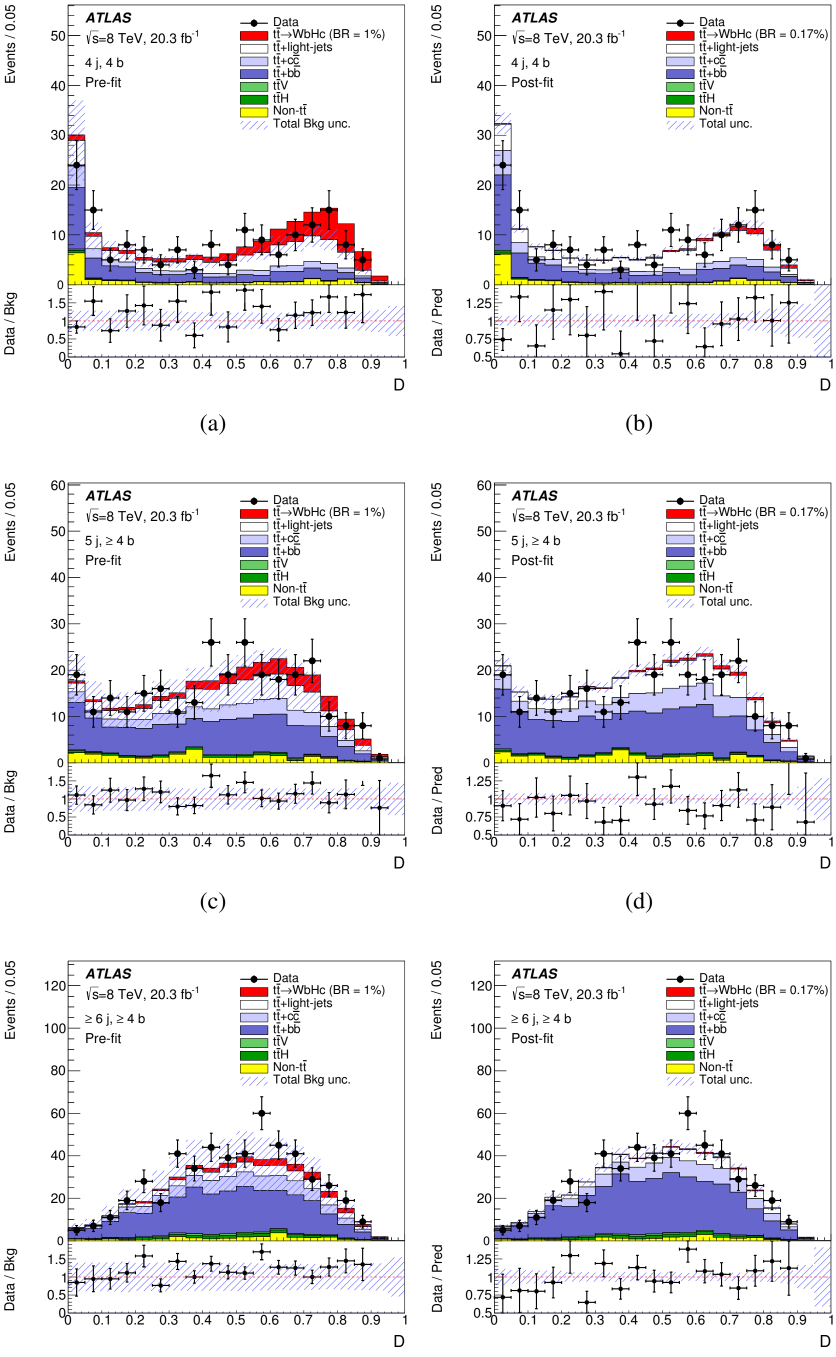

(a) (b) (c) (d) (e) (f)

Figure 6: $t\bar{t} \to WbHc, H \to b\bar{b}$ search: comparison between the data and prediction for the distribution of the D discriminant used in the (4 j, 4 b) channel (a) before the fit and (b) after the fit, in the (5 j, ≥4 b) channel (c) before the fit and (d) after the fit, and in the (≥6 j, ≥4 b) channel (e) before the fit and (f) after the fit. The fit is performed on data under the signal-plus-background hypothesis. In the pre-fit distributions the $t\bar{t} \to WbHc$ signal (solid red) is normalised to BR($t \to Hc$) = 1% and the $t\bar{t} \to WbWb$ background is normalised to the SM prediction, while in the post-fit distributions both signal and $t\bar{t} \to WbWb$ background are normalised using the best-fit BR($t \to Hc$). The small contributions from W/Z+jets, single top, diboson and multijet backgrounds are combined into a single background source referred to as "Non-$t\bar{t}$". The bottom panels display the ratios of data to either the SM background prediction before the fit ("Bkg") or the total signal-plus-background prediction after the fit ("Pred"). The hashed area represents the total uncertainty on the background.

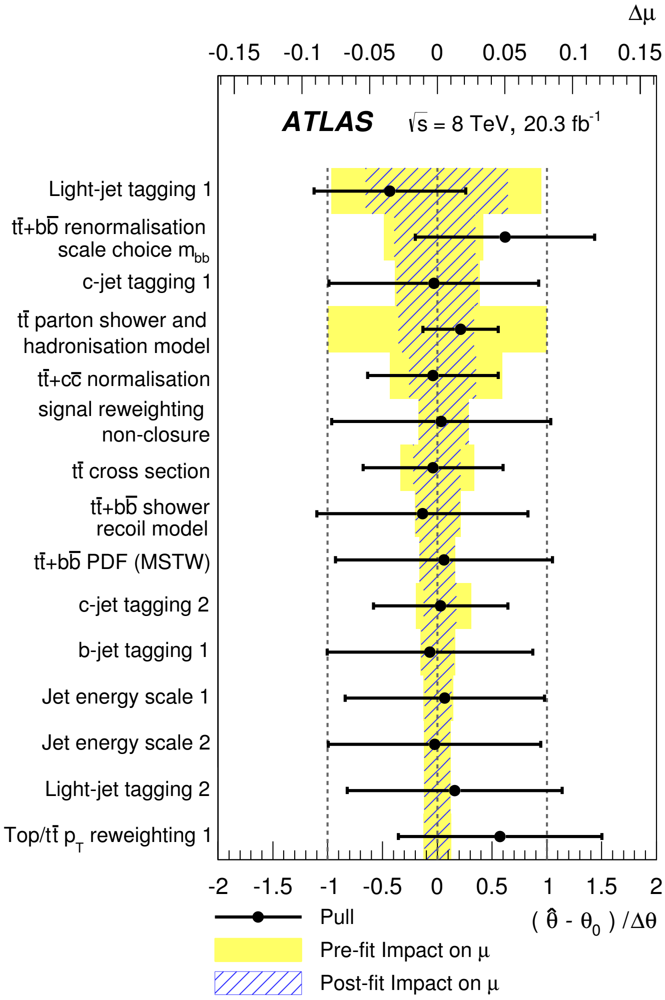

Figure 7: $t\bar{t} \to WbHc, H \to b\bar{b}$ search: the fitted values of the nuisance parameters for the most important sources of systematic uncertainty and their impact on the measured signal strength. The points, which are drawn conforming to the scale of the bottom axis, show the deviation of each of the fitted nuisance parameters, $\hat{\theta}$, from θ_0, which is the nominal value of that nuisance parameter, in units of the pre-fit standard deviation $\Delta\theta$. The error bars show the post-fit uncertainties, σ_θ, which are close to 1 if the data do not provide any further constraint on that uncertainty. Conversely, a value of σ_θ much smaller than 1 indicates a significant reduction with respect to the original uncertainty. The nuisance parameters are sorted according to their post-fit effect on μ (hashed blue area), conforming to the scale of the top axis, with those with the largest impact at the top.

Recently, the ATLAS Collaboration has published a search for $t\bar{t}H$ production with $H \to WW^*$, $\tau\tau$ and ZZ^* [23] that exploits several multilepton signatures resulting from the leptonic decays of W and Z bosons and/or the presence of τ leptons. That search considered five separate event categories depending on the number of reconstructed electrons or muons and hadronic τ candidates, of which the following three are considered for a reinterpretation in the context of the $t\bar{t} \to WbHq$ search:

- $2\ell 0\tau_{\mathrm{had}}$: two same-charge light leptons (e or μ) with no hadronic τ candidates (τ_{had}) and ≥4 jets with ≥1 b-tagged jets. This channel is sensitive to the process $t\bar{t} \to WbHq \to \ell^{\pm}\ell^{\pm}qqqb2\nu$. To further improve the sensitivity, this category is further subdivided into six subcategories depending on the flavour of the leptons and the number of jets: (ee, $\mu\mu$, $e\mu$)×(4 jets, ≥5 jets).
- 3ℓ: three light leptons with either ≥3 jets of which ≥2 are b-tagged, or ≥4 jets of which ≥1 are b-tagged. This channel is sensitive to the process $t\bar{t} \to WbHq \to \ell^{\pm}\ell^{\pm}\ell^{\mp}qb3\nu$.
- $2\ell 1\tau_{\mathrm{had}}$: two same-charge light leptons (e or μ), one τ_{had} candidate, and ≥4 jets with ≥1 b-tagged jets. This channel is sensitive to the process $t\bar{t} \to WbHq \to \ell^{\pm}\ell^{\pm}\tau^{\mp}qb3\nu$.

The two other categories considered in the $t\bar{t}H$ search in multilepton final states but not in this reinterpretation are: 4ℓ (four light leptons with ≥2 jets and ≥1 b-tagged jets) and $1\ell 2\tau_{\mathrm{had}}$ (one light lepton and two opposite-charge τ_{had} candidates, with ≥3 jets and ≥1 b-tagged jets), which have very small signal acceptance and/or poor signal-to-background ratio due to the large number of jets misidentified as τ_{had} candidates. The minimum number of jets required in the $2\ell 0\tau_{\mathrm{had}}$ category is well matched to the number of partons expected from $t\bar{t} \to WbHq \to W^{\pm}W^{\pm}W^{\mp}bq$ signal events, while the 3ℓ and $2\ell 1\tau_{\mathrm{had}}$ categories effectively require one or two jets beyond leading order. Because of this, and the gain in branching ratio resulting from only requiring two, as opposed to three, W bosons decaying leptonically, the $2\ell 0\tau_{\mathrm{had}}$ category dominates the sensitivity.

The largest background in the most sensitive category, 2ℓ4j, is $t\bar{t}$ or single-top production with one of the leptons originating from a decay of a heavy-flavour hadron (“non-prompt lepton”), followed by $t\bar{t}W$ production. Smaller contributions arise from $t\bar{t}(Z/\gamma^*)$, $t\bar{t}H$, and diboson (primarily WZ) production, and dilepton events from $t\bar{t}$ and Z/γ^* with the wrong charge sign measured for one electron. In the remaining categories the non-prompt lepton background decreases in importance, relative to the prompt-lepton contributions. The prompt contributions are estimated using the simulation, as typically the relevant processes (e.g., $t\bar{t}V$, $V = W, Z$) have not been measured at an accuracy exceeding that of theoretical predictions. The non-prompt lepton background predictions are computed or validated using data control regions with similar lepton kinematic selections but with fewer jets (two or three). Further details are provided in ref. [23]. In the search for $t\bar{t}H$, these regions have almost no contamination from signal, but the same is not necessarily true for the $t\bar{t} \to WbHq$ process, which is characterised by a lower jet multiplicity than the $t\bar{t}H$ process. This could potentially lead to an overestimate of the non-prompt background in this reinterpretation, particularly in the $2\ell 0\tau_{\mathrm{had}}$ categories, where the effect is more pronounced. The 3ℓ category estimates the non-prompt lepton background in the signal region by extrapolating, in terms of lepton quality, from a data sideband region that is sufficiently depleted in signal, using normalisation factors obtained from the simulation.

The non-prompt lepton background estimate for the $2\ell 0\tau_{\mathrm{had}}$ categories is validated using simulation and control regions with two or three jets in which the lower p_{T} (subleading) lepton satisfies $10~\mathrm{GeV} < p_{\mathrm{T}} < 30~\mathrm{GeV}$. Because the number of non-prompt leptons increases significantly as the lepton p_{T} requirement is lowered, this region is dominated by the non-prompt contribution for any non-excluded value of BR$(t \to Hq)$. To extract the non-prompt background yields in these regions, binned likelihood fits to the subleading lepton p_{T} distribution are performed, accounting for non-prompt lepton backgrounds,

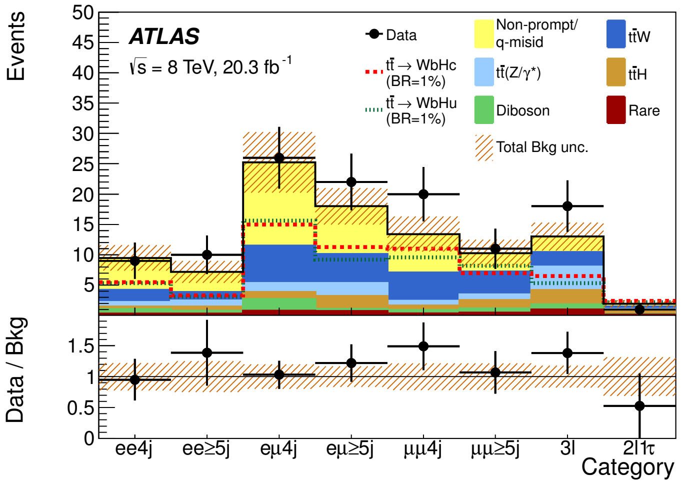

Figure 8: $t\bar{t} \to WbHq, H \to WW^*, \tau\tau$ search: comparison between the data and background prediction for the yields in each of the analysis channels considered before the fit to data. The expected $t\bar{t} \to WbHc$ and $t\bar{t} \to WbHu$ signals (dashed histograms) are shown separately normalised to BR$(t \to Hq)$ = 1%. The sum of instrumental backgrounds originating from non-prompt leptons and lepton charge misidentification is denoted by "Non-prompt/q-misid". The small contribution from rare processes such as tZ, $t\bar{t}WW$, triboson, $t\bar{t}t\bar{t}$ and tH production are combined into a single background source denoted by "Rare". The bottom panel displays the ratio of data to the SM background ("Bkg") prediction. The hashed area represents the total uncertainty on the background.

sources of prompt leptons (normalised to the SM expectation), and a potential $t\bar{t} \to WbHq$ contribution. The fitted $t\bar{t} \to WbHq$ contribution is in all cases found to be compatible with zero. The obtained best-fit non-prompt background yields in these low-p_{T} control regions are used to normalise the simulation and obtain estimates for the background in the $2\ell 0\tau_{\mathrm{had}}$ signal regions. These are found to be compatible with the nominal data-driven predictions within the stated uncertainties. The nominal predictions of the non-prompt backgrounds and their associated uncertainties are therefore used without modification in this reinterpretation.

Figure 8 shows the event yields in each of the categories, which are used as input to the statistical analysis discussed in section 8. A table summarising the expected and observed yields can be found in appendix B. The best-fit branching ratio obtained is BR$(t \to Hc)$ = [0.27 ± 0.18 (stat.) ± 0.21 (syst.)]% assuming that BR$(t \to Hu) = 0$. A similar fit is performed for the $t\bar{t} \to WbHu$ search, yielding BR$(t \to Hu)$ = [0.23 ± 0.18 (stat.) ± 0.21 (syst.)]%, assuming that BR$(t \to Hc) = 0$. The observed (expected) 95% CL upper limits on the branching ratios are BR$(t \to Hc) < 0.79\%$ (0.54%) and BR$(t \to Hu) < 0.78\%$ (0.57%). The corresponding observed (expected) limits on the couplings are $|\lambda_{tcH}| < 0.17$ (0.14) and $|\lambda_{tuH}| < 0.17$ (0.14) at 95% CL.

9.4. Combination of searches

The three searches discussed in the sections 9.1–9.3 are combined using the statistical analysis discussed in section 8. In this combination, the only systematic uncertainties taken to be fully correlated among the three searches are the $t\bar{t}$ cross section and the integrated luminosity for $\sqrt{s}$ = 8 TeV data. The dominant uncertainties on the Higgs boson branching ratios primarily affect the $t\bar{t} \to WbHq, H \to \gamma\gamma$

and $t\bar{t} \to WbHq$, $H \to b\bar{b}$ searches. Other uncertainties such as those associated with leptons, jet energy scale and b-tagging should be partially correlated between the $t\bar{t} \to WbHq$, $H \to \gamma\gamma$ search and the other two searches, but the differences in treatment between analyses (different lepton selection and p_{T} cuts, no uncertainty breakdown for jet energy scale and b-tagging in the $t\bar{t} \to WbHq$, $H \to \gamma\gamma$ search) make it difficult to account for correlations. However, given that the $t\bar{t} \to WbHq$, $H \to \gamma\gamma$ search is completely dominated by the data statistics, the effect of this simplification is negligible. The uncertainties taken as correlated between the $t\bar{t} \to WbHq$, $H \to b\bar{b}$ and $t\bar{t} \to WbHq$, $H \to WW^*, \tau\tau$ searches include those associated with lepton isolation, the leading b-tagging and jet energy scale uncertainties, and the reweighting of top quark p_{T} and $t\bar{t}$ system p_{T}. The rest of the uncertainties are taken to be uncorrelated among the searches. This correlation scheme closely follows the procedure adopted in the combination of $t\bar{t}H$ searches by ATLAS [104].

The first set of combined results is obtained for each branching ratio separately, setting the other branching ratio to zero. The best-fit combined branching ratios are $\mathrm{BR}(t \to Hc) = [0.22 \pm 0.10\,(\mathrm{stat.}) \pm 0.10\,(\mathrm{syst.})]\%$ and $\mathrm{BR}(t \to Hu) = [0.16 \pm 0.11\,(\mathrm{stat.}) \pm 0.12\,(\mathrm{syst.})]\%$. The difference between the central values of $\mathrm{BR}(t \to Hc)$ and $\mathrm{BR}(t \to Hu)$ originates from the ability of the $H \to b\bar{b}$ search to probe both decay modes separately. A comparison of the best-fit branching ratios for the individual searches and their combination can be found in figure 9 for $\mathrm{BR}(t \to Hc)$ and figure 10 for $\mathrm{BR}(t \to Hu)$. Figure 11 shows the $\mathrm{CL_s}$ versus branching ratio for the combination. The observed (expected) 95% CL combined upper limits on the branching ratios are $\mathrm{BR}(t \to Hc) < 0.46\%\,(0.25\%)$ and $\mathrm{BR}(t \to Hu) < 0.45\%\,(0.29\%)$. The corresponding observed (expected) upper limits on the couplings are $|\lambda_{tcH}| < 0.13\,(0.10)$ and $|\lambda_{tuH}| < 0.13\,(0.10)$. A summary of the upper limits on the branching ratios obtained by the individual searches, as well as their combination, can be found in figure 12.

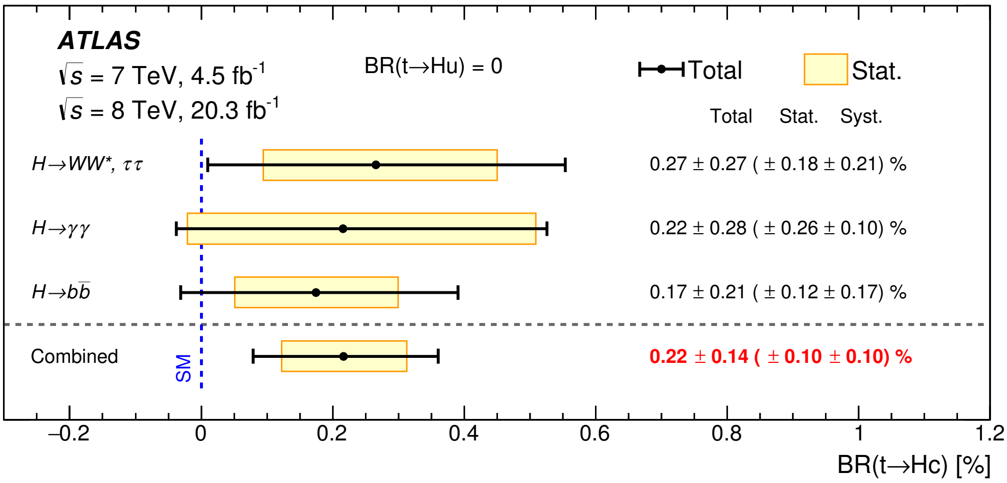

Figure 9: Summary of the best-fit $\mathrm{BR}(t \to Hc)$ for the individual searches as well as their combination, assuming that $\mathrm{BR}(t \to Hu) = 0$.

A similar set of results can be obtained by simultaneously probing both branching ratios. Although the $t\bar{t} \to WbHq$, $H \to \gamma\gamma$ and $t\bar{t} \to WbHq$, $H \to WW^*, \tau\tau$ searches are basically only sensitive to the sum of the two branching ratios, the $t\bar{t} \to WbHq$, $H \to b\bar{b}$ search has different sensitivity to each of them, and a simultaneous fit can be performed. The best-fit branching ratios obtained from the simultaneous fit are $\mathrm{BR}(t \to Hc) = [0.34 \pm 0.22\,(\mathrm{stat.}) \pm 0.15\,(\mathrm{syst.})]\%$ and $\mathrm{BR}(t \to Hu) = [-0.17 \pm 0.25\,(\mathrm{stat.}) \pm 0.17\,(\mathrm{syst.})]\%$,

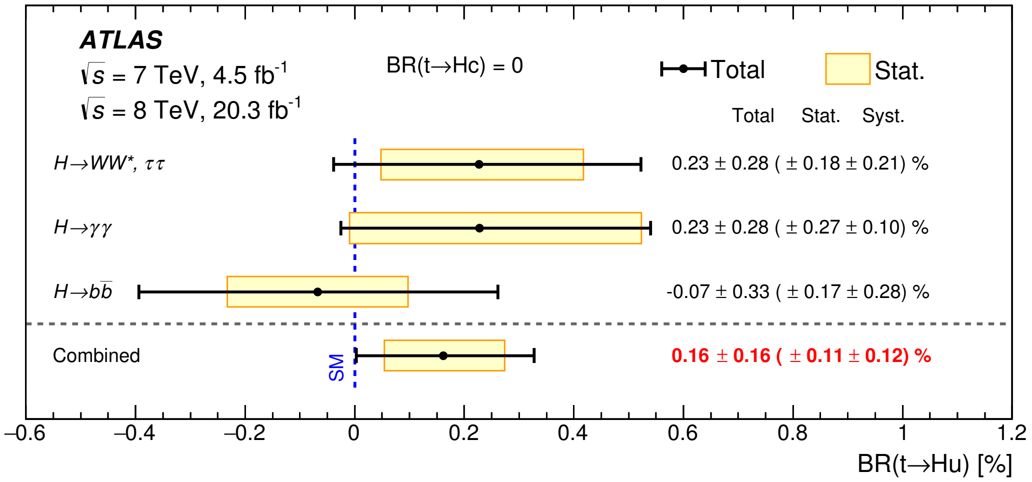

Figure 10: Summary of the best-fit BR($t \to Hu$) for the individual searches as well as their combination, assuming that BR($t \to Hc$) = 0.

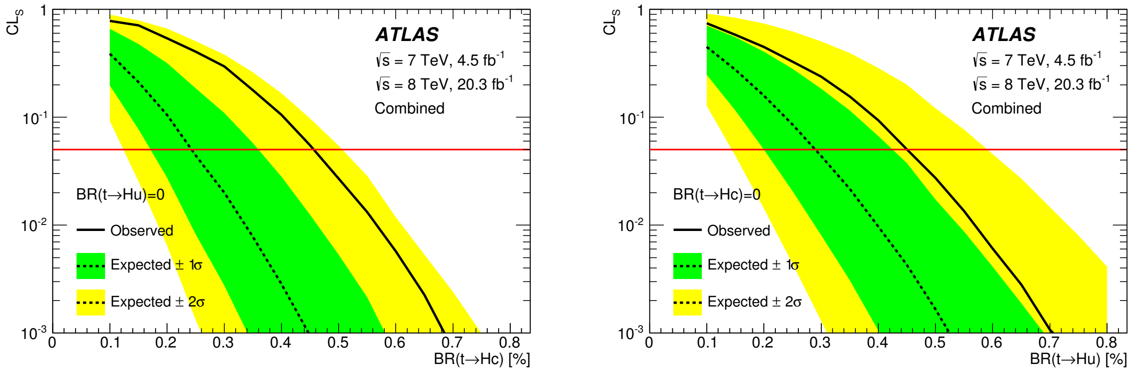

(a) (b)

Figure 11: (a) $\mathrm{CL_s}$ versus BR($t \to Hc$) and (b) $\mathrm{CL_s}$ versus BR($t \to Hu$) for the combination of the searches, assuming that the other branching ratio is zero. The observed $\mathrm{CL_s}$ values (solid black lines) are compared to the expected (median) $\mathrm{CL_s}$ values under the background-only hypothesis (dotted black lines). The surrounding shaded bands correspond to the 68% and 95% CL intervals around the expected $\mathrm{CL_s}$ values, denoted by $\pm 1\sigma$ and $\pm 2\sigma$, respectively. The solid red line at $\mathrm{CL_s}$=0.05 denotes the value below which the hypothesis is excluded at 95% CL.

with a correlation coefficient of −0.84, as shown in figure 13. Figure 14(a) shows the 95% CL upper limits on the branching ratios in the BR($t \to Hu$) versus BR($t \to Hc$) plane. The corresponding upper limits on the couplings in the $|\lambda_{tuH}|$ versus $|\lambda_{tcH}|$ plane can be found in figure 14(b).

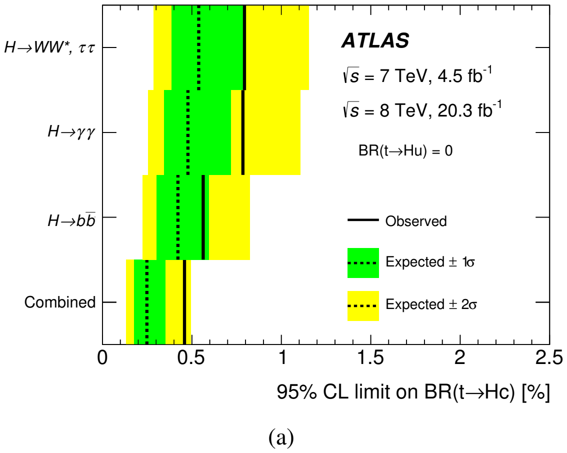

Figure 12: 95% CL upper limits on (a) BR($t \to Hc$) and (b) BR($t \to Hu$) for the individual searches as well as their combination, assuming that the other branching ratio is zero. The observed limits (solid lines) are compared to the expected (median) limits under the background-only hypothesis (dotted lines). The surrounding shaded bands correspond to the 68% and 95% CL intervals around the expected limits, denoted by $\pm 1\sigma$ and $\pm 2\sigma$, respectively. Because the asymptotic approximation is used in the calculation of CL$_s$, the results of the $H \to \gamma\gamma$ search reported in this figure differ slightly from those published in ref. [17], which remain the most accurate results.

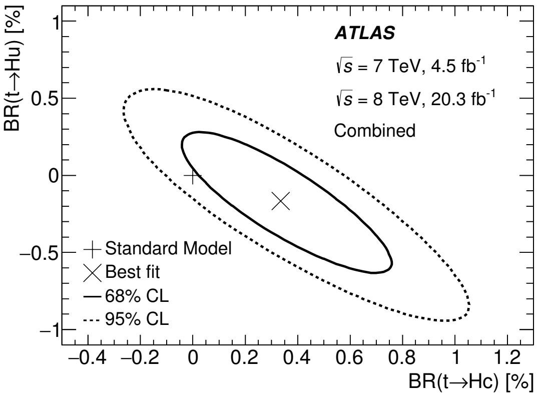

Figure 13: Best-fit BR($t \to Hc$) and BR($t \to Hu$) and the corresponding 68% CL (solid) and 95% CL (dotted) regions for the combination of the searches.

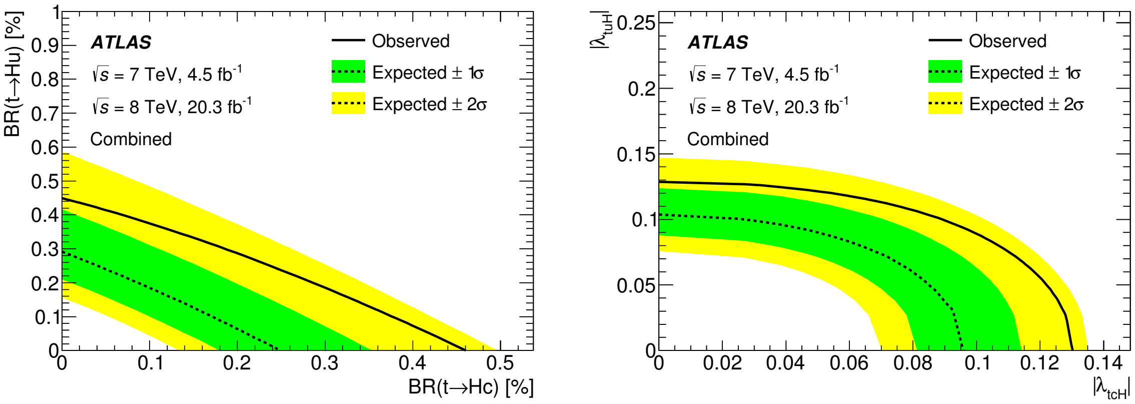

(a)

(b)

Figure 14: 95% CL upper limits (a) on the plane of BR($t \to Hu$) versus BR($t \to Hc$) and (b) on the plane of $|\lambda_{tuH}|$ versus $|\lambda_{tcH}|$ for the combination of the searches. The observed limits (solid lines) are compared to the expected (median) limits under the background-only hypothesis (dotted lines). The surrounding shaded bands correspond to the 68% and 95% CL intervals around the expected limits, denoted by $\pm 1\sigma$ and $\pm 2\sigma$, respectively.

10. Conclusion

A search for flavour-changing neutral current decays of a top quark to an up-type quark ($q = u, c$) and the Standard Model Higgs boson, where the Higgs boson decays to $b\bar{b}$, is presented. The analysis searches for top quark pair events in which one top quark decays to Wb, with the W boson decaying leptonically, and the other top quark decays to Hq. The search is based on pp collisions at $\sqrt{s} = 8$ TeV recorded in 2012 with the ATLAS detector at the CERN Large Hadron Collider and uses an integrated luminosity of 20.3 fb^{-1}. Data are analysed in the lepton-plus-jets final state, characterised by an isolated electron or muon with moderately high transverse momentum and at least four jets. In this search the dominant background process is $t\bar{t} \to WbWb$. To separate the signal from the background, the search exploits the high multiplicity of b-quark jets characteristic of signal events, and employs a likelihood discriminant that combines information from invariant mass distributions and the flavour of the jets. No significant excess of events above the background expectation is found, and observed (expected) 95% CL upper limits of 0.56% (0.42%) and 0.61% (0.64%) are derived for the $t \to Hc$ and $t \to Hu$ branching ratios respectively.

Results from other ATLAS searches are also summarised, including a previous search probing $H \to \gamma\gamma$ decays, and a reinterpretation of a search for $t\bar{t}H$ production in multilepton final states, which exploits the $H \to WW^*, \tau\tau$ decay modes. All searches discussed in this paper have comparable sensitivity, and thus their combination represents a significant improvement over the individual results. The observed (expected) 95% CL combined upper limits on the $t \to Hc$ and $t \to Hu$ branching ratios are 0.46% (0.25%) and 0.45% (0.29%) respectively. The corresponding observed (expected) upper limits on the $|\lambda_{tcH}|$ and $|\lambda_{tuH}|$ couplings are 0.13 (0.10) and 0.13 (0.10) respectively. Upper limits in the $t \to Hc$ versus $t \to Hu$ branching ratio plane, as well as best-fit branching ratios, are also reported. These are the most restrictive direct bounds on tqH ($q = u, c$) interactions measured so far.

Acknowledgements

We thank CERN for the very successful operation of the LHC, as well as the support staff from our institutions without whom ATLAS could not be operated efficiently.

We acknowledge the support of ANPCyT, Argentina; YerPhI, Armenia; ARC, Australia; BMWFW and FWF, Austria; ANAS, Azerbaijan; SSTC, Belarus; CNPq and FAPESP, Brazil; NSERC, NRC and CFI, Canada; CERN; CONICYT, Chile; CAS, MOST and NSFC, China; COLCIENCIAS, Colombia; MSMT CR, MPO CR and VSC CR, Czech Republic; DNRF, DNSRC and Lundbeck Foundation, Denmark; IN2P3-CNRS, CEA-DSM/IRFU, France; GNSF, Georgia; BMBF, HGF, and MPG, Germany; GSRT, Greece; RGC, Hong Kong SAR, China; ISF, I-CORE and Benoziyo Center, Israel; INFN, Italy; MEXT and JSPS, Japan; CNRST, Morocco; FOM and NWO, Netherlands; RCN, Norway; MNiSW and NCN, Poland; FCT, Portugal; MNE/IFA, Romania; MES of Russia and NRC KI, Russian Federation; JINR; MESTD, Serbia; MSSR, Slovakia; ARRS and MIZŠ, Slovenia; DST/NRF, South Africa; MINECO, Spain; SRC and Wallenberg Foundation, Sweden; SERI, SNSF and Cantons of Bern and Geneva, Switzerland; MOST, Taiwan; TAEK, Turkey; STFC, United Kingdom; DOE and NSF, United States of America. In addition, individual groups and members have received support from BCKDF, the Canada Council, CANARIE, CRC, Compute Canada, FQRNT, and the Ontario Innovation Trust, Canada; EPLANET, ERC, FP7, Horizon 2020 and Marie Skłodowska-Curie Actions, European Union; Investissements d'Avenir Labex and Idex, ANR, Region Auvergne and Fondation Partager le Savoir, France; DFG and AvH Foundation, Germany; Herakleitos, Thales and Aristeia programmes co-financed by EU-ESF and the Greek NSRF; BSF, GIF and Minerva, Israel; BRF, Norway; the Royal Society and Leverhulme Trust, United Kingdom.

The crucial computing support from all WLCG partners is acknowledged gratefully, in particular from CERN and the ATLAS Tier-1 facilities at TRIUMF (Canada), NDGF (Denmark, Norway, Sweden), CC-IN2P3 (France), KIT/GridKA (Germany), INFN-CNAF (Italy), NL-T1 (Netherlands), PIC (Spain), ASGC (Taiwan), RAL (UK) and BNL (USA) and in the Tier-2 facilities worldwide.

Appendix

A. Pre-fit and post-fit event yields in the $t\bar{t} \to WbHq, H \to b\bar{b}$ search

Table 3 presents the observed and predicted yields in each of the analysis channels for the $t\bar{t} \to WbHq, H \to b\bar{b}$ search before the fit to data. Table 4 presents the observed and predicted yields in each of the analysis channels for the $t\bar{t} \to WbHc, H \to b\bar{b}$ search, after the fit to the data under the signal-plus-background hypothesis.

B. Pre-fit event yields in the $t\bar{t} \to WbHq, H \to WW^*, \tau\tau$ search

Table 5 presents the observed and predicted yields in each of the analysis channels for the $t\bar{t} \to WbHq, H \to WW^*, \tau\tau$ search before the fit to data.

	4 j, 2 b	4 j, 3 b	4 j, 4 b
$t\bar{t} \to WbHc$	890 ± 100	394 ± 54	41.6 ± 7.2
$t\bar{t} \to WbHu$	851 ± 98	339 ± 49	3.81 ± 0.71
$t\bar{t}$+light-jets	77400 ± 8100	6170 ± 860	53 ± 12
$t\bar{t} + c\bar{c}$	4900 ± 2600	680 ± 370	21 ± 11
$t\bar{t} + b\bar{b}$	1870 ± 990	680 ± 370	44 ± 23
$t\bar{t}V$	121 ± 21	15.5 ± 2.9	0.89 ± 0.19
$t\bar{t}H$	30.5 ± 4.2	12.7 ± 1.9	1.91 ± 0.34
W+jets	4700 ± 1600	217 ± 78	5.4 ± 2.0
Z+jets	1080 ± 450	50 ± 22	0.90 ± 0.50
Single top	4900 ± 1400	340 ± 100	6.8 ± 2.3
Diboson	212 ± 75	11.5 ± 4.1	0.24 ± 0.11
Multijet	1540 ± 550	100 ± 36	3.4 ± 1.2
Total background	96800 ± 9600	8300 ± 1100	138 ± 32
Data	98049	8752	161

	5 j, 2 b	5 j, 3 b	5 j, ≥4 b
$t\bar{t} \to WbHc$	483 ± 96	242 ± 50	35.1 ± 7.7
$t\bar{t} \to WbHu$	473 ± 95	217 ± 46	8.4 ± 2.0
$t\bar{t}$+light-jets	37600 ± 6600	3480 ± 750	61 ± 18
$t\bar{t} + c\bar{c}$	4300 ± 2300	810 ± 460	43 ± 28
$t\bar{t} + b\bar{b}$	1670 ± 860	890 ± 470	115 ± 61
$t\bar{t}V$	145 ± 24	26.5 ± 4.5	3.10 ± 0.60
$t\bar{t}H$	40.9 ± 4.8	22.3 ± 2.9	5.96 ± 0.98
W+jets	1850 ± 790	131 ± 57	5.8 ± 2.7
Z+jets	400 ± 200	29 ± 14	1.47 ± 0.76
Single top	1880 ± 740	195 ± 78	8.3 ± 3.1
Diboson	96 ± 41	8.0 ± 3.5	0.40 ± 0.19
Multijet	450 ± 160	68 ± 24	8.3 ± 3.0
Total background	48400 ± 7800	5700 ± 1100	252 ± 75
Data	49699	6199	286

	≥ 6 j, 2 b	≥6 j, 3 b	≥6 j, ≥4 b
$t\bar{t} \to WbHc$	267 ± 68	145 ± 37	31.1 ± 8.3
$t\bar{t} \to WbHu$	259 ± 67	132 ± 34	10.3 ± 2.8
$t\bar{t}$+light-jets	18800 ± 4800	2000 ± 730	52 ± 40
$t\bar{t} + c\bar{c}$	3700 ± 2000	850 ± 500	79 ± 46
$t\bar{t} + b\bar{b}$	1430 ± 760	970 ± 520	240 ± 130
$t\bar{t}V$	182 ± 32	44.6 ± 8.1	8.4 ± 1.7
$t\bar{t}H$	64.2 ± 8.2	39.8 ± 5.4	16.1 ± 2.6
W+jets	880 ± 440	95 ± 47	8.5 ± 4.5
Z+jets	180 ± 100	19 ± 11	1.5 ± 0.9
Single top	840 ± 410	122 ± 62	11.9 ± 6.2
Diboson	50 ± 26	6.0 ± 3.0	0.54 ± 0.29
Multijet	176 ± 62	20.3 ± 7.2	0.93 ± 0.50
Total background	26400 ± 6100	4200 ± 1200	420 ± 160
Data	26185	4701	516

Table 3: $t\bar{t} \to WbHq, H \to b\bar{b}$ search: predicted and observed yields in each of the analysis channels considered. The prediction is shown before the fit to data. Also shown are the signal expectations for $t\bar{t} \to WbHc$ and $t\bar{t} \to WbHu$ assuming BR($t \to Hc$) = 1% and BR($t \to Hu$) = 1% respectively. The $t\bar{t} \to WbWb$ background is normalised to the SM prediction. The quoted uncertainties are the sum in quadrature of statistical and systematic uncertainties on the yields.

	4 j, 2 b	4 j, 3 b	4 j, 4 b
$t\bar{t} \to WbHc$	155 ± 11	68.5 ± 5.0	7.23 ± 0.56
$t\bar{t}$+light-jets	77300 ± 1700	6240 ± 190	56.1 ± 7.3
$t\bar{t} + c\bar{c}$	5600 ± 1500	810 ± 210	23.4 ± 6.0
$t\bar{t} + b\bar{b}$	2420 ± 360	890 ± 130	54.1 ± 7.5
$t\bar{t}V$	122 ± 19	15.6 ± 2.5	0.90 ± 0.15
$t\bar{t}H$	30.9 ± 3.6	12.8 ± 1.6	1.92 ± 0.26
W+jets	4900 ± 1100	231 ± 55	5.8 ± 1.5
Z+jets	1040 ± 390	48 ± 18	0.78 ± 0.32
Single top	5100 ± 1000	352 ± 71	7.1 ± 1.5
Diboson	209 ± 72	11.6 ± 4.0	0.22 ± 0.08
Multijet	1120 ± 320	75 ± 22	2.41 ± 0.70
Total	98070 ± 370	8756 ± 98	159.9 ± 7.4
Data	98049	8752	161

	5 j, 2 b	5 j, 3 b	5 j, ≥4 b
$t\bar{t} \to WbHc$	85 ± 10	42.4 ± 5.1	6.17 ± 0.77
$t\bar{t}$+light-jets	37600 ± 1200	3570 ± 160	66.4 ± 8.1
$t\bar{t} + c\bar{c}$	4700 ± 1200	970 ± 240	59 ± 16
$t\bar{t} + b\bar{b}$	2140 ± 310	1150 ± 160	144 ± 17
$t\bar{t}V$	145 ± 23	26.6 ± 4.2	3.12 ± 0.50
$t\bar{t}H$	41.0 ± 4.5	22.4 ± 2.6	5.98 ± 0.74
W+jets	1940 ± 560	140 ± 41	6.0 ± 1.8
Z+jets	380 ± 170	27.6 ± 12.4	1.38 ± 0.63
Single top	2090 ± 630	219 ± 66	10.1 ± 3.1
Diboson	93 ± 39	7.8 ± 3.3	0.37 ± 0.16
Multijet	332 ± 96	46 ± 13	6.2 ± 1.9
Total	49570 ± 250	6223 ± 66	308 ± 11
Data	49699	6199	286

	≥6 j, 2 b	≥6 j, 3 b	≥6 j, ≥4 b
$t\bar{t} \to WbHc$	46.1 ± 4.2	25.0 ± 2.3	5.41 ± 0.52
$t\bar{t}$+light-jets	18590 ± 800	2080 ± 140	54.2 ± 8.4
$t\bar{t} + c\bar{c}$	3820 ± 920	980 ± 240	85 ± 20
$t\bar{t} + b\bar{b}$	1860 ± 270	1260 ± 170	320 ± 35
$t\bar{t}V$	178 ± 27	43.7 ± 6.8	8.3 ± 1.3
$t\bar{t}H$	64.0 ± 7.2	39.6 ± 4.5	15.9 ± 1.8
W+jets	680 ± 220	75 ± 24	7.0 ± 2.7
Z+jets	159 ± 78	16.8 ± 8.3	1.48 ± 0.75
Single top	740 ± 270	108 ± 40	10.6 ± 4.0
Diboson	48 ± 23	5.7 ± 2.7	0.51 ± 0.25
Multijet	120 ± 34	13.9 ± 4.0	1.12 ± 0.65
Total	26300 ± 160	4652 ± 62	508 ± 22
Data	26185	4701	516

Table 4: $t\bar{t} \to WbHc, H \to b\bar{b}$ search: predicted and observed yields in each of the analysis channels considered. The background prediction is shown after the fit to data under the signal-plus-background hypothesis. The quoted uncertainties are the sum in quadrature of statistical and systematic uncertainties on the yields, computed taking into account correlations among nuisance parameters and among processes.

	ee4j	$e\mu$4j	$\mu\mu$4j
$t\bar{t} \to WbHc$	$5.4\,^{+0.8}_{-0.6}$	$15.0\,^{+1.7}_{-1.4}$	$11.1\,^{+1.1}_{-1.2}$
$t\bar{t} \to WbHu$	5.5 ± 0.7	$15.9\,^{+1.7}_{-1.5}$	$9.7\,^{+1.5}_{-1.0}$
Non-prompt	3.4 ± 1.7	12 ± 4	6.3 ± 2.6
q mis-id	1.8 ± 0.7	1.4 ± 0.6	–
$t\bar{t}W$	2.0 ± 0.4	6.2 ± 1.0	4.7 ± 0.9
$t\bar{t}(Z/\gamma^*)$	0.75 ± 0.20	1.5 ± 0.3	0.80 ± 0.22
Diboson	0.7 ± 0.4	1.9 ± 1.0	0.53 ± 0.30
$t\bar{t}H$	0.44 ± 0.06	1.16 ± 0.14	0.74 ± 0.10
Rare	$0.25\,^{+0.04}_{-0.02}$	0.72 ± 0.05	$0.34\,^{+0.04}_{-0.03}$
Total background	9.5 ± 2.1	25 ± 5	13.4 ± 2.9
Data	9	26	20

	ee≥5j	$e\mu$≥5j	$\mu\mu$≥5j
$t\bar{t} \to WbHc$	2.9 ± 0.6	$10.2\,^{+2.0}_{-1.6}$	$6.6\,^{+1.5}_{-1.3}$
$t\bar{t} \to WbHu$	2.7 ± 0.8	$8.2\,^{+1.6}_{-1.2}$	$7.2\,^{+1.2}_{-1.4}$
Non-prompt	2.3 ± 1.2	6.7 ± 2.4	2.9 ± 1.4
q mis-id	1.1 ± 0.5	0.85 ± 0.35	–
$t\bar{t}W$	1.4 ± 0.4	4.8 ± 1.2	3.8 ± 0.9
$t\bar{t}(Z/\gamma^*)$	0.98 ± 0.26	2.1 ± 0.5	0.95 ± 0.25
Diboson	0.47 ± 0.29	0.38 ± 0.30	0.7 ± 0.4
$t\bar{t}H$	0.73 ± 0.14	2.1 ± 0.4	1.41 ± 0.28
Rare	0.27 ± 0.02	$0.79\,^{+0.05}_{-0.04}$	0.38 ± 0.02
Total background	7.2 ± 1.8	17 ± 3	10.0 ± 2.2
Data	10	22	11

	3ℓ	$2\ell 1\tau_{\mathrm{had}}$
$t\bar{t} \to WbHc$	6.4 ± 0.9	2.4 ± 0.4
$t\bar{t} \to WbHu$	$5.2\,^{+1.0}_{-0.8}$	$2.1\,^{+0.5}_{-0.4}$
Non-prompt	3.2 ± 0.7	$0.4\,^{+0.6}_{-0.4}$
q mis-id	–	–
$t\bar{t}W$	2.3 ± 0.7	0.38 ± 0.12
$t\bar{t}(Z/\gamma^*)$	3.9 ± 0.8	0.37 ± 0.08
Diboson	0.86 ± 0.55	0.12 ± 0.11
$t\bar{t}H$	2.34 ± 0.35	0.47 ± 0.08
Rare	$0.92\,^{+0.07}_{-0.06}$	$0.10\,^{+0.02}_{-0.01}$
Total background	13.7 ± 2.3	1.9 ± 0.6
Data	18	1

Table 5: $t\bar{t} \to WbHq, H \to WW^*, \tau\tau$ search: predicted and observed yields in each of the event categories considered. The prediction is shown before the fit to data. Also shown are the signal expectations for $t\bar{t} \to WbHc$ and $t\bar{t} \to WbHu$ assuming $\mathrm{BR}(t \to Hc) = 1\%$ and $\mathrm{BR}(t \to Hu) = 1\%$ respectively. The quoted uncertainties are the sum in quadrature of statistical and systematic uncertainties on the yields.

References

[1] ATLAS Collaboration, *Observation of a new particle in the search for the Standard Model Higgs boson with the ATLAS detector at the LHC*, Phys. Lett. B **716** (2012) 1, arXiv:`1207.7214 [hep-ex]`.

[2] CMS Collaboration, *Observation of a new boson at a mass of 125 GeV with the CMS experiment at the LHC*, Phys. Lett. B **716** (2012) 30, arXiv:`1207.7235 [hep-ex]`.

[3] ATLAS and CMS Collaborations, *Combined Measurement of the Higgs Boson Mass in pp Collisions at* $\sqrt{s} = 7$ *and 8 TeV with the ATLAS and CMS Experiments*, Phys. Rev. Lett. **114** (2015) 191803, arXiv:`1503.07589 [hep-ex]`.

[4] S. Glashow, J. Iliopoulos and L. Maiani, *Weak Interactions with Lepton-Hadron Symmetry*, Phys. Rev. D **2** (1970) 1285.

[5] G. Eilam, J. L. Hewett and A. Soni, *Rare decays of the top quark in the standard and two Higgs doublet models*, Phys. Rev. D **44** (1991) 1473, Erratum-ibid. D **59** (1999) 039901.

[6] B. Mele, S. Petrarca and A. Soddu, *A New evaluation of the* $t \to cH$ *decay width in the standard model*, Phys. Lett. B **435** (1998) 401, arXiv:`hep-ph/9805498 [hep-ph]`.

[7] J. A. Aguilar-Saavedra, *Top flavor-changing neutral interactions: Theoretical expectations and experimental detection*, Acta Phys. Polon. B **35** (2004) 2695, arXiv:`hep-ph/0409342 [hep-ph]`.

[8] C. Zhang and F. Maltoni, *Top-quark decay into Higgs boson and a light quark at next-to-leading order in QCD*, Phys. Rev. D **88** (2013) 054005, arXiv:`1305.7386 [hep-ph]`.

[9] J. A. Aguilar-Saavedra, *Effects of mixing with quark singlets*, Phys. Rev. D **67** (2003) 035003, Erratum-ibid. D **69** (2004) 09990, arXiv:`hep-ph/0210112 [hep-ph]`.

[10] S. Bejar, J. Guasch and J. Solà, *Loop induced flavor changing neutral decays of the top quark in a general two Higgs doublet model*, Nucl. Phys. B **600** (2001) 21, arXiv:`hep-ph/0011091 [hep-ph]`.

[11] J. Guasch and J. Solà, *FCNC top quark decays: A Door to SUSY physics in high luminosity colliders?*, Nucl. Phys. B **562** (1999) 3, arXiv:`hep-ph/9906268 [hep-ph]`.

[12] J. J. Cao et al., *SUSY-induced FCNC top-quark processes at the large hadron collider*, Phys. Rev D. **75** (2007) 075021, arXiv:`hep-ph/0702264 [hep-ph]`.

[13] G. Eilam et al., *Top quark rare decay* $t \to ch$ *in R-parity violating SUSY*, Phys. Lett. B **510** (2001) 227, arXiv:`hep-ph/0102037 [hep-ph]`.

[14] T. P. Cheng and M. Sher, *Mass Matrix Ansatz and Flavor Nonconservation in Models with Multiple Higgs Doublets*, Phys. Rev. D **35** (1987) 3484.

[15] I. Baum, G. Eilam and S. Bar-Shalom, *Scalar flavor changing neutral currents and rare top quark decays in a two Higgs doublet model 'for the top quark'*, Phys. Rev. D **77** (2008) 113008, arXiv:`0802.2622 [hep-ph]`.

[16] K.-F. Chen et al., *When the Higgs meets the Top: Search for* $t \to ch^0$ *at the LHC*, Phys. Lett. B **725** (2013) 378, arXiv:`1304.8037 [hep-ph]`.

[17] ATLAS Collaboration, *Search for top quark decays* $t \to qH$ *with* $H \to \gamma\gamma$ *using the ATLAS detector*, JHEP **1406** (2014) 008, arXiv:`1403.6293 [hep-ex]`.

[18] CMS Collaboration, *Searches for heavy Higgs bosons in two-Higgs-doublet models and for $t \to ch$ decay using multilepton and diphoton final states in pp collisions at 8 TeV*, Phys. Rev. D **90** (2014) 112013, arXiv:`1410.2751 [hep-ex]`.

[19] A. Denner and T. Sack, *The Top width*, Nucl. Phys. B **358** (1991) 46.

[20] J. A. Aguilar-Saavedra and G. C. Branco, *Probing top flavor changing neutral scalar couplings at the CERN LHC*, Phys. Lett. B **495** (2000) 347, arXiv:`hep-ph/0004190 [hep-ph]`.

[21] ATLAS Collaboration, *Search for the Standard Model Higgs boson produced in association with top quarks and decaying into $b\bar{b}$ in pp collisions at $\sqrt{s}$ = 8 TeV with the ATLAS detector*, Eur. Phys. J. C **75** (2015) 349, arXiv:`1503.05066 [hep-ex]`.

[22] ATLAS Collaboration, *Search for production of vector-like quark pairs and of four top quarks in the lepton-plus-jets final state in pp collisions at $\sqrt{s}$ = 8 TeV with the ATLAS detector*, JHEP **08** (2015) 105, arXiv:`1505.04306 [hep-ex]`.

[23] ATLAS Collaboration, *Search for the associated production of the Higgs boson with a top quark pair in multilepton final states with the ATLAS detector*, Phys. Lett. B **749** (2015) 519, arXiv:`1506.05988 [hep-ex]`.

[24] ATLAS Collaboration, *The ATLAS Experiment at the CERN Large Hadron Collider*, JINST **3** (2008) S08003.

[25] ATLAS Collaboration, *Performance of the ATLAS Trigger System in 2010*, Eur. Phys. J. C **72** (2012) 1849, arXiv:`1110.1530 [hep-ex]`.

[26] ATLAS Collaboration, *Electron reconstruction and identification efficiency measurements with the ATLAS detector using the 2011 LHC proton-proton collision data*, Eur. Phys. J. C **74** (2014) 2941, arXiv:`1404.2240 [hep-ex]`.

[27] ATLAS Collaboration, *Muon reconstruction efficiency and momentum resolution of the ATLAS experiment in proton-proton collisions at $\sqrt{s}$ = 7 TeV in 2010*, Eur. Phys. J. C **74** (2014) 3034, arXiv:`1404.4562 [hep-ex]`.

[28] ATLAS Collaboration, *Measurement of the muon reconstruction performance of the ATLAS detector using 2011 and 2012 LHC proton-proton collision data*, Eur. Phys. J. C **74** (2014) 3130, arXiv:`1407.3935 [hep-ex]`.

[29] M. Cacciari, G. P. Salam and G. Soyez, *The anti-k_t jet clustering algorithm*, JHEP **0804** (2008) 063, arXiv:`0802.1189 [hep-ph]`.

[30] M. Cacciari and G. P. Salam, *Dispelling the N^3 myth for the k_t jet-finder*, Phys. Lett. B **641** (2006) 57, arXiv:`hep-ph/0512210`.

[31] M. Cacciari, G. P. Salam and G. Soyez, *FastJet User Manual*, Eur. Phys. J. C **72** (2012) 1896, arXiv:`1111.6097 [hep-ph]`.

[32] C. Cojocaru et al., *Hadronic calibration of the ATLAS liquid argon end-cap calorimeter in the pseudorapidity region* $1.6 < |\eta| < 1.8$ *in beam tests*, Nucl. Instrum. Meth. A **531** (2004) 481, arXiv:`physics/0407009 [physics.ins-det]`.

[33] W. Lampl et al., *Calorimeter Clustering Algorithms : Description and Performance*, ATL-LARG-PUB-2008-002 (2008), `http://cds.cern.ch/record/1099735`.

[34] ATLAS Collaboration, *Jet energy measurement with the ATLAS detector in proton-proton collisions at $\sqrt{s}$ = 7 TeV*, Eur. Phys. J. C **73** (2013) 2304, arXiv:`1112.6426 [hep-ex]`.

[35] ATLAS Collaboration, *Jet energy measurement and its systematic uncertainty in proton-proton collisions at $\sqrt{s} = 7$ TeV with the ATLAS detector*, Eur. Phys. J. C **75** (2015) 17, arXiv:`1406.0076 [hep-ex]`.

[36] ATLAS Collaboration, *Calibration of the performance of b-tagging for c and light-flavour jets in the 2012 ATLAS data*, ATLAS-CONF-2014-046 (2014), `http://cds.cern.ch/record/1741020`.

[37] ATLAS Collaboration, *Performance of Missing Transverse Momentum Reconstruction in Proton-Proton Collisions at 7 TeV with ATLAS*, Eur. Phys. J. C **72** (2012) 1844, arXiv:`1108.5602 [hep-ex]`.

[38] ATLAS Collaboration, *Improved luminosity determination in pp collisions at $\sqrt{s} = 7$ TeV using the ATLAS detector at the LHC*, Eur. Phys. J. C **73** (2013) 2518, arXiv:`1302.4393 [hep-ex]`.

[39] ATLAS Collaboration, *Measurement of the top quark-pair production cross section with ATLAS in pp collisions at $\sqrt{s} = 7$ TeV*, Eur. Phys. J. C **71** (2011) 1577, arXiv:`1012.1792 [hep-ex]`.

[40] S. Frixione, P. Nason and G. Ridolfi, *A Positive-weight next-to-leading-order Monte Carlo for heavy flavour hadroproduction*, JHEP **0709** (2007) 126, arXiv:`0707.3088 [hep-ph]`.

[41] P. Nason, *A New method for combining NLO QCD with shower Monte Carlo algorithms*, JHEP **0411** (2004) 040, arXiv:`hep-ph/0409146`.

[42] S. Frixione, P. Nason and C. Oleari, *Matching NLO QCD computations with Parton Shower simulations: the POWHEG method*, JHEP **0711** (2007) 070, arXiv:`0709.2092 [hep-ph]`.

[43] S. Alioli et al., *A general framework for implementing NLO calculations in shower Monte Carlo programs: the POWHEG BOX*, JHEP **1006** (2010) 043, arXiv:`1002.2581 [hep-ph]`.

[44] H.-L. Lai et al., *New parton distributions for collider physics*, Phys. Rev. D **82** (2010) 074024, arXiv:`1007.2241 [hep-ph]`.

[45] T. Sjöstrand, S. Mrenna and P. Z. Skands, *PYTHIA 6.4 Physics and Manual*, JHEP **0605** (2006) 026, arXiv:`hep-ph/0603175`.

[46] P. Z. Skands, *Tuning Monte Carlo Generators: The Perugia Tunes*, Phys. Rev. D **82** (2010) 074018, arXiv:`1005.3457 [hep-ph]`.

[47] G. Corcella et al., *HERWIG 6: An Event generator for hadron emission reactions with interfering gluons (including supersymmetric processes)*, JHEP **0101** (2001) 010, arXiv:`hep-ph/0011363`.

[48] J. M. Butterworth, J. R. Forshaw and M. H. Seymour, *Multiparton interactions in photoproduction at HERA*, Z. Phys. C **72** (1996) 637, arXiv:`hep-ph/9601371`.

[49] M. Czakon and A. Mitov, *Top++: A Program for the Calculation of the Top-Pair Cross-Section at Hadron Colliders*, Comput. Phys. Commun. **185** (2014) 2930, arXiv:`1112.5675 [hep-ph]`.

[50] M. Cacciari et al., *Top-pair production at hadron colliders with next-to-next-to-leading logarithmic soft-gluon resummation*, Phys. Lett. B **710** (2012) 612, arXiv:`1111.5869 [hep-ph]`.

[51] P. Bärnreuther, M. Czakon and A. Mitov, *Percent-Level-Precision Physics at the Tevatron: Next-to-Next-to-Leading Order QCD Corrections to $q\bar{q} \to t\bar{t} + X$*, Phys. Rev. Lett. **109** (2012) 132001, arXiv:`1204.5201 [hep-ph]`.

[52] M. Czakon and A. Mitov, *NNLO corrections to top-pair production at hadron colliders: the all-fermionic scattering channels*, JHEP **1212** (2012) 054, arXiv:`1207.0236 [hep-ph]`.

[53] M. Czakon and A. Mitov, *NNLO corrections to top pair production at hadron colliders: the quark-gluon reaction*, JHEP **1301** (2013) 080, arXiv:`1210.6832 [hep-ph]`.

[54] M. Czakon, P. Fiedler and A. Mitov, *Total Top-Quark Pair-Production Cross Section at Hadron Colliders Through* $O(\alpha_S^4)$, Phys. Rev. Lett. **110** (2013) 252004, arXiv:`1303.6254 [hep-ph]`.

[55] A. D. Martin et al., *Parton distributions for the LHC*, Eur. Phys. J. C **63** (2009) 189, arXiv:`0901.0002 [hep-ph]`.

[56] A. D. Martin et al., *Uncertainties on* α_S *in global PDF analyses and implications for predicted hadronic cross sections*, Eur. Phys. J. C **64** (2009) 653, arXiv:`0905.3531 [hep-ph]`.

[57] M. Botje et al., *The PDF4LHC Working Group Interim Recommendations* (2011), arXiv:`1101.0538 [hep-ph]`.

[58] J. Gao et al., *CT10 next-to-next-to-leading order global analysis of QCD*, Phys. Rev. D **89** (2014) 033009, arXiv:`1302.6246 [hep-ph]`.

[59] R. D. Ball et al., *Parton distributions with LHC data*, Nucl. Phys. B **867** (2013) 244, arXiv:`1207.1303 [hep-ph]`.

[60] J. Alwall et al., *MadGraph 5 : Going Beyond*, JHEP **1106** (2011) 128, arXiv:`1106.0522 [hep-ph]`.

[61] ATLAS Collaboration, *Measurements of normalized differential cross sections for* $t\bar{t}$ *production in pp collisions at* $\sqrt{s} = 7$ *TeV using the ATLAS detector*, Phys. Rev. D **90** (2014) 072004, arXiv:`1407.0371 [hep-ex]`.

[62] F. Cascioli et al., *NLO matching for* $t\bar{t}b\bar{b}$ *production with massive b-quarks*, Phys. Lett. B **734** (2014) 210, arXiv:`1309.5912 [hep-ph]`.

[63] T. Gleisberg et al., *Event generation with SHERPA 1.1*, JHEP **0902** (2009) 007, arXiv:`0811.4622 [hep-ph]`.

[64] F. Cascioli, P. Maierhofer and S. Pozzorini, *Scattering Amplitudes with Open Loops*, Phys. Rev. Lett. **108** (2012) 111601, arXiv:`1111.5206 [hep-ph]`.

[65] S. Alioli et al., *NLO single-top production matched with shower in POWHEG: s- and t-channel contributions*, JHEP **0909** (2009) 111, arXiv:`0907.4076 [hep-ph]`.

[66] E. Re, *Single-top Wt-channel production matched with parton showers using the POWHEG method*, Eur. Phys. J. C **71** (2011) 1547, arXiv:`1009.2450 [hep-ph]`.

[67] S. Frixione et al., *Single-top production in MC@NLO*, JHEP **0603** (2006) 092, arXiv:`hep-ph/0512250`.

[68] N. Kidonakis, *Next-to-next-to-leading-order collinear and soft gluon corrections for t-channel single top quark production*, Phys. Rev. D **83** (2011) 091503, arXiv:`1103.2792 [hep-ph]`.

[69] N. Kidonakis, *Two-loop soft anomalous dimensions for single top quark associated production with a* W^- *or* H^-, Phys. Rev. D **82** (2010) 054018, arXiv:`1005.4451 [hep-ph]`.

[70] N. Kidonakis, *NNLL resummation for s-channel single top quark production*, Phys. Rev. D **81** (2010) 054028, arXiv:`1001.5034 [hep-ph]`.

[71] M. L. Mangano et al., *ALPGEN, a generator for hard multiparton processes in hadronic collisions*, JHEP **0307** (2003) 001, arXiv:`hep-ph/0206293`.

[72] M. L. Mangano, M. Moretti and R. Pittau, *Multijet matrix elements and shower evolution in hadronic collisions: $Wb\bar{b} + n$ jets as a case study*, Nucl. Phys. B **632** (2002) 343, arXiv:hep-ph/0108069.

[73] K. Melnikov and F. Petriello, *Electroweak gauge boson production at hadron colliders through $O(\alpha_S^2)$*, Phys. Rev. D **74** (2006) 114017, arXiv:hep-ph/0609070.

[74] ATLAS Collaboration, *Measurement of the charge asymmetry in top-quark pair production in the lepton-plus-jets final state in pp collision data at $\sqrt{s} = 8$ TeV with the ATLAS detector* (2015), submitted to Eur. Phys. J. C, arXiv:1509.02358 [hep-ex].

[75] J. M. Campbell and R. K. Ellis, *An Update on vector boson pair production at hadron colliders*, Phys. Rev. D **60** (1999) 113006, arXiv:hep-ph/9905386.

[76] ATLAS Collaboration, *ATLAS tunes of PYTHIA6 and PYTHIA8 for MC11*, ATL-PHYS-PUB-2011-009 (2011), http://cds.cern.ch/record/1363300.

[77] M. V. Garzelli et al., *Standard Model Higgs boson production in association with a top anti-top pair at NLO with parton showering*, Europhys. Lett. **96** (2011) 11001, arXiv:1108.0387 [hep-ph].

[78] G. Bevilacqua et al., *HELAC-NLO*, Comput. Phys. Commun. **184** (2013) 986, arXiv:1110.1499 [hep-ph].

[79] T. Sjöstrand, S. Mrenna and P. Z. Skands, *A Brief Introduction to PYTHIA 8.1*, Comput. Phys. Commun. **178** (2008) 852, arXiv:0710.3820 [hep-ph].

[80] ATLAS Collaboration, *New ATLAS event generator tunes to 2010 data*, ATL-PHYS-PUB-2011-008 (2011), http://cds.cern.ch/record/1345343.

[81] M. V. Garzelli et al., *$t\bar{t}W^{+-}$ and $t\bar{t}Z$ Hadroproduction at NLO accuracy in QCD with Parton Shower and Hadronization effects*, JHEP **1211** (2012) 056, arXiv:1208.2665 [hep-ph].

[82] S. Dawson et al., *Associated Higgs production with top quarks at the Large Hadron Collider: NLO QCD corrections*, Phys. Rev. D **68** (2003) 034022, arXiv:hep-ph/0305087.

[83] W. Beenakker et al., *NLO QCD corrections to $t\bar{t}H$ production in hadron collisions*, Nucl. Phys. B **653** (2003) 151, arXiv:hep-ph/0211352.

[84] W. Beenakker et al., *Higgs radiation off top quarks at the Tevatron and the LHC*, Phys. Rev. Lett. **87** (2001) 201805, arXiv:hep-ph/0107081.

[85] A. Djouadi, J. Kalinowski and M. Spira, *HDECAY: A Program for Higgs boson decays in the standard model and its supersymmetric extension*, Comput. Phys. Commun. **108** (1998) 56, arXiv:hep-ph/9704448.

[86] A. Bredenstein et al., *Precise predictions for the Higgs-boson decay $H \to WW/ZZ \to 4$ leptons*, Phys. Rev. D **74** (2006) 013004, arXiv:hep-ph/0604011.

[87] S. Actis et al., *NNLO Computational Techniques: The Cases $H \to \gamma\gamma$ and $H \to gg$*, Nucl. Phys. B **811** (2009) 182, arXiv:0809.3667 [hep-ph].

[88] A. Denner et al., *Standard Model Higgs-Boson Branching Ratios with Uncertainties*, Eur. Phys. J. C **71** (2011) 1753, arXiv:1107.5909 [hep-ph].

[89] LHC Higgs Cross Section Working Group, S. Dittmaier et al., *Handbook of LHC Higgs Cross Sections: 1. Inclusive Observables* (2011), arXiv:1101.0593 [hep-ph].

[90] J. A. Aguilar-Saavedra, *PROTOS, a PROgram for TOp Simulations*, `http://jaguilar.web.cern.ch/jaguilar/protos/`.

[91] J. A. Aguilar-Saavedra, *A Minimal set of top-Higgs anomalous couplings*, Nucl. Phys. B **821** (2009) 215, arXiv:`0904.2387 [hep-ph]`.

[92] ATLAS Collaboration, *The ATLAS Simulation Infrastructure*, Eur. Phys. J. C **70** (2010) 823, arXiv:`1005.4568 [physics.ins-det]`.

[93] S. Agostinelli et al., *GEANT4: A Simulation toolkit*, Nucl. Instrum. Meth. A **506** (2003) 250.

[94] ATLAS Collaboration, *Summary of ATLAS Pythia 8 tunes*, ATL-PHYS-PUB-2012-003 (2012), `http://cds.cern.ch/record/1474107`.

[95] ATLAS Collaboration, *Calibration of b-tagging using dileptonic top pair events in a combinatorial likelihood approach with the ATLAS experiment*, ATLAS-CONF-2014-004 (2014), `http://cds.cern.ch/record/1664335`.

[96] J. Alwall et al., *Comparative study of various algorithms for the merging of parton showers and matrix elements in hadronic collisions*, Eur. Phys. J. C **53** (2008) 473, arXiv:`0706.2569 [hep-ph]`.

[97] S. Frixione et al., *Single-top hadroproduction in association with a W boson*, JHEP **0807** (2008) 029, arXiv:`0805.3067 [hep-ph]`.

[98] J. M. Campbell and R. K. Ellis, $t\bar{t}W^{+-}$ *production and decay at NLO*, JHEP **1207** (2012) 052, arXiv:`1204.5678 [hep-ph]`.

[99] W. Verkerke and D. P. Kirkby, *The RooFit toolkit for data modeling*, eConf **C0303241** (2003) MOLT007, arXiv:`physics/0306116 [physics.data-an]`.

[100] W. Verkerke and D. P. Kirkby, *RooFit Users Manual*, `http://roofit.sourceforge.net/`.

[101] G. Cowan et al., *Asymptotic formulae for likelihood-based tests of new physics*, Eur. Phys. J. C **71** (2011) 1554, Erratum-ibid. C **73** (2013) 2501, arXiv:`1007.1727 [physics.data-an]`.

[102] T. Junk, *Confidence level computation for combining searches with small statistics*, Nucl. Instrum. Meth. A **434** (1999) 435, arXiv:`hep-ex/9902006`.

[103] A. L. Read, *Presentation of search results: The CL(s) technique*, J. Phys. G **28** (2002) 2693.

[104] ATLAS Collaboration, *Measurements of the Higgs boson production and decay rates and coupling strengths using pp collision data at* $\sqrt{s} = 7$ *and* 8 *TeV in the ATLAS experiment* (2015), submitted to Eur. Phys. J. C, arXiv:`1507.04548 [hep-ex]`.

The ATLAS Collaboration

G. Aad[85], B. Abbott[113], J. Abdallah[151], O. Abdinov[11], R. Aben[107], M. Abolins[90], O.S. AbouZeid[158], H. Abramowicz[153], H. Abreu[152], R. Abreu[116], Y. Abulaiti[146a,146b], B.S. Acharya[164a,164b,a], L. Adamczyk[38a], D.L. Adams[25], J. Adelman[108], S. Adomeit[100], T. Adye[131], A.A. Affolder[74], T. Agatonovic-Jovin[13], J. Agricola[54], J.A. Aguilar-Saavedra[126a,126f], S.P. Ahlen[22], F. Ahmadov[65,b], G. Aielli[133a,133b], H. Akerstedt[146a,146b], T.P.A. Åkesson[81], A.V. Akimov[96], G.L. Alberghi[20a,20b], J. Albert[169], S. Albrand[55], M.J. Alconada Verzini[71], M. Aleksa[30], I.N. Aleksandrov[65], C. Alexa[26b], G. Alexander[153], T. Alexopoulos[10], M. Alhroob[113], G. Alimonti[91a], L. Alio[85], J. Alison[31], S.P. Alkire[35], B.M.M. Allbrooke[149], P.P. Allport[18], A. Aloisio[104a,104b], A. Alonso[36], F. Alonso[71], C. Alpigiani[138], A. Altheimer[35], B. Alvarez Gonzalez[30], D. Álvarez Piqueras[167], M.G. Alviggi[104a,104b], B.T. Amadio[15], K. Amako[66], Y. Amaral Coutinho[24a], C. Amelung[23], D. Amidei[89], S.P. Amor Dos Santos[126a,126c], A. Amorim[126a,126b], S. Amoroso[48], N. Amram[153], G. Amundsen[23], C. Anastopoulos[139], L.S. Ancu[49], N. Andari[108], T. Andeen[35], C.F. Anders[58b], G. Anders[30], J.K. Anders[74], K.J. Anderson[31], A. Andreazza[91a,91b], V. Andrei[58a], S. Angelidakis[9], I. Angelozzi[107], P. Anger[44], A. Angerami[35], F. Anghinolfi[30], A.V. Anisenkov[109,c], N. Anjos[12], A. Annovi[124a,124b], M. Antonelli[47], A. Antonov[98], J. Antos[144b], F. Anulli[132a], M. Aoki[66], L. Aperio Bella[18], G. Arabidze[90], Y. Arai[66], J.P. Araque[126a], A.T.H. Arce[45], F.A. Arduh[71], J-F. Arguin[95], S. Argyropoulos[63], M. Arik[19a], A.J. Armbruster[30], O. Arnaez[30], H. Arnold[48], M. Arratia[28], O. Arslan[21], A. Artamonov[97], G. Artoni[23], S. Asai[155], N. Asbah[42], A. Ashkenazi[153], B. Åsman[146a,146b], L. Asquith[149], K. Assamagan[25], R. Astalos[144a], M. Atkinson[165], N.B. Atlay[141], K. Augsten[128], M. Aurousseau[145b], G. Avolio[30], B. Axen[15], M.K. Ayoub[117], G. Azuelos[95,d], M.A. Baak[30], A.E. Baas[58a], M.J. Baca[18], C. Bacci[134a,134b], H. Bachacou[136], K. Bachas[154], M. Backes[30], M. Backhaus[30], P. Bagiacchi[132a,132b], P. Bagnaia[132a,132b], Y. Bai[33a], T. Bain[35], J.T. Baines[131], O.K. Baker[176], E.M. Baldin[109,c], P. Balek[129], T. Balestri[148], F. Balli[84], W.K. Balunas[122], E. Banas[39], Sw. Banerjee[173,e], A.A.E. Bannoura[175], L. Barak[30], E.L. Barberio[88], D. Barberis[50a,50b], M. Barbero[85], T. Barillari[101], M. Barisonzi[164a,164b], T. Barklow[143], N. Barlow[28], S.L. Barnes[84], B.M. Barnett[131], R.M. Barnett[15], Z. Barnovska[5], A. Baroncelli[134a], G. Barone[23], A.J. Barr[120], F. Barreiro[82], J. Barreiro Guimarães da Costa[57], R. Bartoldus[143], A.E. Barton[72], P. Bartos[144a], A. Basalaev[123], A. Bassalat[117], A. Basye[165], R.L. Bates[53], S.J. Batista[158], J.R. Batley[28], M. Battaglia[137], M. Bauce[132a,132b], F. Bauer[136], H.S. Bawa[143,f], J.B. Beacham[111], M.D. Beattie[72], T. Beau[80], P.H. Beauchemin[161], R. Beccherle[124a,124b], P. Bechtle[21], H.P. Beck[17,g], K. Becker[120], M. Becker[83], M. Beckingham[170], C. Becot[117], A.J. Beddall[19b], A. Beddall[19b], V.A. Bednyakov[65], C.P. Bee[148], L.J. Beemster[107], T.A. Beermann[30], M. Begel[25], J.K. Behr[120], C. Belanger-Champagne[87], W.H. Bell[49], G. Bella[153], L. Bellagamba[20a], A. Bellerive[29], M. Bellomo[86], K. Belotskiy[98], O. Beltramello[30], O. Benary[153], D. Benchekroun[135a], M. Bender[100], K. Bendtz[146a,146b], N. Benekos[10], Y. Benhammou[153], E. Benhar Noccioli[49], J.A. Benitez Garcia[159b], D.P. Benjamin[45], J.R. Bensinger[23], S. Bentvelsen[107], L. Beresford[120], M. Beretta[47], D. Berge[107], E. Bergeaas Kuutmann[166], N. Berger[5], F. Berghaus[169], J. Beringer[15], C. Bernard[22], N.R. Bernard[86], C. Bernius[110], F.U. Bernlochner[21], T. Berry[77], P. Berta[129], C. Bertella[83], G. Bertoli[146a,146b], F. Bertolucci[124a,124b], C. Bertsche[113], D. Bertsche[113], M.I. Besana[91a], G.J. Besjes[36], O. Bessidskaia Bylund[146a,146b], M. Bessner[42], N. Besson[136], C. Betancourt[48], S. Bethke[101], A.J. Bevan[76], W. Bhimji[15], R.M. Bianchi[125], L. Bianchini[23], M. Bianco[30], O. Biebel[100], D. Biedermann[16], N.V. Biesuz[124a,124b], M. Biglietti[134a], J. Bilbao De Mendizabal[49], H. Bilokon[47], M. Bindi[54], S. Binet[117], A. Bingul[19b], C. Bini[132a,132b], S. Biondi[20a,20b], D.M. Bjergaard[45], C.W. Black[150], J.E. Black[143], K.M. Black[22], D. Blackburn[138], R.E. Blair[6], J.-B. Blanchard[136], J.E. Blanco[77], T. Blazek[144a], I. Bloch[42], C. Blocker[23], W. Blum[83,*], U. Blumenschein[54], S. Blunier[32a],

G.J. Bobbink[107], V.S. Bobrovnikov[109,c], S.S. Bocchetta[81], A. Bocci[45], C. Bock[100], M. Boehler[48],
J.A. Bogaerts[30], D. Bogavac[13], A.G. Bogdanchikov[109], C. Bohm[146a], V. Boisvert[77], T. Bold[38a],
V. Boldea[26b], A.S. Boldyrev[99], M. Bomben[80], M. Bona[76], M. Boonekamp[136], A. Borisov[130],
G. Borissov[72], S. Borroni[42], J. Bortfeldt[100], V. Bortolotto[60a,60b,60c], K. Bos[107], D. Boscherini[20a],
M. Bosman[12], J. Boudreau[125], J. Bouffard[2], E.V. Bouhova-Thacker[72], D. Boumediene[34],
C. Bourdarios[117], N. Bousson[114], S.K. Boutle[53], A. Boveia[30], J. Boyd[30], I.R. Boyko[65], I. Bozic[13],
J. Bracinik[18], A. Brandt[8], G. Brandt[54], O. Brandt[58a], U. Bratzler[156], B. Brau[86], J.E. Brau[116],
H.M. Braun[175,*], W.D. Breaden Madden[53], K. Brendlinger[122], A.J. Brennan[88], L. Brenner[107],
R. Brenner[166], S. Bressler[172], T.M. Bristow[46], D. Britton[53], D. Britzger[42], F.M. Brochu[28], I. Brock[21],
R. Brock[90], J. Bronner[101], G. Brooijmans[35], T. Brooks[77], W.K. Brooks[32b], J. Brosamer[15], E. Brost[116],
P.A. Bruckman de Renstrom[39], D. Bruncko[144b], R. Bruneliere[48], A. Bruni[20a], G. Bruni[20a],
M. Bruschi[20a], N. Bruscino[21], L. Bryngemark[81], T. Buanes[14], Q. Buat[142], P. Buchholz[141],
A.G. Buckley[53], I.A. Budagov[65], F. Buehrer[48], L. Bugge[119], M.K. Bugge[119], O. Bulekov[98], D. Bullock[8],
H. Burckhart[30], S. Burdin[74], C.D. Burgard[48], B. Burghgrave[108], S. Burke[131], I. Burmeister[43],
E. Busato[34], D. Büscher[48], V. Büscher[83], P. Bussey[53], J.M. Butler[22], A.I. Butt[3], C.M. Buttar[53],
J.M. Butterworth[78], P. Butti[107], W. Buttinger[25], A. Buzatu[53], A.R. Buzykaev[109,c], S. Cabrera Urbán[167],
D. Caforio[128], V.M. Cairo[37a,37b], O. Cakir[4a], N. Calace[49], P. Calafiura[15], A. Calandri[136], G. Calderini[80],
P. Calfayan[100], L.P. Caloba[24a], D. Calvet[34], S. Calvet[34], R. Camacho Toro[31], S. Camarda[42],
P. Camarri[133a,133b], D. Cameron[119], R. Caminal Armadans[165], S. Campana[30], M. Campanelli[78],
A. Campoverde[148], V. Canale[104a,104b], A. Canepa[159a], M. Cano Bret[33e], J. Cantero[82], R. Cantrill[126a],
T. Cao[40], M.D.M. Capeans Garrido[30], I. Caprini[26b], M. Caprini[26b], M. Capua[37a,37b], R. Caputo[83],
R.M. Carbone[35], R. Cardarelli[133a], F. Cardillo[48], T. Carli[30], G. Carlino[104a], L. Carminati[91a,91b],
S. Caron[106], E. Carquin[32a], G.D. Carrillo-Montoya[30], J.R. Carter[28], J. Carvalho[126a,126c], D. Casadei[78],
M.P. Casado[12], M. Casolino[12], D.W. Casper[163], E. Castaneda-Miranda[145a], A. Castelli[107],
V. Castillo Gimenez[167], N.F. Castro[126a,h], P. Catastini[57], A. Catinaccio[30], J.R. Catmore[119], A. Cattai[30],
J. Caudron[83], V. Cavaliere[165], D. Cavalli[91a], M. Cavalli-Sforza[12], V. Cavasinni[124a,124b],
F. Ceradini[134a,134b], L. Cerda Alberich[167], B.C. Cerio[45], K. Cerny[129], A.S. Cerqueira[24b], A. Cerri[149],
L. Cerrito[76], F. Cerutti[15], M. Cerv[30], A. Cervelli[17], S.A. Cetin[19c], A. Chafaq[135a], D. Chakraborty[108],
I. Chalupkova[129], Y.L. Chan[60a], P. Chang[165], J.D. Chapman[28], D.G. Charlton[18], C.C. Chau[158],
C.A. Chavez Barajas[149], S. Cheatham[152], A. Chegwidden[90], S. Chekanov[6], S.V. Chekulaev[159a],
G.A. Chelkov[65,i], M.A. Chelstowska[89], C. Chen[64], H. Chen[25], K. Chen[148], L. Chen[33d,j], S. Chen[33c],
S. Chen[155], X. Chen[33f], Y. Chen[67], H.C. Cheng[89], Y. Cheng[31], A. Cheplakov[65], E. Cheremushkina[130],
R. Cherkaoui El Moursli[135e], V. Chernyatin[25,*], E. Cheu[7], L. Chevalier[136], V. Chiarella[47],
G. Chiarelli[124a,124b], G. Chiodini[73a], A.S. Chisholm[18], R.T. Chislett[78], A. Chitan[26b], M.V. Chizhov[65],
K. Choi[61], S. Chouridou[9], B.K.B. Chow[100], V. Christodoulou[78], D. Chromek-Burckhart[30],
J. Chudoba[127], A.J. Chuinard[87], J.J. Chwastowski[39], L. Chytka[115], G. Ciapetti[132a,132b], A.K. Ciftci[4a],
D. Cinca[53], V. Cindro[75], I.A. Cioara[21], A. Ciocio[15], F. Cirotto[104a,104b], Z.H. Citron[172], M. Ciubancan[26b],
A. Clark[49], B.L. Clark[57], P.J. Clark[46], R.N. Clarke[15], C. Clement[146a,146b], Y. Coadou[85],
M. Cobal[164a,164c], A. Coccaro[49], J. Cochran[64], L. Coffey[23], J.G. Cogan[143], L. Colasurdo[106], B. Cole[35],
S. Cole[108], A.P. Colijn[107], J. Collot[55], T. Colombo[58c], G. Compostella[101], P. Conde Muiño[126a,126b],
E. Coniavitis[48], S.H. Connell[145b], I.A. Connelly[77], V. Consorti[48], S. Constantinescu[26b], C. Conta[121a,121b],
G. Conti[30], F. Conventi[104a,k], M. Cooke[15], B.D. Cooper[78], A.M. Cooper-Sarkar[120], T. Cornelissen[175],
M. Corradi[20a], F. Corriveau[87,l], A. Corso-Radu[163], A. Cortes-Gonzalez[12], G. Cortiana[101], G. Costa[91a],
M.J. Costa[167], D. Costanzo[139], D. Côté[8], G. Cottin[28], G. Cowan[77], B.E. Cox[84], K. Cranmer[110],
G. Cree[29], S. Crépé-Renaudin[55], F. Crescioli[80], W.A. Cribbs[146a,146b], M. Crispin Ortuzar[120],
M. Cristinziani[21], V. Croft[106], G. Crosetti[37a,37b], T. Cuhadar Donszelmann[139], J. Cummings[176],
M. Curatolo[47], J. Cúth[83], C. Cuthbert[150], H. Czirr[141], P. Czodrowski[3], S. D'Auria[53], M. D'Onofrio[74],

M.J. Da Cunha Sargedas De Sousa[126a,126b], C. Da Via[84], W. Dabrowski[38a], A. Dafinca[120], T. Dai[89],
O. Dale[14], F. Dallaire[95], C. Dallapiccola[86], M. Dam[36], J.R. Dandoy[31], N.P. Dang[48], A.C. Daniells[18],
M. Danninger[168], M. Dano Hoffmann[136], V. Dao[48], G. Darbo[50a], S. Darmora[8], J. Dassoulas[3],
A. Dattagupta[61], W. Davey[21], C. David[169], T. Davidek[129], E. Davies[120,m], M. Davies[153], P. Davison[78],
Y. Davygora[58a], E. Dawe[88], I. Dawson[139], R.K. Daya-Ishmukhametova[86], K. De[8], R. de Asmundis[104a],
A. De Benedetti[113], S. De Castro[20a,20b], S. De Cecco[80], N. De Groot[106], P. de Jong[107], H. De la Torre[82],
F. De Lorenzi[64], D. De Pedis[132a], A. De Salvo[132a], U. De Sanctis[149], A. De Santo[149],
J.B. De Vivie De Regie[117], W.J. Dearnaley[72], R. Debbe[25], C. Debenedetti[137], D.V. Dedovich[65],
I. Deigaard[107], J. Del Peso[82], T. Del Prete[124a,124b], D. Delgove[117], F. Deliot[136], C.M. Delitzsch[49],
M. Deliyergiyev[75], A. Dell'Acqua[30], L. Dell'Asta[22], M. Dell'Orso[124a,124b], M. Della Pietra[104a,k],
D. della Volpe[49], M. Delmastro[5], P.A. Delsart[55], C. Deluca[107], D.A. DeMarco[158], S. Demers[176],
M. Demichev[65], A. Demilly[80], S.P. Denisov[130], D. Derendarz[39], J.E. Derkaoui[135d], F. Derue[80],
P. Dervan[74], K. Desch[21], C. Deterre[42], K. Dette[43], P.O. Deviveiros[30], A. Dewhurst[131], S. Dhaliwal[23],
A. Di Ciaccio[133a,133b], L. Di Ciaccio[5], A. Di Domenico[132a,132b], C. Di Donato[104a,104b], A. Di Girolamo[30],
B. Di Girolamo[30], A. Di Mattia[152], B. Di Micco[134a,134b], R. Di Nardo[47], A. Di Simone[48], R. Di Sipio[158],
D. Di Valentino[29], C. Diaconu[85], M. Diamond[158], F.A. Dias[46], M.A. Diaz[32a], E.B. Diehl[89], J. Dietrich[16],
S. Diglio[85], A. Dimitrievska[13], J. Dingfelder[21], P. Dita[26b], S. Dita[26b], F. Dittus[30], F. Djama[85],
T. Djobava[51b], J.I. Djuvsland[58a], M.A.B. do Vale[24c], D. Dobos[30], M. Dobre[26b], C. Doglioni[81],
T. Dohmae[155], J. Dolejsi[129], Z. Dolezal[129], B.A. Dolgoshein[98,*], M. Donadelli[24d], S. Donati[124a,124b],
P. Dondero[121a,121b], J. Donini[34], J. Dopke[131], A. Doria[104a], M.T. Dova[71], A.T. Doyle[53], E. Drechsler[54],
M. Dris[10], Y. Du[33d], E. Dubreuil[34], E. Duchovni[172], G. Duckeck[100], O.A. Ducu[26b,85], D. Duda[107],
A. Dudarev[30], L. Duflot[117], L. Duguid[77], M. Dührssen[30], M. Dunford[58a], H. Duran Yildiz[4a],
M. Düren[52], A. Durglishvili[51b], D. Duschinger[44], B. Dutta[42], M. Dyndal[38a], C. Eckardt[42],
K.M. Ecker[101], R.C. Edgar[89], W. Edson[2], N.C. Edwards[46], W. Ehrenfeld[21], T. Eifert[30], G. Eigen[14],
K. Einsweiler[15], T. Ekelof[166], M. El Kacimi[135c], M. Ellert[166], S. Elles[5], F. Ellinghaus[175], A.A. Elliot[169],
N. Ellis[30], J. Elmsheuser[100], M. Elsing[30], D. Emeliyanov[131], Y. Enari[155], O.C. Endner[83], M. Endo[118],
J. Erdmann[43], A. Ereditato[17], G. Ernis[175], J. Ernst[2], M. Ernst[25], S. Errede[165], E. Ertel[83], M. Escalier[117],
H. Esch[43], C. Escobar[125], B. Esposito[47], A.I. Etienvre[136], E. Etzion[153], H. Evans[61], A. Ezhilov[123],
L. Fabbri[20a,20b], G. Facini[31], R.M. Fakhrutdinov[130], S. Falciano[132a], R.J. Falla[78], J. Faltova[129],
Y. Fang[33a], M. Fanti[91a,91b], A. Farbin[8], A. Farilla[134a], T. Farooque[12], S. Farrell[15], S.M. Farrington[170],
P. Farthouat[30], F. Fassi[135e], P. Fassnacht[30], D. Fassouliotis[9], M. Faucci Giannelli[77], A. Favareto[50a,50b],
L. Fayard[117], O.L. Fedin[123,n], W. Fedorko[168], S. Feigl[30], L. Feligioni[85], C. Feng[33d], E.J. Feng[30],
H. Feng[89], A.B. Fenyuk[130], L. Feremenga[8], P. Fernandez Martinez[167], S. Fernandez Perez[30],
J. Ferrando[53], A. Ferrari[166], P. Ferrari[107], R. Ferrari[121a], D.E. Ferreira de Lima[53], A. Ferrer[167],
D. Ferrere[49], C. Ferretti[89], A. Ferretto Parodi[50a,50b], M. Fiascaris[31], F. Fiedler[83], A. Filipčič[75],
M. Filipuzzi[42], F. Filthaut[106], M. Fincke-Keeler[169], K.D. Finelli[150], M.C.N. Fiolhais[126a,126c],
L. Fiorini[167], A. Firan[40], A. Fischer[2], C. Fischer[12], J. Fischer[175], W.C. Fisher[90], N. Flaschel[42],
I. Fleck[141], P. Fleischmann[89], G.T. Fletcher[139], G. Fletcher[76], R.R.M. Fletcher[122], T. Flick[175],
A. Floderus[81], L.R. Flores Castillo[60a], M.J. Flowerdew[101], A. Formica[136], A. Forti[84], D. Fournier[117],
H. Fox[72], S. Fracchia[12], P. Francavilla[80], M. Franchini[20a,20b], D. Francis[30], L. Franconi[119],
M. Franklin[57], M. Frate[163], M. Fraternali[121a,121b], D. Freeborn[78], S.T. French[28],
S.M. Fressard-Batraneanu[30], F. Friedrich[44], D. Froidevaux[30], J.A. Frost[120], C. Fukunaga[156],
E. Fullana Torregrosa[83], B.G. Fulsom[143], T. Fusayasu[102], J. Fuster[167], C. Gabaldon[55], O. Gabizon[175],
A. Gabrielli[20a,20b], A. Gabrielli[15], G.P. Gach[18], S. Gadatsch[30], S. Gadomski[49], G. Gagliardi[50a,50b],
P. Gagnon[61], C. Galea[106], B. Galhardo[126a,126c], E.J. Gallas[120], B.J. Gallop[131], P. Gallus[128], G. Galster[36],
K.K. Gan[111], J. Gao[33b,85], Y. Gao[46], Y.S. Gao[143,f], F.M. Garay Walls[46], F. Garberson[176], C. García[167],
J.E. García Navarro[167], M. Garcia-Sciveres[15], R.W. Gardner[31], N. Garelli[143], V. Garonne[119], C. Gatti[47],

A. Gaudiello[50a,50b], G. Gaudio[121a], B. Gaur[141], L. Gauthier[95], P. Gauzzi[132a,132b], I.L. Gavrilenko[96], C. Gay[168], G. Gaycken[21], E.N. Gazis[10], P. Ge[33d], Z. Gecse[168], C.N.P. Gee[131], Ch. Geich-Gimbel[21], M.P. Geisler[58a], C. Gemme[50a], M.H. Genest[55], C. Geng[33b,o], S. Gentile[132a,132b], M. George[54], S. George[77], D. Gerbaudo[163], A. Gershon[153], S. Ghasemi[141], H. Ghazlane[135b], B. Giacobbe[20a], S. Giagu[132a,132b], V. Giangiobbe[12], P. Giannetti[124a,124b], B. Gibbard[25], S.M. Gibson[77], M. Gignac[168], M. Gilchriese[15], T.P.S. Gillam[28], D. Gillberg[30], G. Gilles[34], D.M. Gingrich[3,d], N. Giokaris[9], M.P. Giordani[164a,164c], F.M. Giorgi[20a], F.M. Giorgi[16], P.F. Giraud[136], P. Giromini[47], D. Giugni[91a], C. Giuliani[101], M. Giulini[58b], B.K. Gjelsten[119], S. Gkaitatzis[154], I. Gkialas[154], E.L. Gkougkousis[117], L.K. Gladilin[99], C. Glasman[82], J. Glatzer[30], P.C.F. Glaysher[46], A. Glazov[42], M. Goblirsch-Kolb[101], J.R. Goddard[76], J. Godlewski[39], S. Goldfarb[89], T. Golling[49], D. Golubkov[130], A. Gomes[126a,126b,126d], R. Gonçalo[126a], J. Goncalves Pinto Firmino Da Costa[136], L. Gonella[21], S. González de la Hoz[167], G. Gonzalez Parra[12], S. Gonzalez-Sevilla[49], L. Goossens[30], P.A. Gorbounov[97], H.A. Gordon[25], I. Gorelov[105], B. Gorini[30], E. Gorini[73a,73b], A. Gorišek[75], E. Gornicki[39], A.T. Goshaw[45], C. Gössling[43], M.I. Gostkin[65], D. Goujdami[135c], A.G. Goussiou[138], N. Govender[145b], E. Gozani[152], H.M.X. Grabas[137], L. Graber[54], I. Grabowska-Bold[38a], P.O.J. Gradin[166], P. Grafström[20a,20b], J. Gramling[49], E. Gramstad[119], S. Grancagnolo[16], V. Gratchev[123], H.M. Gray[30], E. Graziani[134a], Z.D. Greenwood[79,p], C. Grefe[21], K. Gregersen[78], I.M. Gregor[42], P. Grenier[143], J. Griffiths[8], A.A. Grillo[137], K. Grimm[72], S. Grinstein[12,q], Ph. Gris[34], J.-F. Grivaz[117], J.P. Grohs[44], A. Grohsjean[42], E. Gross[172], J. Grosse-Knetter[54], G.C. Grossi[79], Z.J. Grout[149], L. Guan[89], J. Guenther[128], F. Guescini[49], D. Guest[163], O. Gueta[153], E. Guido[50a,50b], T. Guillemin[117], S. Guindon[2], U. Gul[53], C. Gumpert[30], J. Guo[33e], Y. Guo[33b,o], S. Gupta[120], G. Gustavino[132a,132b], P. Gutierrez[113], N.G. Gutierrez Ortiz[78], C. Gutschow[44], C. Guyot[136], C. Gwenlan[120], C.B. Gwilliam[74], A. Haas[110], C. Haber[15], H.K. Hadavand[8], N. Haddad[135e], P. Haefner[21], S. Hageböck[21], Z. Hajduk[39], H. Hakobyan[177], M. Haleem[42], J. Haley[114], D. Hall[120], G. Halladjian[90], G.D. Hallewell[85], K. Hamacher[175], P. Hamal[115], K. Hamano[169], A. Hamilton[145a], G.N. Hamity[139], P.G. Hamnett[42], L. Han[33b], K. Hanagaki[66,r], K. Hanawa[155], M. Hance[137], B. Haney[122], P. Hanke[58a], R. Hanna[136], J.B. Hansen[36], J.D. Hansen[36], M.C. Hansen[21], P.H. Hansen[36], K. Hara[160], A.S. Hard[173], T. Harenberg[175], F. Hariri[117], S. Harkusha[92], R.D. Harrington[46], P.F. Harrison[170], F. Hartjes[107], M. Hasegawa[67], Y. Hasegawa[140], A. Hasib[113], S. Hassani[136], S. Haug[17], R. Hauser[90], L. Hauswald[44], M. Havranek[127], C.M. Hawkes[18], R.J. Hawkings[30], A.D. Hawkins[81], T. Hayashi[160], D. Hayden[90], C.P. Hays[120], J.M. Hays[76], H.S. Hayward[74], S.J. Haywood[131], S.J. Head[18], T. Heck[83], V. Hedberg[81], L. Heelan[8], S. Heim[122], T. Heim[175], B. Heinemann[15], L. Heinrich[110], J. Hejbal[127], L. Helary[22], S. Hellman[146a,146b], C. Helsens[12], J. Henderson[120], R.C.W. Henderson[72], Y. Heng[173], C. Hengler[42], S. Henkelmann[168], A. Henrichs[176], A.M. Henriques Correia[30], S. Henrot-Versille[117], G.H. Herbert[16], Y. Hernández Jiménez[167], G. Herten[48], R. Hertenberger[100], L. Hervas[30], G.G. Hesketh[78], N.P. Hessey[107], J.W. Hetherly[40], R. Hickling[76], E. Higón-Rodriguez[167], E. Hill[169], J.C. Hill[28], K.H. Hiller[42], S.J. Hillier[18], I. Hinchliffe[15], E. Hines[122], R.R. Hinman[15], M. Hirose[157], D. Hirschbuehl[175], J. Hobbs[148], N. Hod[107], M.C. Hodgkinson[139], P. Hodgson[139], A. Hoecker[30], M.R. Hoeferkamp[105], F. Hoenig[100], M. Hohlfeld[83], D. Hohn[21], T.R. Holmes[15], M. Homann[43], T.M. Hong[125], W.H. Hopkins[116], Y. Horii[103], A.J. Horton[142], J-Y. Hostachy[55], S. Hou[151], A. Hoummada[135a], J. Howard[120], J. Howarth[42], M. Hrabovsky[115], I. Hristova[16], J. Hrivnac[117], T. Hryn'ova[5], A. Hrynevich[93], C. Hsu[145c], P.J. Hsu[151,s], S.-C. Hsu[138], D. Hu[35], Q. Hu[33b], X. Hu[89], Y. Huang[42], Z. Hubacek[128], F. Hubaut[85], F. Huegging[21], T.B. Huffman[120], E.W. Hughes[35], G. Hughes[72], M. Huhtinen[30], T.A. Hülsing[83], N. Huseynov[65,b], J. Huston[90], J. Huth[57], G. Iacobucci[49], G. Iakovidis[25], I. Ibragimov[141], L. Iconomidou-Fayard[117], E. Ideal[176], Z. Idrissi[135e], P. Iengo[30], O. Igonkina[107], T. Iizawa[171], Y. Ikegami[66], K. Ikematsu[141], M. Ikeno[66], Y. Ilchenko[31,t], D. Iliadis[154], N. Ilic[143], T. Ince[101], G. Introzzi[121a,121b], P. Ioannou[9], M. Iodice[134a], K. Iordanidou[35], V. Ippolito[57], A. Irles Quiles[167], C. Isaksson[166], M. Ishino[68], M. Ishitsuka[157], R. Ishmukhametov[111], C. Issever[120],

S. Istin[19a], J.M. Iturbe Ponce[84], R. Iuppa[133a,133b], J. Ivarsson[81], W. Iwanski[39], H. Iwasaki[66], J.M. Izen[41], V. Izzo[104a], S. Jabbar[3], B. Jackson[122], M. Jackson[74], P. Jackson[1], M.R. Jaekel[30], V. Jain[2], K. Jakobs[48], S. Jakobsen[30], T. Jakoubek[127], J. Jakubek[128], D.O. Jamin[114], D.K. Jana[79], E. Jansen[78], R. Jansky[62], J. Janssen[21], M. Janus[54], G. Jarlskog[81], N. Javadov[65,b], T. Javůrek[48], L. Jeanty[15], J. Jejelava[51a,u], G.-Y. Jeng[150], D. Jennens[88], P. Jenni[48,v], J. Jentzsch[43], C. Jeske[170], S. Jézéquel[5], H. Ji[173], J. Jia[148], Y. Jiang[33b], S. Jiggins[78], J. Jimenez Pena[167], S. Jin[33a], A. Jinaru[26b], O. Jinnouchi[157], M.D. Joergensen[36], P. Johansson[139], K.A. Johns[7], W.J. Johnson[138], K. Jon-And[146a,146b], G. Jones[170], R.W.L. Jones[72], T.J. Jones[74], J. Jongmanns[58a], P.M. Jorge[126a,126b], K.D. Joshi[84], J. Jovicevic[159a], X. Ju[173], A. Juste Rozas[12,q], M. Kaci[167], A. Kaczmarska[39], M. Kado[117], H. Kagan[111], M. Kagan[143], S.J. Kahn[85], E. Kajomovitz[45], C.W. Kalderon[120], S. Kama[40], A. Kamenshchikov[130], N. Kanaya[155], S. Kaneti[28], V.A. Kantserov[98], J. Kanzaki[66], B. Kaplan[110], L.S. Kaplan[173], A. Kapliy[31], D. Kar[145c], K. Karakostas[10], A. Karamaoun[3], N. Karastathis[10,107], M.J. Kareem[54], E. Karentzos[10], M. Karnevskiy[83], S.N. Karpov[65], Z.M. Karpova[65], K. Karthik[110], V. Kartvelishvili[72], A.N. Karyukhin[130], K. Kasahara[160], L. Kashif[173], R.D. Kass[111], A. Kastanas[14], Y. Kataoka[155], C. Kato[155], A. Katre[49], J. Katzy[42], K. Kawade[103], K. Kawagoe[70], T. Kawamoto[155], G. Kawamura[54], S. Kazama[155], V.F. Kazanin[109,c], R. Keeler[169], R. Kehoe[40], J.S. Keller[42], J.J. Kempster[77], H. Keoshkerian[84], O. Kepka[127], B.P. Kerševan[75], S. Kersten[175], R.A. Keyes[87], F. Khalil-zada[11], H. Khandanyan[146a,146b], A. Khanov[114], A.G. Kharlamov[109,c], T.J. Khoo[28], V. Khovanskiy[97], E. Khramov[65], J. Khubua[51b,w], S. Kido[67], H.Y. Kim[8], S.H. Kim[160], Y.K. Kim[31], N. Kimura[154], O.M. Kind[16], B.T. King[74], M. King[167], S.B. King[168], J. Kirk[131], A.E. Kiryunin[101], T. Kishimoto[67], D. Kisielewska[38a], F. Kiss[48], K. Kiuchi[160], O. Kivernyk[136], E. Kladiva[144b], M.H. Klein[35], M. Klein[74], U. Klein[74], K. Kleinknecht[83], P. Klimek[146a,146b], A. Klimentov[25], R. Klingenberg[43], J.A. Klinger[139], T. Klioutchnikova[30], E.-E. Kluge[58a], P. Kluit[107], S. Kluth[101], J. Knapik[39], E. Kneringer[62], E.B.F.G. Knoops[85], A. Knue[53], A. Kobayashi[155], D. Kobayashi[157], T. Kobayashi[155], M. Kobel[44], M. Kocian[143], P. Kodys[129], T. Koffas[29], E. Koffeman[107], L.A. Kogan[120], S. Kohlmann[175], Z. Kohout[128], T. Kohriki[66], T. Koi[143], H. Kolanoski[16], M. Kolb[58b], I. Koletsou[5], A.A. Komar[96,*], Y. Komori[155], T. Kondo[66], N. Kondrashova[42], K. Köneke[48], A.C. König[106], T. Kono[66], R. Konoplich[110,x], N. Konstantinidis[78], R. Kopeliansky[152], S. Koperny[38a], L. Köpke[83], A.K. Kopp[48], K. Korcyl[39], K. Kordas[154], A. Korn[78], A.A. Korol[109,c], I. Korolkov[12], E.V. Korolkova[139], O. Kortner[101], S. Kortner[101], T. Kosek[129], V.V. Kostyukhin[21], V.M. Kotov[65], A. Kotwal[45], A. Kourkoumeli-Charalampidi[154], C. Kourkoumelis[9], V. Kouskoura[25], A. Koutsman[159a], R. Kowalewski[169], T.Z. Kowalski[38a], W. Kozanecki[136], A.S. Kozhin[130], V.A. Kramarenko[99], G. Kramberger[75], D. Krasnopevtsev[98], M.W. Krasny[80], A. Krasznahorkay[30], J.K. Kraus[21], A. Kravchenko[25], S. Kreiss[110], M. Kretz[58c], J. Kretzschmar[74], K. Kreutzfeldt[52], P. Krieger[158], K. Krizka[31], K. Kroeninger[43], H. Kroha[101], J. Kroll[122], J. Kroseberg[21], J. Krstic[13], U. Kruchonak[65], H. Krüger[21], N. Krumnack[64], A. Kruse[173], M.C. Kruse[45], M. Kruskal[22], T. Kubota[88], H. Kucuk[78], S. Kuday[4b], S. Kuehn[48], A. Kugel[58c], F. Kuger[174], A. Kuhl[137], T. Kuhl[42], V. Kukhtin[65], R. Kukla[136], Y. Kulchitsky[92], S. Kuleshov[32b], M. Kuna[132a,132b], T. Kunigo[68], A. Kupco[127], H. Kurashige[67], Y.A. Kurochkin[92], V. Kus[127], E.S. Kuwertz[169], M. Kuze[157], J. Kvita[115], T. Kwan[169], D. Kyriazopoulos[139], A. La Rosa[137], J.L. La Rosa Navarro[24d], L. La Rotonda[37a,37b], C. Lacasta[167], F. Lacava[132a,132b], J. Lacey[29], H. Lacker[16], D. Lacour[80], V.R. Lacuesta[167], E. Ladygin[65], R. Lafaye[5], B. Laforge[80], T. Lagouri[176], S. Lai[54], L. Lambourne[78], S. Lammers[61], C.L. Lampen[7], W. Lampl[7], E. Lançon[136], U. Landgraf[48], M.P.J. Landon[76], V.S. Lang[58a], J.C. Lange[12], A.J. Lankford[163], F. Lanni[25], K. Lantzsch[21], A. Lanza[121a], S. Laplace[80], C. Lapoire[30], J.F. Laporte[136], T. Lari[91a], F. Lasagni Manghi[20a,20b], M. Lassnig[30], P. Laurelli[47], W. Lavrijsen[15], A.T. Law[137], P. Laycock[74], T. Lazovich[57], O. Le Dortz[80], E. Le Guirriec[85], E. Le Menedeu[12], M. LeBlanc[169], T. LeCompte[6], F. Ledroit-Guillon[55], C.A. Lee[145a], S.C. Lee[151], L. Lee[1], G. Lefebvre[80], M. Lefebvre[169], F. Legger[100], C. Leggett[15], A. Lehan[74], G. Lehmann Miotto[30], X. Lei[7], W.A. Leight[29], A. Leisos[154,y], A.G. Leister[176], M.A.L. Leite[24d], R. Leitner[129], D. Lellouch[172], B. Lemmer[54], K.J.C. Leney[78], T. Lenz[21], B. Lenzi[30], R. Leone[7], S. Leone[124a,124b], C. Leonidopoulos[46], S. Leontsinis[10], C. Leroy[95], C.G. Lester[28], M. Levchenko[123], J. Levêque[5], D. Levin[89], L.J. Levinson[172], M. Levy[18], A. Lewis[120], A.M. Leyko[21], M. Leyton[41], B. Li[33b,z], H. Li[148], H.L. Li[31], L. Li[45], L. Li[33e], S. Li[45], X. Li[84], Y. Li[33c,aa], Z. Liang[137], H. Liao[34], B. Liberti[133a], A. Liblong[158], P. Lichard[30], K. Lie[165], J. Liebal[21], W. Liebig[14], C. Limbach[21], A. Limosani[150], S.C. Lin[151,ab], T.H. Lin[83], F. Linde[107], B.E. Lindquist[148], J.T. Linnemann[90], E. Lipeles[122], A. Lipniacka[14], M. Lisovyi[58b], T.M. Liss[165], D. Lissauer[25], A. Lister[168], A.M. Litke[137], B. Liu[151,ac], D. Liu[151], H. Liu[89], J. Liu[85], J.B. Liu[33b], K. Liu[85], L. Liu[165], M. Liu[45], M. Liu[33b], Y. Liu[33b], M. Livan[121a,121b], A. Lleres[55], J. Llorente Merino[82], S.L. Lloyd[76], F. Lo Sterzo[151], E. Lobodzinska[42], P. Loch[7], W.S. Lockman[137], F.K. Loebinger[84], A.E. Loevschall-Jensen[36], K.M. Loew[23], A. Loginov[176], T. Lohse[16], K. Lohwasser[42], M. Lokajicek[127], B.A. Long[22], J.D. Long[165], R.E. Long[72], K.A. Looper[111], L. Lopes[126a], D. Lopez Mateos[57], B. Lopez Paredes[139], I. Lopez Paz[12], J. Lorenz[100], N. Lorenzo Martinez[61], M. Losada[162], P.J. Lösel[100], X. Lou[33a], A. Lounis[117], J. Love[6], P.A. Love[72], H. Lu[60a], N. Lu[89], H.J. Lubatti[138], C. Luci[132a,132b], A. Lucotte[55], C. Luedtke[48], F. Luehring[61], W. Lukas[62], L. Luminari[132a], O. Lundberg[146a,146b], B. Lund-Jensen[147], D. Lynn[25], R. Lysak[127], E. Lytken[81], H. Ma[25], L.L. Ma[33d], G. Maccarrone[47], A. Macchiolo[101], C.M. Macdonald[139], B. Maček[75], J. Machado Miguens[122,126b], D. Macina[30], D. Madaffari[85], R. Madar[34], H.J. Maddocks[72], W.F. Mader[44], A. Madsen[166], J. Maeda[67], S. Maeland[14], T. Maeno[25], A. Maevskiy[99], E. Magradze[54], K. Mahboubi[48], J. Mahlstedt[107], C. Maiani[136], C. Maidantchik[24a], A.A. Maier[101], T. Maier[100], A. Maio[126a,126b,126d], S. Majewski[116], Y. Makida[66], N. Makovec[117], B. Malaescu[80], Pa. Malecki[39], V.P. Maleev[123], F. Malek[55], U. Mallik[63], D. Malon[6], C. Malone[143], S. Maltezos[10], V.M. Malyshev[109], S. Malyukov[30], J. Mamuzic[42], G. Mancini[47], B. Mandelli[30], L. Mandelli[91a], I. Mandić[75], R. Mandrysch[63], J. Maneira[126a,126b], L. Manhaes de Andrade Filho[24b], J. Manjarres Ramos[159b], A. Mann[100], A. Manousakis-Katsikakis[9], B. Mansoulie[136], R. Mantifel[87], M. Mantoani[54], L. Mapelli[30], L. March[145c], G. Marchiori[80], M. Marcisovsky[127], C.P. Marino[169], M. Marjanovic[13], D.E. Marley[89], F. Marroquim[24a], S.P. Marsden[84], Z. Marshall[15], L.F. Marti[17], S. Marti-Garcia[167], B. Martin[90], T.A. Martin[170], V.J. Martin[46], B. Martin dit Latour[14], M. Martinez[12,q], S. Martin-Haugh[131], V.S. Martoiu[26b], A.C. Martyniuk[78], M. Marx[138], F. Marzano[132a], A. Marzin[30], L. Masetti[83], T. Mashimo[155], R. Mashinistov[96], J. Masik[84], A.L. Maslennikov[109,c], I. Massa[20a,20b], L. Massa[20a,20b], P. Mastrandrea[5], A. Mastroberardino[37a,37b], T. Masubuchi[155], P. Mättig[175], J. Mattmann[83], J. Maurer[26b], S.J. Maxfield[74], D.A. Maximov[109,c], R. Mazini[151], S.M. Mazza[91a,91b], G. Mc Goldrick[158], S.P. Mc Kee[89], A. McCarn[89], R.L. McCarthy[148], T.G. McCarthy[29], N.A. McCubbin[131], K.W. McFarlane[56,*], J.A. Mcfayden[78], G. Mchedlidze[54], S.J. McMahon[131], R.A. McPherson[169,l], M. Medinnis[42], S. Meehan[138], S. Mehlhase[100], A. Mehta[74], K. Meier[58a], C. Meineck[100], B. Meirose[41], B.R. Mellado Garcia[145c], F. Meloni[17], A. Mengarelli[20a,20b], S. Menke[101], E. Meoni[161], K.M. Mercurio[57], S. Mergelmeyer[21], P. Mermod[49], L. Merola[104a,104b], C. Meroni[91a], F.S. Merritt[31], A. Messina[132a,132b], J. Metcalfe[25], A.S. Mete[163], C. Meyer[83], C. Meyer[122], J-P. Meyer[136], J. Meyer[107], H. Meyer Zu Theenhausen[58a], R.P. Middleton[131], S. Miglioranzi[164a,164c], L. Mijović[21], G. Mikenberg[172], M. Mikestikova[127], M. Mikuž[75], M. Milesi[88], A. Milic[30], D.W. Miller[31], C. Mills[46], A. Milov[172], D.A. Milstead[146a,146b], A.A. Minaenko[130], Y. Minami[155], I.A. Minashvili[65], A.I. Mincer[110], B. Mindur[38a], M. Mineev[65], Y. Ming[173], L.M. Mir[12], K.P. Mistry[122], T. Mitani[171], J. Mitrevski[100], V.A. Mitsou[167], A. Miucci[49], P.S. Miyagawa[139], J.U. Mjörnmark[81], T. Moa[146a,146b], K. Mochizuki[85], S. Mohapatra[35], W. Mohr[48], S. Molander[146a,146b], R. Moles-Valls[21], R. Monden[68], K. Mönig[42], C. Monini[55], J. Monk[36], E. Monnier[85], A. Montalbano[148], J. Montejo Berlingen[12], F. Monticelli[71], S. Monzani[132a,132b], R.W. Moore[3], N. Morange[117], D. Moreno[162], M. Moreno Llácer[54], P. Morettini[50a], D. Mori[142], T. Mori[155], M. Morii[57], M. Morinaga[155], V. Morisbak[119], S. Moritz[83], A.K. Morley[150], G. Mornacchi[30], J.D. Morris[76], S.S. Mortensen[36], A. Morton[53], L. Morvaj[103], M. Mosidze[51b], J. Moss[143], K. Motohashi[157], R. Mount[143], E. Mountricha[25], S.V. Mouraviev[96,*],

E.J.W. Moyse[86], S. Muanza[85], R.D. Mudd[18], F. Mueller[101], J. Mueller[125], R.S.P. Mueller[100],
T. Mueller[28], D. Muenstermann[49], P. Mullen[53], G.A. Mullier[17], F.J. Munoz Sanchez[84],
J.A. Murillo Quijada[18], W.J. Murray[170,131], H. Musheghyan[54], E. Musto[152], A.G. Myagkov[130,ad],
M. Myska[128], B.P. Nachman[143], O. Nackenhorst[54], J. Nadal[54], K. Nagai[120], R. Nagai[157], Y. Nagai[85],
K. Nagano[66], A. Nagarkar[111], Y. Nagasaka[59], K. Nagata[160], M. Nagel[101], E. Nagy[85], A.M. Nairz[30],
Y. Nakahama[30], K. Nakamura[66], T. Nakamura[155], I. Nakano[112], H. Namasivayam[41],
R.F. Naranjo Garcia[42], R. Narayan[31], D.I. Narrias Villar[58a], T. Naumann[42], G. Navarro[162], R. Nayyar[7],
H.A. Neal[89], P.Yu. Nechaeva[96], T.J. Neep[84], P.D. Nef[143], A. Negri[121a,121b], M. Negrini[20a],
S. Nektarijevic[106], C. Nellist[117], A. Nelson[163], S. Nemecek[127], P. Nemethy[110], A.A. Nepomuceno[24a],
M. Nessi[30,ae], M.S. Neubauer[165], M. Neumann[175], R.M. Neves[110], P. Nevski[25], P.R. Newman[18],
D.H. Nguyen[6], R.B. Nickerson[120], R. Nicolaidou[136], B. Nicquevert[30], J. Nielsen[137], N. Nikiforou[35],
A. Nikiforov[16], V. Nikolaenko[130,ad], I. Nikolic-Audit[80], K. Nikolopoulos[18], J.K. Nilsen[119], P. Nilsson[25],
Y. Ninomiya[155], A. Nisati[132a], R. Nisius[101], T. Nobe[155], M. Nomachi[118], I. Nomidis[29], T. Nooney[76],
S. Norberg[113], M. Nordberg[30], O. Novgorodova[44], S. Nowak[101], M. Nozaki[66], L. Nozka[115], K. Ntekas[10],
G. Nunes Hanninger[88], T. Nunnemann[100], E. Nurse[78], F. Nuti[88], F. O'grady[7], D.C. O'Neil[142],
V. O'Shea[53], F.G. Oakham[29,d], H. Oberlack[101], T. Obermann[21], J. Ocariz[80], A. Ochi[67], I. Ochoa[35],
J.P. Ochoa-Ricoux[32a], S. Oda[70], S. Odaka[66], H. Ogren[61], A. Oh[84], S.H. Oh[45], C.C. Ohm[15],
H. Ohman[166], H. Oide[30], W. Okamura[118], H. Okawa[160], Y. Okumura[31], T. Okuyama[66], A. Olariu[26b],
S.A. Olivares Pino[46], D. Oliveira Damazio[25], A. Olszewski[39], J. Olszowska[39], A. Onofre[126a,126e],
K. Onogi[103], P.U.E. Onyisi[31,t], C.J. Oram[159a], M.J. Oreglia[31], Y. Oren[153], D. Orestano[134a,134b],
N. Orlando[154], C. Oropeza Barrera[53], R.S. Orr[158], B. Osculati[50a,50b], R. Ospanov[84],
G. Otero y Garzon[27], H. Otono[70], M. Ouchrif[135d], F. Ould-Saada[119], A. Ouraou[136], K.P. Oussoren[107],
Q. Ouyang[33a], A. Ovcharova[15], M. Owen[53], R.E. Owen[18], V.E. Ozcan[19a], N. Ozturk[8], K. Pachal[142],
A. Pacheco Pages[12], C. Padilla Aranda[12], M. Pagáčová[48], S. Pagan Griso[15], E. Paganis[139], F. Paige[25],
P. Pais[86], K. Pajchel[119], G. Palacino[159b], S. Palestini[30], M. Palka[38b], D. Pallin[34], A. Palma[126a,126b],
Y.B. Pan[173], E.St. Panagiotopoulou[10], C.E. Pandini[80], J.G. Panduro Vazquez[77], P. Pani[146a,146b],
S. Panitkin[25], D. Pantea[26b], L. Paolozzi[49], Th.D. Papadopoulou[10], K. Papageorgiou[154], A. Paramonov[6],
D. Paredes Hernandez[154], M.A. Parker[28], K.A. Parker[139], F. Parodi[50a,50b], J.A. Parsons[35], U. Parzefall[48],
E. Pasqualucci[132a], S. Passaggio[50a], F. Pastore[134a,134b,*], Fr. Pastore[77], G. Pásztor[29], S. Pataraia[175],
N.D. Patel[150], J.R. Pater[84], T. Pauly[30], J. Pearce[169], B. Pearson[113], L.E. Pedersen[36], M. Pedersen[119],
S. Pedraza Lopez[167], R. Pedro[126a,126b], S.V. Peleganchuk[109,c], D. Pelikan[166], O. Penc[127], C. Peng[33a],
H. Peng[33b], B. Penning[31], J. Penwell[61], D.V. Perepelitsa[25], E. Perez Codina[159a],
M.T. Pérez García-Estañ[167], L. Perini[91a,91b], H. Pernegger[30], S. Perrella[104a,104b], R. Peschke[42],
V.D. Peshekhonov[65], K. Peters[30], R.F.Y. Peters[84], B.A. Petersen[30], T.C. Petersen[36], E. Petit[42],
A. Petridis[1], C. Petridou[154], P. Petroff[117], E. Petrolo[132a], F. Petrucci[134a,134b], N.E. Pettersson[157],
R. Pezoa[32b], P.W. Phillips[131], G. Piacquadio[143], E. Pianori[170], A. Picazio[49], E. Piccaro[76],
M. Piccinini[20a,20b], M.A. Pickering[120], R. Piegaia[27], D.T. Pignotti[111], J.E. Pilcher[31], A.D. Pilkington[84],
A.W.J. Pin[84], J. Pina[126a,126b,126d], M. Pinamonti[164a,164c,af], J.L. Pinfold[3], A. Pingel[36], S. Pires[80],
H. Pirumov[42], M. Pitt[172], C. Pizio[91a,91b], L. Plazak[144a], M.-A. Pleier[25], V. Pleskot[129], E. Plotnikova[65],
P. Plucinski[146a,146b], D. Pluth[64], R. Poettgen[146a,146b], L. Poggioli[117], D. Pohl[21], G. Polesello[121a],
A. Poley[42], A. Policicchio[37a,37b], R. Polifka[158], A. Polini[20a], C.S. Pollard[53], V. Polychronakos[25],
K. Pommès[30], L. Pontecorvo[132a], B.G. Pope[90], G.A. Popeneciu[26c], D.S. Popovic[13], A. Poppleton[30],
S. Pospisil[128], K. Potamianos[15], I.N. Potrap[65], C.J. Potter[149], C.T. Potter[116], G. Poulard[30], J. Poveda[30],
V. Pozdnyakov[65], M.E. Pozo Astigarraga[30], P. Pralavorio[85], A. Pranko[15], S. Prasad[30], S. Prell[64],
D. Price[84], L.E. Price[6], M. Primavera[73a], S. Prince[87], M. Proissl[46], K. Prokofiev[60c], F. Prokoshin[32b],
E. Protopapadaki[136], S. Protopopescu[25], J. Proudfoot[6], M. Przybycien[38a], E. Ptacek[116],
D. Puddu[134a,134b], E. Pueschel[86], D. Puldon[148], M. Purohit[25,ag], P. Puzo[117], J. Qian[89], G. Qin[53], Y. Qin[84],

A. Quadt[54], D.R. Quarrie[15], W.B. Quayle[164a,164b], M. Queitsch-Maitland[84], D. Quilty[53], S. Raddum[119],
V. Radeka[25], V. Radescu[42], S.K. Radhakrishnan[148], P. Radloff[116], P. Rados[88], F. Ragusa[91a,91b],
G. Rahal[178], S. Rajagopalan[25], M. Rammensee[30], C. Rangel-Smith[166], F. Rauscher[100], S. Rave[83],
T. Ravenscroft[53], M. Raymond[30], A.L. Read[119], N.P. Readioff[74], D.M. Rebuzzi[121a,121b],
A. Redelbach[174], G. Redlinger[25], R. Reece[137], K. Reeves[41], L. Rehnisch[16], J. Reichert[122], H. Reisin[27],
C. Rembser[30], H. Ren[33a], A. Renaud[117], M. Rescigno[132a], S. Resconi[91a], O.L. Rezanova[109,c],
P. Reznicek[129], R. Rezvani[95], R. Richter[101], S. Richter[78], E. Richter-Was[38b], O. Ricken[21], M. Ridel[80],
P. Rieck[16], C.J. Riegel[175], J. Rieger[54], O. Rifki[113], M. Rijssenbeek[148], A. Rimoldi[121a,121b], L. Rinaldi[20a],
B. Ristić[49], E. Ritsch[30], I. Riu[12], F. Rizatdinova[114], E. Rizvi[76], S.H. Robertson[87,l],
A. Robichaud-Veronneau[87], D. Robinson[28], J.E.M. Robinson[42], A. Robson[53], C. Roda[124a,124b], S. Roe[30],
O. Røhne[119], A. Romaniouk[98], M. Romano[20a,20b], S.M. Romano Saez[34], E. Romero Adam[167],
N. Rompotis[138], M. Ronzani[48], L. Roos[80], E. Ros[167], S. Rosati[132a], K. Rosbach[48], P. Rose[137],
P.L. Rosendahl[14], O. Rosenthal[141], V. Rossetti[146a,146b], E. Rossi[104a,104b], L.P. Rossi[50a], J.H.N. Rosten[28],
R. Rosten[138], M. Rotaru[26b], I. Roth[172], J. Rothberg[138], D. Rousseau[117], C.R. Royon[136], A. Rozanov[85],
Y. Rozen[152], X. Ruan[145c], F. Rubbo[143], I. Rubinskiy[42], V.I. Rud[99], C. Rudolph[44], M.S. Rudolph[158],
F. Rühr[48], A. Ruiz-Martinez[30], Z. Rurikova[48], N.A. Rusakovich[65], A. Ruschke[100], H.L. Russell[138],
J.P. Rutherfoord[7], N. Ruthmann[30], Y.F. Ryabov[123], M. Rybar[165], G. Rybkin[117], N.C. Ryder[120],
A.F. Saavedra[150], G. Sabato[107], S. Sacerdoti[27], A. Saddique[3], H.F-W. Sadrozinski[137], R. Sadykov[65],
F. Safai Tehrani[132a], P. Saha[108], M. Sahinsoy[58a], M. Saimpert[136], T. Saito[155], H. Sakamoto[155],
Y. Sakurai[171], G. Salamanna[134a,134b], A. Salamon[133a], J.E. Salazar Loyola[32b], M. Saleem[113], D. Salek[107],
P.H. Sales De Bruin[138], D. Salihagic[101], A. Salnikov[143], J. Salt[167], D. Salvatore[37a,37b], F. Salvatore[149],
A. Salvucci[60a], A. Salzburger[30], D. Sammel[48], D. Sampsonidis[154], A. Sanchez[104a,104b], J. Sánchez[167],
V. Sanchez Martinez[167], H. Sandaker[119], R.L. Sandbach[76], H.G. Sander[83], M.P. Sanders[100],
M. Sandhoff[175], C. Sandoval[162], R. Sandstroem[101], D.P.C. Sankey[131], M. Sannino[50a,50b], A. Sansoni[47],
C. Santoni[34], R. Santonico[133a,133b], H. Santos[126a], I. Santoyo Castillo[149], K. Sapp[125], A. Sapronov[65],
J.G. Saraiva[126a,126d], B. Sarrazin[21], O. Sasaki[66], Y. Sasaki[155], K. Sato[160], G. Sauvage[5,*], E. Sauvan[5],
G. Savage[77], P. Savard[158,d], C. Sawyer[131], L. Sawyer[79,p], J. Saxon[31], C. Sbarra[20a], A. Sbrizzi[20a,20b],
T. Scanlon[78], D.A. Scannicchio[163], M. Scarcella[150], V. Scarfone[37a,37b], J. Schaarschmidt[172],
P. Schacht[101], D. Schaefer[30], R. Schaefer[42], J. Schaeffer[83], S. Schaepe[21], S. Schaetzel[58b], U. Schäfer[83],
A.C. Schaffer[117], D. Schaile[100], R.D. Schamberger[148], V. Scharf[58a], V.A. Schegelsky[123], D. Scheirich[129],
M. Schernau[163], C. Schiavi[50a,50b], C. Schillo[48], M. Schioppa[37a,37b], S. Schlenker[30], K. Schmieden[30],
C. Schmitt[83], S. Schmitt[58b], S. Schmitt[42], S. Schmitz[83], B. Schneider[159a], Y.J. Schnellbach[74],
U. Schnoor[44], L. Schoeffel[136], A. Schoening[58b], B.D. Schoenrock[90], E. Schopf[21],
A.L.S. Schorlemmer[54], M. Schott[83], D. Schouten[159a], J. Schovancova[8], S. Schramm[49], M. Schreyer[174],
N. Schuh[83], M.J. Schultens[21], H.-C. Schultz-Coulon[58a], H. Schulz[16], M. Schumacher[48],
B.A. Schumm[137], Ph. Schune[136], C. Schwanenberger[84], A. Schwartzman[143], T.A. Schwarz[89],
Ph. Schwegler[101], H. Schweiger[84], Ph. Schwemling[136], R. Schwienhorst[90], J. Schwindling[136],
T. Schwindt[21], F.G. Sciacca[17], E. Scifo[117], G. Sciolla[23], F. Scuri[124a,124b], F. Scutti[21], J. Searcy[89],
G. Sedov[42], E. Sedykh[123], P. Seema[21], S.C. Seidel[105], A. Seiden[137], F. Seifert[128], J.M. Seixas[24a],
G. Sekhniaidze[104a], K. Sekhon[89], S.J. Sekula[40], D.M. Seliverstov[123,*], N. Semprini-Cesari[20a,20b],
C. Serfon[30], L. Serin[117], L. Serkin[164a,164b], T. Serre[85], M. Sessa[134a,134b], R. Seuster[159a], H. Severini[113],
T. Sfiligoj[75], F. Sforza[30], A. Sfyrla[30], E. Shabalina[54], M. Shamim[116], L.Y. Shan[33a], R. Shang[165],
J.T. Shank[22], M. Shapiro[15], P.B. Shatalov[97], K. Shaw[164a,164b], S.M. Shaw[84], A. Shcherbakova[146a,146b],
C.Y. Shehu[149], P. Sherwood[78], L. Shi[151,ah], S. Shimizu[67], C.O. Shimmin[163], M. Shimojima[102],
M. Shiyakova[65], A. Shmeleva[96], D. Shoaleh Saadi[95], M.J. Shochet[31], S. Shojaii[91a,91b], S. Shrestha[111],
E. Shulga[98], M.A. Shupe[7], P. Sicho[127], P.E. Sidebo[147], O. Sidiropoulou[174], D. Sidorov[114],
A. Sidoti[20a,20b], F. Siegert[44], Dj. Sijacki[13], J. Silva[126a,126d], Y. Silver[153], S.B. Silverstein[146a],

V. Simak[128], O. Simard[5], Lj. Simic[13], S. Simion[117], E. Simioni[83], B. Simmons[78], D. Simon[34], P. Sinervo[158], N.B. Sinev[116], M. Sioli[20a,20b], G. Siragusa[174], A.N. Sisakyan[65,*], S.Yu. Sivoklokov[99], J. Sjölin[146a,146b], T.B. Sjursen[14], M.B. Skinner[72], H.P. Skottowe[57], P. Skubic[113], M. Slater[18], T. Slavicek[128], M. Slawinska[107], K. Sliwa[161], V. Smakhtin[172], B.H. Smart[46], L. Smestad[14], S.Yu. Smirnov[98], Y. Smirnov[98], L.N. Smirnova[99,ai], O. Smirnova[81], M.N.K. Smith[35], R.W. Smith[35], M. Smizanska[72], K. Smolek[128], A.A. Snesarev[96], G. Snidero[76], S. Snyder[25], R. Sobie[169,l], F. Socher[44], A. Soffer[153], D.A. Soh[151,ah], G. Sokhrannyi[75], C.A. Solans[30], M. Solar[128], J. Solc[128], E.Yu. Soldatov[98], U. Soldevila[167], A.A. Solodkov[130], A. Soloshenko[65], O.V. Solovyanov[130], V. Solovyev[123], P. Sommer[48], H.Y. Song[33b,z], N. Soni[1], A. Sood[15], A. Sopczak[128], B. Sopko[128], V. Sopko[128], V. Sorin[12], D. Sosa[58b], M. Sosebee[8], C.L. Sotiropoulou[124a,124b], R. Soualah[164a,164c], A.M. Soukharev[109,c], D. South[42], B.C. Sowden[77], S. Spagnolo[73a,73b], M. Spalla[124a,124b], M. Spangenberg[170], F. Spanò[77], W.R. Spearman[57], D. Sperlich[16], F. Spettel[101], R. Spighi[20a], G. Spigo[30], L.A. Spiller[88], M. Spousta[129], R.D. St. Denis[53,*], A. Stabile[91a], S. Staerz[30], J. Stahlman[122], R. Stamen[58a], S. Stamm[16], E. Stanecka[39], C. Stanescu[134a], M. Stanescu-Bellu[42], M.M. Stanitzki[42], S. Stapnes[119], E.A. Starchenko[130], J. Stark[55], P. Staroba[127], P. Starovoitov[58a], R. Staszewski[39], P. Steinberg[25], B. Stelzer[142], H.J. Stelzer[30], O. Stelzer-Chilton[159a], H. Stenzel[52], G.A. Stewart[53], J.A. Stillings[21], M.C. Stockton[87], M. Stoebe[87], G. Stoicea[26b], P. Stolte[54], S. Stonjek[101], A.R. Stradling[8], A. Straessner[44], M.E. Stramaglia[17], J. Strandberg[147], S. Strandberg[146a,146b], A. Strandlie[119], E. Strauss[143], M. Strauss[113], P. Strizenec[144b], R. Ströhmer[174], D.M. Strom[116], R. Stroynowski[40], A. Strubig[106], S.A. Stucci[17], B. Stugu[14], N.A. Styles[42], D. Su[143], J. Su[125], R. Subramaniam[79], A. Succurro[12], S. Suchek[58a], Y. Sugaya[118], M. Suk[128], V.V. Sulin[96], S. Sultansoy[4c], T. Sumida[68], S. Sun[57], X. Sun[33a], J.E. Sundermann[48], K. Suruliz[149], G. Susinno[37a,37b], M.R. Sutton[149], S. Suzuki[66], M. Svatos[127], M. Swiatlowski[31], I. Sykora[144a], T. Sykora[129], D. Ta[48], C. Taccini[134a,134b], K. Tackmann[42], J. Taenzer[158], A. Taffard[163], R. Tafirout[159a], N. Taiblum[153], H. Takai[25], R. Takashima[69], H. Takeda[67], T. Takeshita[140], Y. Takubo[66], M. Talby[85], A.A. Talyshev[109,c], J.Y.C. Tam[174], K.G. Tan[88], J. Tanaka[155], R. Tanaka[117], S. Tanaka[66], B.B. Tannenwald[111], S. Tapia Araya[32b], S. Tapprogge[83], S. Tarem[152], F. Tarrade[29], G.F. Tartarelli[91a], P. Tas[129], M. Tasevsky[127], T. Tashiro[68], E. Tassi[37a,37b], A. Tavares Delgado[126a,126b], Y. Tayalati[135d], F.E. Taylor[94], G.N. Taylor[88], P.T.E. Taylor[88], W. Taylor[159b], F.A. Teischinger[30], M. Teixeira Dias Castanheira[76], P. Teixeira-Dias[77], K.K. Temming[48], D. Temple[142], H. Ten Kate[30], P.K. Teng[151], J.J. Teoh[118], F. Tepel[175], S. Terada[66], K. Terashi[155], J. Terron[82], S. Terzo[101], M. Testa[47], R.J. Teuscher[158,l], T. Theveneaux-Pelzer[34], J.P. Thomas[18], J. Thomas-Wilsker[77], E.N. Thompson[35], P.D. Thompson[18], R.J. Thompson[84], A.S. Thompson[53], L.A. Thomsen[176], E. Thomson[122], M. Thomson[28], R.P. Thun[89,*], M.J. Tibbetts[15], R.E. Ticse Torres[85], V.O. Tikhomirov[96,aj], Yu.A. Tikhonov[109,c], S. Timoshenko[98], E. Tiouchichine[85], P. Tipton[176], S. Tisserant[85], K. Todome[157], T. Todorov[5,*], S. Todorova-Nova[129], J. Tojo[70], S. Tokár[144a], K. Tokushuku[66], K. Tollefson[90], E. Tolley[57], L. Tomlinson[84], M. Tomoto[103], L. Tompkins[143,ak], K. Toms[105], E. Torrence[116], H. Torres[142], E. Torró Pastor[138], J. Toth[85,al], F. Touchard[85], D.R. Tovey[139], T. Trefzger[174], L. Tremblet[30], A. Tricoli[30], I.M. Trigger[159a], S. Trincaz-Duvoid[80], M.F. Tripiana[12], W. Trischuk[158], B. Trocmé[55], C. Troncon[91a], M. Trottier-McDonald[15], M. Trovatelli[169], L. Truong[164a,164c], M. Trzebinski[39], A. Trzupek[39], C. Tsarouchas[30], J.C-L. Tseng[120], P.V. Tsiareshka[92], D. Tsionou[154], G. Tsipolitis[10], N. Tsirintanis[9], S. Tsiskaridze[12], V. Tsiskaridze[48], E.G. Tskhadadze[51a], K.M. Tsui[60a], I.I. Tsukerman[97], V. Tsulaia[15], S. Tsuno[66], D. Tsybychev[148], A. Tudorache[26b], V. Tudorache[26b], A.N. Tuna[57], S.A. Tupputi[20a,20b], S. Turchikhin[99,ai], D. Turecek[128], R. Turra[91a,91b], A.J. Turvey[40], P.M. Tuts[35], A. Tykhonov[49], M. Tylmad[146a,146b], M. Tyndel[131], I. Ueda[155], R. Ueno[29], M. Ughetto[146a,146b], F. Ukegawa[160], G. Unal[30], A. Undrus[25], G. Unel[163], F.C. Ungaro[48], Y. Unno[66], C. Unverdorben[100], J. Urban[144b], P. Urquijo[88], P. Urrejola[83], G. Usai[8], A. Usanova[62], L. Vacavant[85], V. Vacek[128], B. Vachon[87], C. Valderanis[83], N. Valencic[107], S. Valentinetti[20a,20b], A. Valero[167], L. Valery[12], S. Valkar[129], S. Vallecorsa[49], J.A. Valls Ferrer[167], W. Van Den Wollenberg[107], P.C. Van Der Deijl[107], R. van der Geer[107], H. van der Graaf[107], N. van Eldik[152], P. van Gemmeren[6], J. Van Nieuwkoop[142], I. van Vulpen[107], M.C. van Woerden[30], M. Vanadia[132a,132b], W. Vandelli[30], R. Vanguri[122], A. Vaniachine[6], F. Vannucci[80], G. Vardanyan[177], R. Vari[132a], E.W. Varnes[7], T. Varol[40], D. Varouchas[80], A. Vartapetian[8], K.E. Varvell[150], F. Vazeille[34], T. Vazquez Schroeder[87], J. Veatch[7], L.M. Veloce[158], F. Veloso[126a,126c], T. Velz[21], S. Veneziano[132a], A. Ventura[73a,73b], D. Ventura[86], M. Venturi[169], N. Venturi[158], A. Venturini[23], V. Vercesi[121a], M. Verducci[132a,132b], W. Verkerke[107], J.C. Vermeulen[107], A. Vest[44], M.C. Vetterli[142,d], O. Viazlo[81], I. Vichou[165], T. Vickey[139], O.E. Vickey Boeriu[139], G.H.A. Viehhauser[120], S. Viel[15], R. Vigne[62], M. Villa[20a,20b], M. Villaplana Perez[91a,91b], E. Vilucchi[47], M.G. Vincter[29], V.B. Vinogradov[65], I. Vivarelli[149], F. Vives Vaque[3], S. Vlachos[10], D. Vladoiu[100], M. Vlasak[128], M. Vogel[32a], P. Vokac[128], G. Volpi[124a,124b], M. Volpi[88], H. von der Schmitt[101], H. von Radziewski[48], E. von Toerne[21], V. Vorobel[129], K. Vorobev[98], M. Vos[167], R. Voss[30], J.H. Vossebeld[74], N. Vranjes[13], M. Vranjes Milosavljevic[13], V. Vrba[127], M. Vreeswijk[107], R. Vuillermet[30], I. Vukotic[31], Z. Vykydal[128], P. Wagner[21], W. Wagner[175], H. Wahlberg[71], S. Wahrmund[44], J. Wakabayashi[103], J. Walder[72], R. Walker[100], W. Walkowiak[141], C. Wang[151], F. Wang[173], H. Wang[15], H. Wang[40], J. Wang[42], J. Wang[150], K. Wang[87], R. Wang[6], S.M. Wang[151], T. Wang[21], T. Wang[35], X. Wang[176], C. Wanotayaroj[116], A. Warburton[87], C.P. Ward[28], D.R. Wardrope[78], A. Washbrook[46], C. Wasicki[42], P.M. Watkins[18], A.T. Watson[18], I.J. Watson[150], M.F. Watson[18], G. Watts[138], S. Watts[84], B.M. Waugh[78], S. Webb[84], M.S. Weber[17], S.W. Weber[174], J.S. Webster[31], A.R. Weidberg[120], B. Weinert[61], J. Weingarten[54], C. Weiser[48], H. Weits[107], P.S. Wells[30], T. Wenaus[25], T. Wengler[30], S. Wenig[30], N. Wermes[21], M. Werner[48], P. Werner[30], M. Wessels[58a], J. Wetter[161], K. Whalen[116], A.M. Wharton[72], A. White[8], M.J. White[1], R. White[32b], S. White[124a,124b], D. Whiteson[163], F.J. Wickens[131], W. Wiedenmann[173], M. Wielers[131], P. Wienemann[21], C. Wiglesworth[36], L.A.M. Wiik-Fuchs[21], A. Wildauer[101], H.G. Wilkens[30], H.H. Williams[122], S. Williams[107], C. Willis[90], S. Willocq[86], A. Wilson[89], J.A. Wilson[18], I. Wingerter-Seez[5], F. Winklmeier[116], B.T. Winter[21], M. Wittgen[143], J. Wittkowski[100], S.J. Wollstadt[83], M.W. Wolter[39], H. Wolters[126a,126c], B.K. Wosiek[39], J. Wotschack[30], M.J. Woudstra[84], K.W. Wozniak[39], M. Wu[55], M. Wu[31], S.L. Wu[173], X. Wu[49], Y. Wu[89], T.R. Wyatt[84], B.M. Wynne[46], S. Xella[36], D. Xu[33a], L. Xu[25], B. Yabsley[150], S. Yacoob[145a], R. Yakabe[67], M. Yamada[66], D. Yamaguchi[157], Y. Yamaguchi[118], A. Yamamoto[66], S. Yamamoto[155], T. Yamanaka[155], K. Yamauchi[103], Y. Yamazaki[67], Z. Yan[22], H. Yang[33e], H. Yang[173], Y. Yang[151], W-M. Yao[15], Y.C. Yap[80], Y. Yasu[66], E. Yatsenko[5], K.H. Yau Wong[21], J. Ye[40], S. Ye[25], I. Yeletskikh[65], A.L. Yen[57], E. Yildirim[42], K. Yorita[171], R. Yoshida[6], K. Yoshihara[122], C. Young[143], C.J.S. Young[30], S. Youssef[22], D.R. Yu[15], J. Yu[8], J.M. Yu[89], J. Yu[114], L. Yuan[67], S.P.Y. Yuen[21], A. Yurkewicz[108], I. Yusuff[28,am], B. Zabinski[39], R. Zaidan[63], A.M. Zaitsev[130,ad], J. Zalieckas[14], A. Zaman[148], S. Zambito[57], L. Zanello[132a,132b], D. Zanzi[88], C. Zeitnitz[175], M. Zeman[128], A. Zemla[38a], Q. Zeng[143], K. Zengel[23], O. Zenin[130], T. Ženiš[144a], D. Zerwas[117], D. Zhang[89], F. Zhang[173], G. Zhang[33b], H. Zhang[33c], J. Zhang[6], L. Zhang[48], R. Zhang[33b,j], X. Zhang[33d], Z. Zhang[117], X. Zhao[40], Y. Zhao[33d,117], Z. Zhao[33b], A. Zhemchugov[65], J. Zhong[120], B. Zhou[89], C. Zhou[45], L. Zhou[35], L. Zhou[40], M. Zhou[148], N. Zhou[33f], C.G. Zhu[33d], H. Zhu[33a], J. Zhu[89], Y. Zhu[33b], X. Zhuang[33a], K. Zhukov[96], A. Zibell[174], D. Zieminska[61], N.I. Zimine[65], C. Zimmermann[83], S. Zimmermann[48], Z. Zinonos[54], M. Zinser[83], M. Ziolkowski[141], L. Živković[13], G. Zobernig[173], A. Zoccoli[20a,20b], M. zur Nedden[16], G. Zurzolo[104a,104b], L. Zwalinski[30].

[1] Department of Physics, University of Adelaide, Adelaide, Australia

[2] Physics Department, SUNY Albany, Albany NY, United States of America

[3] Department of Physics, University of Alberta, Edmonton AB, Canada

[4] [(a)] Department of Physics, Ankara University, Ankara; [(b)] Istanbul Aydin University, Istanbul; [(c)] Division of Physics, TOBB University of Economics and Technology, Ankara, Turkey

[5] LAPP, CNRS/IN2P3 and Université Savoie Mont Blanc, Annecy-le-Vieux, France
[6] High Energy Physics Division, Argonne National Laboratory, Argonne IL, United States of America
[7] Department of Physics, University of Arizona, Tucson AZ, United States of America
[8] Department of Physics, The University of Texas at Arlington, Arlington TX, United States of America
[9] Physics Department, University of Athens, Athens, Greece
[10] Physics Department, National Technical University of Athens, Zografou, Greece
[11] Institute of Physics, Azerbaijan Academy of Sciences, Baku, Azerbaijan
[12] Institut de Física d'Altes Energies and Departament de Física de la Universitat Autònoma de Barcelona, Barcelona, Spain
[13] Institute of Physics, University of Belgrade, Belgrade, Serbia
[14] Department for Physics and Technology, University of Bergen, Bergen, Norway
[15] Physics Division, Lawrence Berkeley National Laboratory and University of California, Berkeley CA, United States of America
[16] Department of Physics, Humboldt University, Berlin, Germany
[17] Albert Einstein Center for Fundamental Physics and Laboratory for High Energy Physics, University of Bern, Bern, Switzerland
[18] School of Physics and Astronomy, University of Birmingham, Birmingham, United Kingdom
[19] (a) Department of Physics, Bogazici University, Istanbul; (b) Department of Physics Engineering, Gaziantep University, Gaziantep; (c) Department of Physics, Dogus University, Istanbul, Turkey
[20] (a) INFN Sezione di Bologna; (b) Dipartimento di Fisica e Astronomia, Università di Bologna, Bologna, Italy
[21] Physikalisches Institut, University of Bonn, Bonn, Germany
[22] Department of Physics, Boston University, Boston MA, United States of America
[23] Department of Physics, Brandeis University, Waltham MA, United States of America
[24] (a) Universidade Federal do Rio De Janeiro COPPE/EE/IF, Rio de Janeiro; (b) Electrical Circuits Department, Federal University of Juiz de Fora (UFJF), Juiz de Fora; (c) Federal University of Sao Joao del Rei (UFSJ), Sao Joao del Rei; (d) Instituto de Fisica, Universidade de Sao Paulo, Sao Paulo, Brazil
[25] Physics Department, Brookhaven National Laboratory, Upton NY, United States of America
[26] (a) Transilvania University of Brasov, Brasov; (b) National Institute of Physics and Nuclear Engineering, Bucharest; (c) National Institute for Research and Development of Isotopic and Molecular Technologies, Physics Department, Cluj Napoca; (d) University Politehnica Bucharest, Bucharest; (e) West University in Timisoara, Timisoara, Romania
[27] Departamento de Física, Universidad de Buenos Aires, Buenos Aires, Argentina
[28] Cavendish Laboratory, University of Cambridge, Cambridge, United Kingdom
[29] Department of Physics, Carleton University, Ottawa ON, Canada
[30] CERN, Geneva, Switzerland
[31] Enrico Fermi Institute, University of Chicago, Chicago IL, United States of America
[32] (a) Departamento de Física, Pontificia Universidad Católica de Chile, Santiago; (b) Departamento de Física, Universidad Técnica Federico Santa María, Valparaíso, Chile
[33] (a) Institute of High Energy Physics, Chinese Academy of Sciences, Beijing; (b) Department of Modern Physics, University of Science and Technology of China, Anhui; (c) Department of Physics, Nanjing University, Jiangsu; (d) School of Physics, Shandong University, Shandong; (e) Department of Physics and Astronomy, Shanghai Key Laboratory for Particle Physics and Cosmology, Shanghai Jiao Tong University, Shanghai; (f) Physics Department, Tsinghua University, Beijing 100084, China
[34] Laboratoire de Physique Corpusculaire, Clermont Université and Université Blaise Pascal and CNRS/IN2P3, Clermont-Ferrand, France
[35] Nevis Laboratory, Columbia University, Irvington NY, United States of America

[36] Niels Bohr Institute, University of Copenhagen, Kobenhavn, Denmark
[37] (a) INFN Gruppo Collegato di Cosenza, Laboratori Nazionali di Frascati; (b) Dipartimento di Fisica, Università della Calabria, Rende, Italy
[38] (a) AGH University of Science and Technology, Faculty of Physics and Applied Computer Science, Krakow; (b) Marian Smoluchowski Institute of Physics, Jagiellonian University, Krakow, Poland
[39] Institute of Nuclear Physics Polish Academy of Sciences, Krakow, Poland
[40] Physics Department, Southern Methodist University, Dallas TX, United States of America
[41] Physics Department, University of Texas at Dallas, Richardson TX, United States of America
[42] DESY, Hamburg and Zeuthen, Germany
[43] Institut für Experimentelle Physik IV, Technische Universität Dortmund, Dortmund, Germany
[44] Institut für Kern- und Teilchenphysik, Technische Universität Dresden, Dresden, Germany
[45] Department of Physics, Duke University, Durham NC, United States of America
[46] SUPA - School of Physics and Astronomy, University of Edinburgh, Edinburgh, United Kingdom
[47] INFN Laboratori Nazionali di Frascati, Frascati, Italy
[48] Fakultät für Mathematik und Physik, Albert-Ludwigs-Universität, Freiburg, Germany
[49] Section de Physique, Université de Genève, Geneva, Switzerland
[50] (a) INFN Sezione di Genova; (b) Dipartimento di Fisica, Università di Genova, Genova, Italy
[51] (a) E. Andronikashvili Institute of Physics, Iv. Javakhishvili Tbilisi State University, Tbilisi; (b) High Energy Physics Institute, Tbilisi State University, Tbilisi, Georgia
[52] II Physikalisches Institut, Justus-Liebig-Universität Giessen, Giessen, Germany
[53] SUPA - School of Physics and Astronomy, University of Glasgow, Glasgow, United Kingdom
[54] II Physikalisches Institut, Georg-August-Universität, Göttingen, Germany
[55] Laboratoire de Physique Subatomique et de Cosmologie, Université Grenoble-Alpes, CNRS/IN2P3, Grenoble, France
[56] Department of Physics, Hampton University, Hampton VA, United States of America
[57] Laboratory for Particle Physics and Cosmology, Harvard University, Cambridge MA, United States of America
[58] (a) Kirchhoff-Institut für Physik, Ruprecht-Karls-Universität Heidelberg, Heidelberg; (b) Physikalisches Institut, Ruprecht-Karls-Universität Heidelberg, Heidelberg; (c) ZITI Institut für technische Informatik, Ruprecht-Karls-Universität Heidelberg, Mannheim, Germany
[59] Faculty of Applied Information Science, Hiroshima Institute of Technology, Hiroshima, Japan
[60] (a) Department of Physics, The Chinese University of Hong Kong, Shatin, N.T., Hong Kong; (b) Department of Physics, The University of Hong Kong, Hong Kong; (c) Department of Physics, The Hong Kong University of Science and Technology, Clear Water Bay, Kowloon, Hong Kong, China
[61] Department of Physics, Indiana University, Bloomington IN, United States of America
[62] Institut für Astro- und Teilchenphysik, Leopold-Franzens-Universität, Innsbruck, Austria
[63] University of Iowa, Iowa City IA, United States of America
[64] Department of Physics and Astronomy, Iowa State University, Ames IA, United States of America
[65] Joint Institute for Nuclear Research, JINR Dubna, Dubna, Russia
[66] KEK, High Energy Accelerator Research Organization, Tsukuba, Japan
[67] Graduate School of Science, Kobe University, Kobe, Japan
[68] Faculty of Science, Kyoto University, Kyoto, Japan
[69] Kyoto University of Education, Kyoto, Japan
[70] Department of Physics, Kyushu University, Fukuoka, Japan
[71] Instituto de Física La Plata, Universidad Nacional de La Plata and CONICET, La Plata, Argentina
[72] Physics Department, Lancaster University, Lancaster, United Kingdom
[73] (a) INFN Sezione di Lecce; (b) Dipartimento di Matematica e Fisica, Università del Salento, Lecce,

Italy
[74] Oliver Lodge Laboratory, University of Liverpool, Liverpool, United Kingdom
[75] Department of Physics, Jožef Stefan Institute and University of Ljubljana, Ljubljana, Slovenia
[76] School of Physics and Astronomy, Queen Mary University of London, London, United Kingdom
[77] Department of Physics, Royal Holloway University of London, Surrey, United Kingdom
[78] Department of Physics and Astronomy, University College London, London, United Kingdom
[79] Louisiana Tech University, Ruston LA, United States of America
[80] Laboratoire de Physique Nucléaire et de Hautes Energies, UPMC and Université Paris-Diderot and CNRS/IN2P3, Paris, France
[81] Fysiska institutionen, Lunds universitet, Lund, Sweden
[82] Departamento de Fisica Teorica C-15, Universidad Autonoma de Madrid, Madrid, Spain
[83] Institut für Physik, Universität Mainz, Mainz, Germany
[84] School of Physics and Astronomy, University of Manchester, Manchester, United Kingdom
[85] CPPM, Aix-Marseille Université and CNRS/IN2P3, Marseille, France
[86] Department of Physics, University of Massachusetts, Amherst MA, United States of America
[87] Department of Physics, McGill University, Montreal QC, Canada
[88] School of Physics, University of Melbourne, Victoria, Australia
[89] Department of Physics, The University of Michigan, Ann Arbor MI, United States of America
[90] Department of Physics and Astronomy, Michigan State University, East Lansing MI, United States of America
[91] (a) INFN Sezione di Milano; (b) Dipartimento di Fisica, Università di Milano, Milano, Italy
[92] B.I. Stepanov Institute of Physics, National Academy of Sciences of Belarus, Minsk, Republic of Belarus
[93] National Scientific and Educational Centre for Particle and High Energy Physics, Minsk, Republic of Belarus
[94] Department of Physics, Massachusetts Institute of Technology, Cambridge MA, United States of America
[95] Group of Particle Physics, University of Montreal, Montreal QC, Canada
[96] P.N. Lebedev Institute of Physics, Academy of Sciences, Moscow, Russia
[97] Institute for Theoretical and Experimental Physics (ITEP), Moscow, Russia
[98] National Research Nuclear University MEPhI, Moscow, Russia
[99] D.V. Skobeltsyn Institute of Nuclear Physics, M.V. Lomonosov Moscow State University, Moscow, Russia
[100] Fakultät für Physik, Ludwig-Maximilians-Universität München, München, Germany
[101] Max-Planck-Institut für Physik (Werner-Heisenberg-Institut), München, Germany
[102] Nagasaki Institute of Applied Science, Nagasaki, Japan
[103] Graduate School of Science and Kobayashi-Maskawa Institute, Nagoya University, Nagoya, Japan
[104] (a) INFN Sezione di Napoli; (b) Dipartimento di Fisica, Università di Napoli, Napoli, Italy
[105] Department of Physics and Astronomy, University of New Mexico, Albuquerque NM, United States of America
[106] Institute for Mathematics, Astrophysics and Particle Physics, Radboud University Nijmegen/Nikhef, Nijmegen, Netherlands
[107] Nikhef National Institute for Subatomic Physics and University of Amsterdam, Amsterdam, Netherlands
[108] Department of Physics, Northern Illinois University, DeKalb IL, United States of America
[109] Budker Institute of Nuclear Physics, SB RAS, Novosibirsk, Russia
[110] Department of Physics, New York University, New York NY, United States of America

[111] Ohio State University, Columbus OH, United States of America
[112] Faculty of Science, Okayama University, Okayama, Japan
[113] Homer L. Dodge Department of Physics and Astronomy, University of Oklahoma, Norman OK, United States of America
[114] Department of Physics, Oklahoma State University, Stillwater OK, United States of America
[115] Palacký University, RCPTM, Olomouc, Czech Republic
[116] Center for High Energy Physics, University of Oregon, Eugene OR, United States of America
[117] LAL, Université Paris-Sud and CNRS/IN2P3, Orsay, France
[118] Graduate School of Science, Osaka University, Osaka, Japan
[119] Department of Physics, University of Oslo, Oslo, Norway
[120] Department of Physics, Oxford University, Oxford, United Kingdom
[121] (a) INFN Sezione di Pavia; (b) Dipartimento di Fisica, Università di Pavia, Pavia, Italy
[122] Department of Physics, University of Pennsylvania, Philadelphia PA, United States of America
[123] National Research Centre "Kurchatov Institute" B.P.Konstantinov Petersburg Nuclear Physics Institute, St. Petersburg, Russia
[124] (a) INFN Sezione di Pisa; (b) Dipartimento di Fisica E. Fermi, Università di Pisa, Pisa, Italy
[125] Department of Physics and Astronomy, University of Pittsburgh, Pittsburgh PA, United States of America
[126] (a) Laboratório de Instrumentação e Física Experimental de Partículas - LIP, Lisboa; (b) Faculdade de Ciências, Universidade de Lisboa, Lisboa; (c) Department of Physics, University of Coimbra, Coimbra; (d) Centro de Física Nuclear da Universidade de Lisboa, Lisboa; (e) Departamento de Fisica, Universidade do Minho, Braga; (f) Departamento de Fisica Teorica y del Cosmos and CAFPE, Universidad de Granada, Granada (Spain); (g) Dep Fisica and CEFITEC of Faculdade de Ciencias e Tecnologia, Universidade Nova de Lisboa, Caparica, Portugal
[127] Institute of Physics, Academy of Sciences of the Czech Republic, Praha, Czech Republic
[128] Czech Technical University in Prague, Praha, Czech Republic
[129] Faculty of Mathematics and Physics, Charles University in Prague, Praha, Czech Republic
[130] State Research Center Institute for High Energy Physics (Protvino), NRC KI, Russia
[131] Particle Physics Department, Rutherford Appleton Laboratory, Didcot, United Kingdom
[132] (a) INFN Sezione di Roma; (b) Dipartimento di Fisica, Sapienza Università di Roma, Roma, Italy
[133] (a) INFN Sezione di Roma Tor Vergata; (b) Dipartimento di Fisica, Università di Roma Tor Vergata, Roma, Italy
[134] (a) INFN Sezione di Roma Tre; (b) Dipartimento di Matematica e Fisica, Università Roma Tre, Roma, Italy
[135] (a) Faculté des Sciences Ain Chock, Réseau Universitaire de Physique des Hautes Energies - Université Hassan II, Casablanca; (b) Centre National de l'Energie des Sciences Techniques Nucleaires, Rabat; (c) Faculté des Sciences Semlalia, Université Cadi Ayyad, LPHEA-Marrakech; (d) Faculté des Sciences, Université Mohamed Premier and LPTPM, Oujda; (e) Faculté des sciences, Université Mohammed V, Rabat, Morocco
[136] DSM/IRFU (Institut de Recherches sur les Lois Fondamentales de l'Univers), CEA Saclay (Commissariat à l'Energie Atomique et aux Energies Alternatives), Gif-sur-Yvette, France
[137] Santa Cruz Institute for Particle Physics, University of California Santa Cruz, Santa Cruz CA, United States of America
[138] Department of Physics, University of Washington, Seattle WA, United States of America
[139] Department of Physics and Astronomy, University of Sheffield, Sheffield, United Kingdom
[140] Department of Physics, Shinshu University, Nagano, Japan
[141] Fachbereich Physik, Universität Siegen, Siegen, Germany

[142] Department of Physics, Simon Fraser University, Burnaby BC, Canada
[143] SLAC National Accelerator Laboratory, Stanford CA, United States of America
[144] (a) Faculty of Mathematics, Physics & Informatics, Comenius University, Bratislava; (b) Department of Subnuclear Physics, Institute of Experimental Physics of the Slovak Academy of Sciences, Kosice, Slovak Republic
[145] (a) Department of Physics, University of Cape Town, Cape Town; (b) Department of Physics, University of Johannesburg, Johannesburg; (c) School of Physics, University of the Witwatersrand, Johannesburg, South Africa
[146] (a) Department of Physics, Stockholm University; (b) The Oskar Klein Centre, Stockholm, Sweden
[147] Physics Department, Royal Institute of Technology, Stockholm, Sweden
[148] Departments of Physics & Astronomy and Chemistry, Stony Brook University, Stony Brook NY, United States of America
[149] Department of Physics and Astronomy, University of Sussex, Brighton, United Kingdom
[150] School of Physics, University of Sydney, Sydney, Australia
[151] Institute of Physics, Academia Sinica, Taipei, Taiwan
[152] Department of Physics, Technion: Israel Institute of Technology, Haifa, Israel
[153] Raymond and Beverly Sackler School of Physics and Astronomy, Tel Aviv University, Tel Aviv, Israel
[154] Department of Physics, Aristotle University of Thessaloniki, Thessaloniki, Greece
[155] International Center for Elementary Particle Physics and Department of Physics, The University of Tokyo, Tokyo, Japan
[156] Graduate School of Science and Technology, Tokyo Metropolitan University, Tokyo, Japan
[157] Department of Physics, Tokyo Institute of Technology, Tokyo, Japan
[158] Department of Physics, University of Toronto, Toronto ON, Canada
[159] (a) TRIUMF, Vancouver BC; (b) Department of Physics and Astronomy, York University, Toronto ON, Canada
[160] Faculty of Pure and Applied Sciences, and Center for Integrated Research in Fundamental Science and Engineering, University of Tsukuba, Tsukuba, Japan
[161] Department of Physics and Astronomy, Tufts University, Medford MA, United States of America
[162] Centro de Investigaciones, Universidad Antonio Narino, Bogota, Colombia
[163] Department of Physics and Astronomy, University of California Irvine, Irvine CA, United States of America
[164] (a) INFN Gruppo Collegato di Udine, Sezione di Trieste, Udine; (b) ICTP, Trieste; (c) Dipartimento di Chimica, Fisica e Ambiente, Università di Udine, Udine, Italy
[165] Department of Physics, University of Illinois, Urbana IL, United States of America
[166] Department of Physics and Astronomy, University of Uppsala, Uppsala, Sweden
[167] Instituto de Física Corpuscular (IFIC) and Departamento de Física Atómica, Molecular y Nuclear and Departamento de Ingeniería Electrónica and Instituto de Microelectrónica de Barcelona (IMB-CNM), University of Valencia and CSIC, Valencia, Spain
[168] Department of Physics, University of British Columbia, Vancouver BC, Canada
[169] Department of Physics and Astronomy, University of Victoria, Victoria BC, Canada
[170] Department of Physics, University of Warwick, Coventry, United Kingdom
[171] Waseda University, Tokyo, Japan
[172] Department of Particle Physics, The Weizmann Institute of Science, Rehovot, Israel
[173] Department of Physics, University of Wisconsin, Madison WI, United States of America
[174] Fakultät für Physik und Astronomie, Julius-Maximilians-Universität, Würzburg, Germany
[175] Fachbereich C Physik, Bergische Universität Wuppertal, Wuppertal, Germany

[176] Department of Physics, Yale University, New Haven CT, United States of America
[177] Yerevan Physics Institute, Yerevan, Armenia
[178] Centre de Calcul de l'Institut National de Physique Nucléaire et de Physique des Particules (IN2P3), Villeurbanne, France
[a] Also at Department of Physics, King's College London, London, United Kingdom
[b] Also at Institute of Physics, Azerbaijan Academy of Sciences, Baku, Azerbaijan
[c] Also at Novosibirsk State University, Novosibirsk, Russia
[d] Also at TRIUMF, Vancouver BC, Canada
[e] Also at Department of Physics & Astronomy, University of Louisville, Louisville, KY, United States of America
[f] Also at Department of Physics, California State University, Fresno CA, United States of America
[g] Also at Department of Physics, University of Fribourg, Fribourg, Switzerland
[h] Also at Departamento de Fisica e Astronomia, Faculdade de Ciencias, Universidade do Porto, Portugal
[i] Also at Tomsk State University, Tomsk, Russia
[j] Also at CPPM, Aix-Marseille Université and CNRS/IN2P3, Marseille, France
[k] Also at Universita di Napoli Parthenope, Napoli, Italy
[l] Also at Institute of Particle Physics (IPP), Canada
[m] Also at Particle Physics Department, Rutherford Appleton Laboratory, Didcot, United Kingdom
[n] Also at Department of Physics, St. Petersburg State Polytechnical University, St. Petersburg, Russia
[o] Also at Department of Physics, The University of Michigan, Ann Arbor MI, United States of America
[p] Also at Louisiana Tech University, Ruston LA, United States of America
[q] Also at Institucio Catalana de Recerca i Estudis Avancats, ICREA, Barcelona, Spain
[r] Also at Graduate School of Science, Osaka University, Osaka, Japan
[s] Also at Department of Physics, National Tsing Hua University, Taiwan
[t] Also at Department of Physics, The University of Texas at Austin, Austin TX, United States of America
[u] Also at Institute of Theoretical Physics, Ilia State University, Tbilisi, Georgia
[v] Also at CERN, Geneva, Switzerland
[w] Also at Georgian Technical University (GTU),Tbilisi, Georgia
[x] Also at Manhattan College, New York NY, United States of America
[y] Also at Hellenic Open University, Patras, Greece
[z] Also at Institute of Physics, Academia Sinica, Taipei, Taiwan
[aa] Also at LAL, Université Paris-Sud and CNRS/IN2P3, Orsay, France
[ab] Also at Academia Sinica Grid Computing, Institute of Physics, Academia Sinica, Taipei, Taiwan
[ac] Also at School of Physics, Shandong University, Shandong, China
[ad] Also at Moscow Institute of Physics and Technology State University, Dolgoprudny, Russia
[ae] Also at Section de Physique, Université de Genève, Geneva, Switzerland
[af] Also at International School for Advanced Studies (SISSA), Trieste, Italy
[ag] Also at Department of Physics and Astronomy, University of South Carolina, Columbia SC, United States of America
[ah] Also at School of Physics and Engineering, Sun Yat-sen University, Guangzhou, China
[ai] Also at Faculty of Physics, M.V.Lomonosov Moscow State University, Moscow, Russia
[aj] Also at National Research Nuclear University MEPhI, Moscow, Russia
[ak] Also at Department of Physics, Stanford University, Stanford CA, United States of America
[al] Also at Institute for Particle and Nuclear Physics, Wigner Research Centre for Physics, Budapest, Hungary
[am] Also at University of Malaya, Department of Physics, Kuala Lumpur, Malaysia
[*] Deceased